



**University of
Zurich^{UZH}**

Geochemical Characteristics of Grain Size Fractions - Detailing Mackenzie River Sediment

ESS 511 Master's Thesis

Author

Bastian Buman
13-717-434

Supervised by

Dr. Alysha Inez Coppola

Faculty representative

Prof. Dr. Michael W.I. Schmidt

28.04.2019

Department of Geography, University of Zurich



Universität
Zürich ^{UZH}

GEOCHEMICAL CHARACTERISTICS OF GRAIN SIZE FRACTIONS

Detailing Mackenzie River Sediment

MASTER THESIS

To obtain the academic degree of
Master of Science in Earth System Science

Presented to the Department of Geography of the University of Zurich

Supervisor

Dr. Alysha I. Coppola

Faculty Member

Prof. Dr. Michael W. I. Schmidt

Mentor

Dr. Samuel Abiven

Author

Bastian S. Buman
Joggelacker 16, 5210 Windisch
13-717-434
bastian.buman@uzh.ch

Windisch, Sunday, April 28, 2019





What is this mind of ours:
what are these atoms with consciousness?
Last week's potatoes!
They now can remember what was going on in my mind a year
ago
—
a mind which has long ago been replaced.

— Richard Feynman about the half-life of phosphorus in the (human) brain,
in Feynman and Leighton (2007).

Abstract

The Arctic has a very important role in the global climate system and is drastically influenced by climate change. The atmosphere is rapidly warming, permafrost is thawing, river discharge and wildfire risk are increased, and the carbon cycle overall is intensified. In this context rivers are integral because they are the main link between processes on land and in the ocean. Rivers transport sediment from its source to its terminal burial in the oceans by a series of routes and processes. Throughout the journey, important constituents of sediment, such as organic substances, are subject to modifications. It is thus important to have a detailed look at sediment transported by a river.

In this thesis the geochemical characteristics of different grain size fractions from sediment of the Mackenzie River and important tributaries are investigated. The delta-head rivers, Mackenzie, Arctic Red and Peel are compared to samples from the delta. The explored geochemical characteristics include the mineral specific surface area, inorganic elements (Al, Si, Ca, Ti), organic carbon (C_{org}) and black carbon (BC).

The results show different grain size distributions in the delta-head rivers and a distribution in the delta that is not simply explained by the inputs. In the delta both smaller and larger particles are lost, while intermediately sized particles increase in importance. Indicators of minerals (Al, Ti) clearly increase with decreasing particle size. C_{org} and BC are associated with smaller particles (highest in $< 20 \mu\text{m}$) but it looks like larger particles do also contain significant amounts. The results highlight that it is important to account for geochemical differences as well as grain size characteristics when sampling – at least during the freshet.

The fluxes of both C_{org} and BC for 2017 were $1.7 \pm 0.7 \text{ Mt}$ and $0.36 \pm 0.09 \text{ Mt}$ respectively. With current estimates of burial efficiency, the amount of particulate organic carbon potentially buried could be $0.994 \pm 0.130 \text{ Mt}$, of which up to $0.208 \pm 0.027 \text{ Mt}$ could be in the form of particulate black carbon.

Acknowledgments

I would like to thank Dr. Alysha Coppola for assisting and supervising me during the thesis. Her comments and ideas helped me to think and write more clearly and express my ideas more accurately. I learned a great deal from her about the work and morale of a scientist. Her dedication to the research fields of biogeochemistry and earth system science were a constant motivation for me. Her introduction into the BPCA method gave me insights into an active field of research.

I'm further very thankful for the advice, assistance and inspiration provided by Dr. Samuel Abiven. His lectures and his personality inspired me to keep my eyes open for interesting facts and ideas.

I would like to express my gratitude towards Melissa Schwab, who provided the samples as well as ideas and knowledge and who helped me in the laboratory.

I thank Reto Bollmann, Jessica Buman, Selina Liechti and Florian Lustenberger, who lectured the thesis as well as Michael Hilf, who always assisted me in the laboratory.

— To my family and friends, and all who helped me during my thesis.

Content

Abstract	i
Acknowledgments	iii
Content	v
Table of Figures	vii
Table of Tables	xi
List of Abbreviations	xiii
1 Introduction	1
1.1 The Arctic	2
1.2 Organic Carbon	4
1.3 Motivation	7
1.4 Research Questions	8
2 Study Setting and Riverine Sediment Transport	9
2.1 Study Setting	9
2.1.1 Mackenzie River Basin	9
2.1.2 Carbon Export	9
2.1.3 Geology and Climate	10
2.1.4 Fire History	12
2.2 Sediment	13
2.2.1 Transport and Erosion	13
2.2.2 Effective Particle Size	15
2.2.3 Further Considerations	15
3 Methods	17
3.1 Sampling	17
3.2 Mineral specific Surface Area	18
3.3 Homogenization	19
3.4 Elemental Composition	19
3.5 Diffuse Reflectance Infrared Fourier Transform	20
3.6 Black Carbon	22
3.7 Carbon and Stable Isotopes	25
3.7.1 Isotope Ratio Mass Spectrometry	25
3.7.2 Cavity Ring-Down Spectrometry	26
3.8 Mixing Model and Export Fluxes	27
4 Results	29

4.1 Mass Balance	29
4.2 Elemental Composition	31
4.3 Surface Area	33
4.4 Carbon Content	35
4.4.1 Total Carbon	35
4.4.2 Organic Carbon	36
4.4.3 Black Carbon	37
4.5 Stable Isotopes	41
4.6 Mid-infrared spectrometry.....	43
5 Discussion	49
5.1 Geochemical Characteristics of Grain Size Fractions.....	49
5.1.1 Grain Size Distribution	49
5.1.2 Geochemical Characteristics	51
5.1.3 Carbon in the Mix	52
5.1.4 Black Carbon	54
5.1.5 Identifying Sources for Higher C _{org} Content.....	55
5.2 Fluxes	56
6 Conclusion	60
7 Outlook	62
8 Limitations	63
References	64
Declaration of Originality	76
Supplements.....	77
S-1. Methods	77
Sieving and Drying	77
Area under the curve.....	77
Partial Least Squares Regression	77
S-2. Treatise of XRF Reproducibility and Error	78
S-3. BPCA Statistics	81
S-4. Mid-infrared spectrometry.....	82
S-5. Estimating the Organic Carbon Content.....	85

Table of Figures

Figure 1-1 Overview of the observed changes to the average surface temperature from 1901 to 2012. White areas represent regions with sparse data availability (less than 70 % complete records and less than 20 % data availability in the first and last 10 % of the time period). Changes are derived from linear regression on temperature data. Significant trends ($\alpha = 10\%$) are indicated by a + sign (IPCC, 2013).	2
Figure 1-2 Distribution of C_{org} in and on river suspended sediment particles. C_{org} can be incorporated into pores and laminar structures of minerals but it can also be distributed onto particle surfaces. Colors indicate sources of C_{org} (green modern; aged brown, and sedimentary rock derived, black). Red colored patches are reactive oxides (e.g. Iron-oxides) that may be present (not relevant to this study), figure based on Blair and Aller (2012).	4
Figure 1-3 (a) The BC continuum as function of pyrolysis temperature. Aromatic ratios H/C and O/C decrease with increasing temperature, while particle size decreases from cm scale to μm scale. Aromaticity, degree of condensation as well as resistance to oxidation increases, while surface reactivity decreases. Particle size relation has exceptions, smoke for example can form under low temperature and contains extremely fine particles. (b) Example for a possible structural molecular representation of black carbon, from Ziolkowski et al. (2011). Highlighted in bold are benzene-polycarboxylic acids (BPCAs); for more details on BPCA please refer to the text (p. 22).	6
Figure 2-1 Map depicts Canada along 60 degrees latitude. Indicated are the large rivers and lakes of the Mackenzie River system, as well as the main physiographic regions. Map created using QGIS software (QGIS Development Team, 2019) and publicly available data from Natural Resources Canada (Natural Resources Canada, 2016) as well as with Natural Earth, free vector and raster map data @ naturalearthdata.com. Projection is Canada Lambert Conformal Conic (CLCC, EPSG:102002). Shaded relief based on NWT Centre for Geomatics (2015).	11
Figure 2-2 Satellite imagery (false color: thermal IR, green and blue) of the section of the Mackenzie Basin relevant to the study. Highlighted are the confluence of Arctic Red and Mackenzie River at Tsiigehtchic, the sampling location on the Peel River as well as on Mackenzie River at Inuvik. Star symbols indicate samples from 2017 analyzed in this thesis, whereas circles indicate samples from other authors (red = Vonk et al., 2015a, yellow = Hilton et al., 2015). Map created using QGIS (QGIS Development Team, 2019) and free satellite orthoimages (geo-referenced) from Natural Resources Canada (2016).	12
Figure 2-3 (a) different size classes used to describe sediment, (Table 2-2, note the logarithmic scale). (b) sketch of the particle transport in a river, including the common terminology used for the description of different particles transported in a river (Parsons et al., 2015).), please note the logarithmic scale.	14
Figure 2-4 Image of a composite particle (Woodward and Walling, 2007).	15
Figure 3-1 Schematic illustration of the methodology used in diffuse reflectance spectrometry, modified from Chen et al. (2015). IR denotes Infrared radiation. A source emits infrared radiation that is redirected by a mirror onto the sample, where it is scattered by the particles. Scattering can be due to reflection, refraction and diffraction. A sensor can finally measure the beam of IR that reemerges from the sample. Analysis of the signal yields information about molecules present in the sample...	21
Figure 3-2 Sketch of the improved BPCA method with individual steps, (Wiedemeier et al., 2016).	23

Figure 3-3 (a) Molecular structure of the marker compounds (benzene polycarboxylic acids, BPCAs) isolated in the BPCA method, figure adapted from Brodowski et al. (2005). (b) Illustrating the approximate retention time in the HPLC for BPCA marker compounds (Wiedemeier et al., 2013). In (b) The specific samples used were (a) a soil sample (chernozem) and (b) grass charcoal (<i>Oryza Sativa</i>).	25
Figure 4-1 Mass balance for the four different sampling locations and rivers (Station / River). Particle sizes were determined by two consecutive rounds of sieving, more info in Table 4-1.....	30
Figure 4-2 (a) Overview of selected elemental shares. Black bars indicate the error range for a specific measurement. The working code is a unique code identifying each sample. MT refers to Tsiigehtchic / Mackenzie, AR to Tsiigehtchic / Arctic Red, PR to Fort Mcpherson / Peel and MD to Inuvik / Mackenzie, the number refers to the particle size, with 1 being associated with bulk and 8 with < 20 μm (more details in Table 3-1). (b) Particle size (grain size fraction) vs. Al/Si ratio.	32
Figure 4-3 Mineral specific surface area for the 2017 samples (BET method, see methods, p. 18). Colors indicate different measurement sites. The working code is a unique code identifying each sample. MT refers to Tsiigehtchic / Mackenzie, AR to Tsiigehtchic / Arctic Red, PR to Fort McPherson / Peel and MD to Inuvik / Mackenzie, the number refers to the particle size, with 1 being associated with bulk and 8 with < 20 μm (more details in Table 3-1).	34
Figure 4-4 Relationship between aluminum and surface area. Linear regression significance levels (* 0.05, ** 0.01, *** 0.001) and R^2 . Colors indicate the different measurement sites (Location / River). Aluminum was determined using XRF (p. 19), mineral specific surface area was determined using BET (p. 18).	34
Figure 4-5 Amount of total carbon (% C). Colors indicate different measurement sites. The working code is a unique code identifying each sample. MT refers to Tsiigehtchic / Mackenzie, AR to Tsiigehtchic / Arctic Red, PR to Fort McPherson / Peel and MD to Inuvik / Mackenzie, the number refers to the particle size, with 1 being associated with bulk and 8 with < 20 μm (more details in Table 3-1).	35
Figure 4-6 Relationship between calcium and carbon. The upper panel (a) includes the extreme values found in Inuvik / Mackenzie (Pearson's $r = 0.35$), while the lower panel (b) ignores these two (Pearson's $r = 0.83$).	36
Figure 4-7 Organic carbon (C_{org}) in the samples. Colors indicate different measurement sites. The Working code is a unique code identifying each sample. MT refers to Tsiigehtchic / Mackenzie, AR to Tsiigehtchic / Arctic Red, PR to Fort McPherson / Peel and MD to Inuvik / Mackenzie, the number refers to the particle size, with 1 being associated with bulk and 8 with < 20 μm (more details in Table 3-1).	37
Figure 4-8 Compilation of the measured BPCA in the samples. (a) Overview by location, giving all size fractions individually, BC in [g BPCA-C / kg sample] is independent of the amount of C_{org} . (b) Overview by particle size, location indicated by the same colors as in (a), same units as (a). (c) same as (a) but BC reported in [g BPCA-C / kg C_{org}]. (d) same as (b) but in units of (c). The working code is a unique code identifying each sample. MT refers to Tsiigehtchic / Mackenzie, AR to Tsiigehtchic / Arctic Red, PR to Fort Mcpherson / Peel and MD to Inuvik / Mackenzie, the number refers to the particle size, with 1 being associated with bulk and 8 with < 20 μm (more details in Table 3-1).	38
Figure 4-9 Mineral specific surface area vs. BPCA-C. (a) C_{org} independent measurement in [g BPCA-C / kg sample], (b) BPCA-C as portion of C_{org} in [g BPCA-C / kg C]. Linear regression significance levels (* 0.05, ** 0.01, *** 0.001) and R^2 . Colors indicate the different measurement sites (Location / River). BPCA-C determined using the method introduced by Wiedemeier et al. (2013) (p.22), mineral specific surface area was determined using BET (p. 18).	39

Figure 4-10 Distribution of the different BPCAs. (a) all samples individually, stacked distribution of the BPCAs. (b) shows the distribution of the different BPCAs between sites. Here the grouping colors indicate statistically significant different groups. For each of the four BPCAs a test for normal distribution was conducted by using the Shapiro method, subsequently a Levene test was used to test for equal variances and finally either a Kruskal-Wallis (K.-W.) or an analysis of variance (ANOVA; AOV) was conducted to see if measurement sites have significantly different BPCA distribution. A Dunn post-hoc test, using the Bonnferoni method, was used to find the different groups. The working code is a unique code identifying each sample. MT refers to Tsiigehtchic / Mackenzie, AR to Tsiigehtchic / Arctic Red, PR to Fort McPherson / Peel and MD to Inuvik / Mackenzie, the number refers to the particle size, with 1 being associated with bulk and 8 with < 20 μm (more details in Table 3-1).	40
Figure 4-11 Stable carbon isotopes (total carbon, C_{tot} , organic + inorganic C) in (a) the different size fractions and the different sampling sites, and in (b) relative to calcium content. Significance levels * $p < 0.05$, ** $p < 0.01$, *** $p < 0.001$. The working code is a unique code identifying each sample. MT refers to Tsiigehtchic / Mackenzie, AR to Tsiigehtchic / Arctic Red, PR to Fort McPherson / Peel and MD to Inuvik / Mackenzie, the number refers to the grain size fraction, with 1 being associated with bulk material and 8 with < 20 μm (more details in Table 3-1).	42
Figure 4-12 Stable carbon isotopes in the different size fractions, determined using isotope ratio mass spectrometry (p. 25). The Working Code is a unique code identifying each sample. MT refers to Tsiigehtchic / Mackenzie, AR to Tsiigehtchic / Arctic Red, PR to Fort McPherson / Peel and MD to Inuvik / Mackenzie, the number refers to the grain size fraction, with 1 being associated with bulk material and 8 with < 20 μm (more details in Table 3-1).	42
Figure 4-13 Overview of the mid-infrared spectral data from diffuse reflectance spectrometry across all samples and all sites. Colors highlight sites, individual spectra represent samples. From top to bottom the particle sizes decrease. Absorbance is a unitless ratio defined as $A = -\log I/I_0$, where I is the measured light intensity and I_0 is the initial intensity.	43
Figure 4-14 Mid-infrared spectral data from diffuse reflectance spectrometry for the site Tsiigehtchic / Mackenzie. Dashed lines indicate absorption bands of compounds related to aromatic structures. Aromatic C-H i-p-b refers to aromatic C-H in-plane bending. Aromatic C-H o-p-b denotes aromatic C-H out-of-plane bending. For more details about the bands and the spectra refer to the text and Table 3-3. Absorbance is a unitless ratio defined as $A = -\log I/I_0$, where I is the measured light intensity and I_0 is the initial intensity.	44
Figure 4-15 C-H stretch absorbance area under curve vs. BPCA-C. (a) AUC vs. g BPCA-C / kg C, no significant relationship (b) AUC vs. g BPCA-C / kg sample showing a significant relationship. Levels of significance * $p < 0.05$, ** $p < 0.01$, *** $p < 0.001$	45
Figure 5-1 Relationship ($SA:C_{\text{org}}$), also referred to as C_{org} loading, between mineral specific surface area (SA) and organic carbon (C_{org}). Superimposed is the typical range for this relationship from 0.4 to 1.0 mg C_{org} / m ² (gray area, calculation based on Blair and Aller, 2012; Mayer, 1994). Color indicates different grain size fractions, whereas shapes represent different sampling sites (Location / River).	53
Figure 5-2 Flux of POC (C_{org} associated with particles) and PBC (black carbon associated with particles) for the year 2017 presented for the different rivers and the different grain size fractions. For Tsiigehtchic / Mackenzie two different estimates for TSS were available, dark blue is the lower limit (51 Mt yr ⁻¹) measured by Gareis and Lesack (2017), light blue is the upper limit (93 Mt yr ⁻¹) estimated by Carson et al. (1998). Please note that the scale is in kt yr ⁻¹ (10 ⁻³ Mt yr ⁻¹). Results for the bulk as well as the < 63 μm grain size fraction are intentionally not presented (see text). The	

working code is a unique code identifying each sample. MT refers to Tsiigehtchic / Mackenzie, AR to Tsiigehtchic / Arctic Red, PR to Fort McPherson / Peel and MD to Inuvik / Mackenzie, the number refers to the grain size fraction, with 1 being associated with bulk material and 8 with < 20 µm (more details in Table 3-1). 57

Figure S-1 Overview of the selected samples (MT1, MT4, MT8, MD1, MD2, MD3, PR8) and elements (Na, Mg, Al, Si, Ca, Ti), as well as the total concentration and the reference series (Ref), see Table S-1. Concentration has variable scales in this figure! Samples are indicated using their working code, where MT refers to Tsiigehtchic / Mackenzie, AR to Tsiigehtchic / Arctic Red, PR to Fort McPherson / Peel and MD to Inuvik / Mackenzie, the number refers to the particle size, with 1 being associated with bulk and 8 with < 20 µm (more details in Table 3-1)..... 78

Figure S-2 Mid-infrared spectral data from diffuse reflectance spectrometry for the site Tsiigehtchic / Arctic Red. Dashed lines indicate absorption bands of compounds related to aromatic structures. Aromatic C-H i-p-b refers to aromatic C-H in-plane bending. Aromatic C-H o-p-b denotes aromatic C-H out-of-plane bending. For more details about the bands and the spectra refer to the text and Table 3-3. Absorbance is a unitless ratio defined as $A = -\log I/I_0$, where I is the measured light intensity and I_0 is the initial intensity. 82

Figure S-3 Mid-infrared spectral data from diffuse reflectance spectrometry for the site Fort McPherson / Peel. Dashed lines indicate absorption bands of compounds related to aromatic structures. Aromatic C-H i-p-b refers to aromatic C-H in-plane bending. Aromatic C-H o-p-b denotes aromatic C-H out-of-plane bending. For more details about the bands and the spectra refer to the text and Table 3-3. Absorbance is a unitless ratio defined as $A = -\log I/I_0$, where I is the measured light intensity and I_0 is the initial intensity..... 83

Figure S-4 Mid-infrared spectral data from diffuse reflectance spectrometry for the site Inuvik / Mackenzie. Dashed lines indicate absorption bands of compounds related to aromatic structures. Aromatic C-H i-p-b refers to aromatic C-H in-plane bending. Aromatic C-H o-p-b denotes aromatic C-H out-of-plane bending. For more details about the bands and the spectra refer to the text and Table 3-3. Absorbance is a unitless ratio defined as $A = -\log I/I_0$, where I is the measured light intensity and I_0 is the initial intensity. 84

Figure S-5 Number of components vs. residual mean squared error of prediction (RMSEP) for the prediction of organic carbon by PLSR on DR-spectrometry data. 85

Figure S-6 Scatterplot matrix of the combinations of the 6 components, percentages in braces indicate the amount of variance explained by the component. 86

Figure S-7 Measured vs. predicted values, the line indicates a 1:1 relationship..... 86

Figure S-8 Components and their loading values..... 87

Table of Tables

Table 2-1 Fine sediment load for the delta-head rivers. Mackenzie River wash load (< 0.125 mm), Arctic Red and Peel Rivers suspended load, additionally added is the relative contribution of the respective load to the total found at Mackenzie / Inuvik, data from(a) Gareis and Lesack (2017) and (b) Carson et al. (1998).....	9
Table 2-2 Particle size classes and their respective particle diameter in μm , (Turnewitsch et al., 2007; Owens, 2008; Viers et al., 2009; Kuhnle, 2013).....	14
Table 3-1 Sample overview. River bank and bedload material sampled in 2017 (Schwab, 2016). The first column (sample code) refers to the code used in other work. The second column (laboratory code) refers to the code attached for the present work in the laboratory and the third column (WC, working code) is a more convenient version for this specific text. MT refers to Tsiigehtchic / Mackenzie, AR to Tsiigehtchic / Arctic Red, PR to Fort McPherson / Peel and MD to Inuvik / Mackenzie, the number refers to the particle size, with 1 being associated with bulk and 8 with < 20 μm . GFR denotes the respective grain size fraction in [μm]......	17
Table 3-2 Continuation of Table 3-1.....	18
Table 3-3 Specific spectral bands for the determination of aromatic structures in a sample, from Coates (2000). Further the table shows bands of further importance (LibreTexts, 2019)......	22
Table 3-4 Overview of the BPCA method steps and reference material. TFA stands for Trifluoroacetic acid, C/R denotes Cation Removal, SPE denotes Solid Phase Extraction (removal of apolar compounds). 23	
Table 3-5 Isotopes of carbon (C) and nitrogen (N) and their relative attribution to the total, from Fry (2006).	26
Table 4-1 Overview of the presentation scheme for the sampled results.....	29
Table 4-2 Results of the simple mixing model, values in [%] of total or in [%] of the grain size fraction < 63 μm , where indicated with a star (*). Calculated using data from (a) Gareis and Lesack (2017) and (b) Carson et al. (1998) and equation III-6. The last column gives the measured contribution (m).....	31
Table 4-3 Area under the curve (AUC) for the samples and the different NIR bands important for aromatic compounds.....	46
Table 4-4 Overview of the results from the different measurements. Individual samples are referred to by their working code (WC). WC is a unique code identifying each sample. MT refers to Tsiigehtchic / Mackenzie, AR to Tsiigehtchic / Arctic Red, PR to Fort McPherson / Peel and MD to Inuvik / Mackenzie, the number refers to the grain size fraction, with 1 being associated with bulk material and 8 with < 20 μm (more details in Table 3-1). L/R denotes the sampling location (L) and the corresponding river (R), GFR denotes the grain size fraction, S1 denote the share of a certain GFR to the total. S2 denotes the share of a certain GFR to < 63 μm . SA denotes mineral specific surface area, C_{org} denotes organic carbon, C_{pred} denotes C_{org} predicted from a partial least squares regression on diffuse reflectance spectrometry data, C_{tot} gives the total carbon content measured with cavity ring-down spectrometry. BPCA denotes benzene poly-carboxylic acid and is the sum of the individual marker compounds (B3CA, B4CA, B5CA and B6CA). BPCA is given in % of C_{org} , in g / kg C_{org} as well as in g / kg S, where S denotes sample mass. Al denotes aluminum, Si denotes silicon, Ca denotes calcium and Ti denotes titanium.....	47
Table 4-5 Continuation of Table 4-4.....	48
Table 5-1 W/C = Working Code, MT = Tsiigehtchic / Mackenzie, AR = Tsiigehtchic / Arctic Red, PR = Fort McPherson / Peel, MD = Inuvik / Mackenzie, L/R = Location / River, TSS = Total Suspended	

Sediment, * conversion factor = 4 ± 1 (Ziolkowski et al., 2011). ^a Hilton et al. (2015), ^b Coppola et al. (2018).	58
Table 5-2 Overview of relevant results found in other work. MT = Mackenzie at Tsiigehtchic, AR = Arctic Red, PR = Peel River, MD = Mackenzie at Inuvik/Delta. SA = Surface Area, C _{org} = organic carbon, POC = Particulate Organic Carbon, DOC = Dissolved Organic Carbon, TSS = Total suspended sediment....	59
Table S-1 Overview of the XRF elemental composition for selected samples and selected elements as well as the total summed up concentration (device internal processing). Samples are indicated using their working code, where MT refers to Tsiigehtchic / Mackenzie, AR to Tsiigehtchic / Arctic Red, PR to Fort McPherson / Peel and MD to Inuvik / Mackenzie, the number refers to the particle size, with 1 being associated with bulk and 8 with < 20 µm (more details in Table 3-1).....	80
Table S-2 Descriptive statistics of the BPCA distribution across measurement sites. MT = Mackenzie at Tsiigehtchic, AR = Arctic Red (at Tsiigehtchic), PR = Peel River, MD = Mackenzie Delta (at Inuvik). For each of the four BPCAs a test of normal distribution was conducted by using the Shapiro method, subsequently a Levene test was used to test for equal variances and finally either a Kruskal-Wallis (K.-W.) or an analysis of variance (ANOVA; AOV) was conducted to see if measurement sites have significantly different BC quality. A Dunn post-hoc test, using the Bonnferoni method, was used to find the different groups. Correlation coefficient was calculated using $r = zn$, effect size is based on Cohen (1992).	81
Table S-3 Descriptive statistics for the relationship between aromatic C-H stretch AUC and BPCA [g/kg sample]. No autocorrelation according to D-W statistics, residuals normally distributed and homoscedastic.....	84

List of Abbreviations

BC, PBC	Black Carbon, Particulate Black Carbon
BPCA	Benzene Poly-Carboxylic Acid; [g BPCA-C / kg Sample] or [g BPCA-C / kg C _{org}]
POC, DOC	Particulate Organic Carbon (POC), Dissolved Organic Carbon (DOC)
SOC	Soil Organic Carbon
OC, C _{org}	Organic Carbon in [%]
C, C _{tot}	Total Carbon in [%] (inorganic carbon + organic carbon)
BET	Brunauer-Emmet-Teller method to determine mineral specific surface area (Brunauer et al., 1938)
SA	Surface area in [m ² /g]
XRF	X-Ray Fluorescence, phenomenon exploited to determine the elemental composition (Jenkins, 2012)
DRIFT	Diffuse Reflectance Infrared Fourier Transform, better referred to as DR-spectrometry, (Griffiths and Haseth, 2007)
IRMS	Isotope Ratio Mass Spectrometry
CRDS	Cavity Ring-Down Spectrometry
PLSR	Partial Least Squares Regression
MT	Mackenzie River at Tsiigehtchic
AR	Arctic Red River (at Tsiigehtchic)
PR	Peel River (at Fort McPherson)
MD	Mackenzie River at Inuvik (delta middle channel, after the confluence of MT, AR and PR)
Tg	Tera-gram, 10 ¹² g = 10 ⁹ kg = 10 ⁶ t (metric tons)
Gg	Giga-gram, 10 ⁹ g = 10 ⁶ kg = 10 ³ t
Mt	Mega-ton, 10 ⁶ t
µm	Micrometer, 10 ⁻⁶ m



The movement of water drives the carbon cycle

— Ward et al. (2017)

1 Introduction

In this thesis I look at river bank and bedload sediment from four different locations in the Mackenzie River basin. Three of which are from the delta-head rivers of the Mackenzie Delta; Mackenzie River itself, Arctic Red River and Peel River. These are the most important sediment contributors to the delta. The last sample is from the middle channel of the delta.

I look at these samples on the level of different grain size fractions, going from larger particles ($> 250 \mu\text{m}$) to very fine particles ($< 20 \mu\text{m}$). Each grain size fraction is analyzed for inorganic elements, for mineral specific surface area and organic matter, including black carbon content. With this I try to answer the question whether different grain size fractions show differences in their geochemical characteristics. It is important to look at these different size fractions because they are not transported equally in a river. Depending on particle characteristics (size, density, shape, porosity) they experience different hydrodynamic sorting along the course of the river (Walling et al., 2000; Williams et al., 2008).

If these hydrodynamic differences were to be further contrasted by differences in the composition (Walling et al., 2000), then there would be implications for the cycling and remineralization of organic matter. Which in turn could influence our understanding of the carbon balance and dynamics in the whole drainage basin, with consequences for the adjacent shelf and open ocean.

1.1 The Arctic

Current changes observed in the global climate system, such as the warming atmosphere and oceans, reduced snow cover, reduced land- and sea-ice (IPCC, 2013) are also affecting, and are being observed in the Arctic (Box et al., 2019). Major feedback mechanisms on all scales are altered by climate change. The air temperature, for instance, is observed to be increasing twice as fast as the global average (Figure 1-1 and Osborne et al., 2018). The hydrological cycle shows increased and earlier river discharge (Overeem and Syvitski, 2016). The sea ice is younger and shows dramatic decreases in extent (Laxon et al., 2013). Snow cover decreases in spring and summer (Estilow et al., 2015) and the arctic tundra is greening (Reichle et al., 2018) due in part to increasing shrub biomass (Box et al., 2019; Martin et al., 2017). The vast areas of permafrost, with huge stocks of soil organic carbon (SOC), are observed to be warming (Tarnocai et al., 2009; Smith et al., 2010) and the risk for wildfire ignition in boreal landscapes by cause of lightning is increasing due to drier conditions and higher maximum air temperatures (Box et al., 2019).

The implications of changes to all these systems are manifold and far-reaching (McGuire et al., 2006). The importance of the Arctic for the global climate system lies in reducing the input of energy the earth receives at and near the equator (McGuire et al., 2006). McGuire et al. (2006) estimate that positive feedback mechanisms are likely to dominate in the near future (next 50 to 100 years), thereby strengthening already existing climatic changes. With these dramatic changes it is clear why the Arctic is an important topic of research. One of the most prominent study objects is the Arctic Ocean (Stein and Macdonald, 2013).

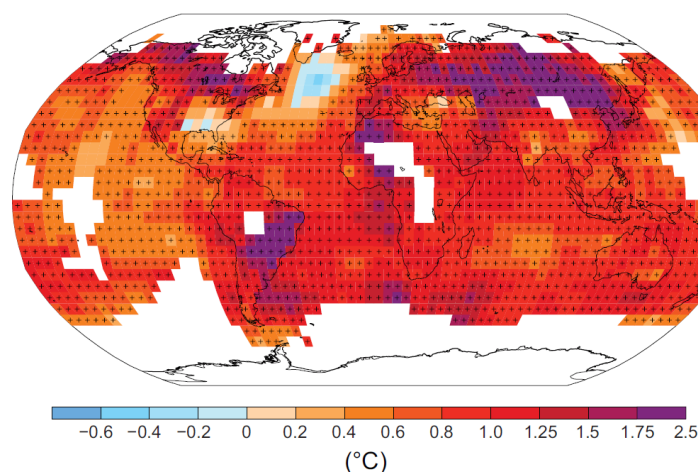


Figure 1-1 Overview of the observed changes to the average surface temperature from 1901 to 2012. White areas represent regions with sparse data availability (less than 70 % complete records and less than 20 % data availability in the first and last 10 % of the time period). Changes are derived from linear regression on temperature data. Significant trends ($\alpha = 10\%$) are indicated by a + sign (IPCC, 2013).

The Arctic Ocean is a shelf-dominated, sea-ice influenced waterbody, with little biological activity (Honjo et al., 2010), and while being a small ocean compared to the rest of the

world's oceans (1 % of the total volume, Menard and Smith, 1966), it is very important for the climate system (McGuire et al., 2006). In contrast to its size, it receives 10 % – 13 % of the global freshwater and 2.2 % of the global sediment discharge (Holmes et al., 2012; Milliman and Farnsworth, 2011), illustrating how important rivers are for arctic land-ocean interactions (McGuire et al., 2006).

Rivers represent the main link between the terrestrial source of material and its terminal burial in oceanic sediments (Freymond et al., 2018; Aufdenkampe et al., 2011; Guo et al., 2018). Only in oceanic sediments organic carbon is stored over geologic timescales (Emerson and Hedges, 1988). Riverine processes are therefore important for feedback mechanisms and regional and global climate on many spatial and temporal scales (Cole et al., 2007; Battin et al., 2009). The transfer of sediment by rivers, from its source through a series of routes and processes to the oceans, is denoted aquatic continuum or sediment cascade / continuum (Koiter et al., 2013; Burt and Allison, 2010; Ward et al., 2017).

In the context of this continuum, rivers are hotspots for transport, modification, redistribution and remineralization of organic matter. And as such, rivers have the potential for the release and burial of large quantities of CO₂, granting them a key yet understudied role in the climate system (Cole et al., 2007; IPCC, 2013; Galy et al., 2007; Aufdenkampe et al., 2011; Regnier et al., 2013; Galy et al., 2015; Ward et al., 2017). Arctic rivers play a key role in the global climate system because they link the Arctic landscapes to the Arctic Ocean.

Arctic landscapes contain about 40 % – 50 % of the global SOC stocks (amounting to 1'100 Pg to 1'672 Pg of SOC, Tarnocai et al., 2009; Hugelius et al., 2014). These massive amounts of SOC are susceptible to increased mobility under future warming and likely to be incorporated in microbial decomposition and also likely to enter rivers (Spencer et al., 2015; Feng et al., 2013; Mann et al., 2015). If remineralized, this amount of SOC could easily double the current amount of carbon in the atmosphere (Spencer et al., 2015). The focus of this study lies on the Mackenzie River system, as it is the largest arctic sediment contributor (Vonk et al., 2015a).

The most important part of the sediment for the climate is the amount, type and reactivity of the organic material that is transported. This part of the sediment can potentially be remineralized to CO₂ and thereby increase atmospheric CO₂ (Blair and Aller, 2012).

1.2 Organic Carbon

Rivers transport organic carbon (C_{org} , OC) both in association with particles (POC, particulate organic carbon) and in solution (DOC, dissolved organic carbon). Organic carbon transported by particles in a river has three main sources: (i) recently produced, (ii) old and altered C_{org} (e.g. soil organic carbon) and (iii) sedimentary rock derived C_{org} (Blair and Aller, 2012). The amount of C_{org} is typically between 0.2 % to 3 % of the particle mass. It is found in association with all particle sizes, where it is distributed onto particle surfaces but is also incorporated into mineral structures. Furthermore, it can form and be integrated into gel-like structures (Blair and Aller, 2012). The contribution of the three components is influenced mainly by the composition of the drainage basin (Blair and Aller, 2012).

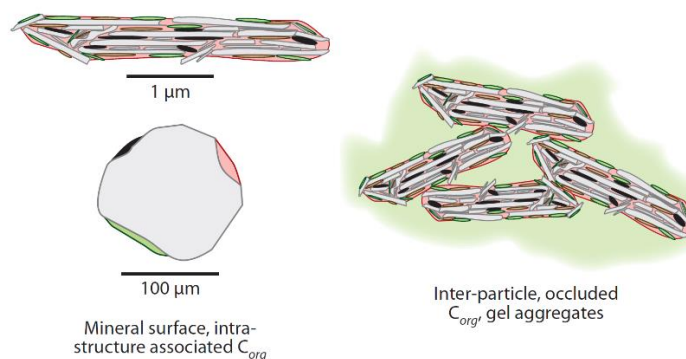


Figure 1-2 Distribution of C_{org} in and on river suspended sediment particles. C_{org} can be incorporated into pores and laminar structures of minerals but it can also be distributed onto particle surfaces. Colors indicate sources of C_{org} (green modern; aged brown, and sedimentary rock derived, black). Red colored patches are reactive oxides (e.g. Iron-oxides) that may be present (not relevant to this study), figure based on Blair and Aller (2012).

The amount and composition of POC in Arctic rivers is heavily influenced by the seasonality. The largest share of exported sediment is transported during the freshet and it comes to a large part from bank erosion (McClelland et al., 2016). The annual yield of POC in Arctic rivers (5.767 Mt) is estimated to be lower than the DOC yield (34.042 Mt, McClelland et al., 2016; Holmes et al., 2012).

DOC is regulated by hydrology and landscape composition (wetlands, permafrost, forests, etc.) and heavily influenced by seasonal forcing (Laudon et al., 2011). Up to 60 % of DOC in the five largest arctic rivers is exported after ice breakup in spring (Raymond et al., 2007). Increases in DOC, which are observed in many rivers of the northern hemisphere, are attributed to numerous drivers (Laudon et al., 2011; Clark et al., 2010). This includes changes to atmospheric chemistry, to precipitation and temperature, to land management or acid rich precipitation (Clark et al., 2010; Carpenter et al., 2011).

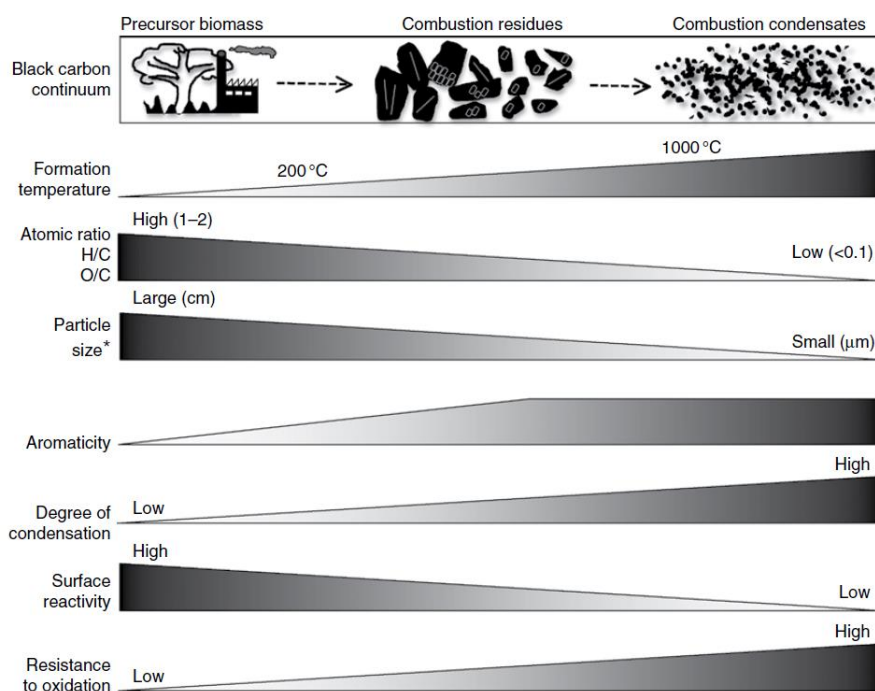
A certain fraction of organic carbon is present in the form of black carbon (BC), which is a variant of organic carbon produced during combustion. BC describes a continuum of

substances formed during pyrolysis. Pyrolysis happens during combustion of organic material under elevated temperatures and low to zero oxygen (Bird and Ascough, 2012, Bird et al., 2015, Scott et al., 2014). It is most often produced from biomass burning (i.e. wildfires) as well as fossil and bio fuels (Bird et al., 2015; Chatterjee et al., 2012; Preston and Schmidt, 2006; Hammes and Abiven, 2013). BC can be found everywhere in the environment, from the atmosphere to soils, to riverine as well as oceanic water and sediments (Bird et al., 2015; Hammes and Abiven, 2013).

Fires occur frequently and in almost all vegetated areas. Each year around 4 % of ice-free land biomes are on average burnt worldwide (Randerson et al., 2012), from which about 27 % of the burnt biomass is transformed into some form of BC (Santín et al., 2015). The main way for BC to enter rivers is through soils and overland flow. The estimated BC stock of soils is around 200 Pg of BC for the uppermost 2 m of soil (Reisser et al., 2016). However, the connection between fire history or climate and black carbon is not yet fully understood (Zimmerman and Mitra, 2017). Total riverine transport of particulate (PBC, $1 < d < 63 \mu\text{m}$) and dissolved (DBC, $d < 1 \mu\text{m}$) BC amounts to an estimated 17-37 Tg yr⁻¹, respectively 27 Tg yr⁻¹ (Coppola et al., 2018).

Since BC is regarded as a continuum (Figure 1-3 a), with a myriad of substances (Hammes and Abiven, 2013), its appearance and characteristics are complex and highly variable (Figure 1-3 b, Bird et al., 2015). The specific type of BC produced in a fire is predominantly moderated by the conditions during formation (Hammes and Abiven, 2013). Common to all forms of BC enclosed in the continuum are aromatic ring structures in varying sizes (Preston and Schmidt, 2006). Chemical functional groups, which are important for biological degradability and are indicated by large molar ratios of H/C and O/C, decrease with increasing thermal alteration (Figure 1-3 a, Preston and Schmidt, 2006). BC represents a slow cycling component of the carbon cycle and a potential sink for atmospheric CO₂ (Santín et al., 2015). Evaluating the fate of BC in river suspended sediment can thus give further insights into the role of rivers in the climate system.

(a)



(b)

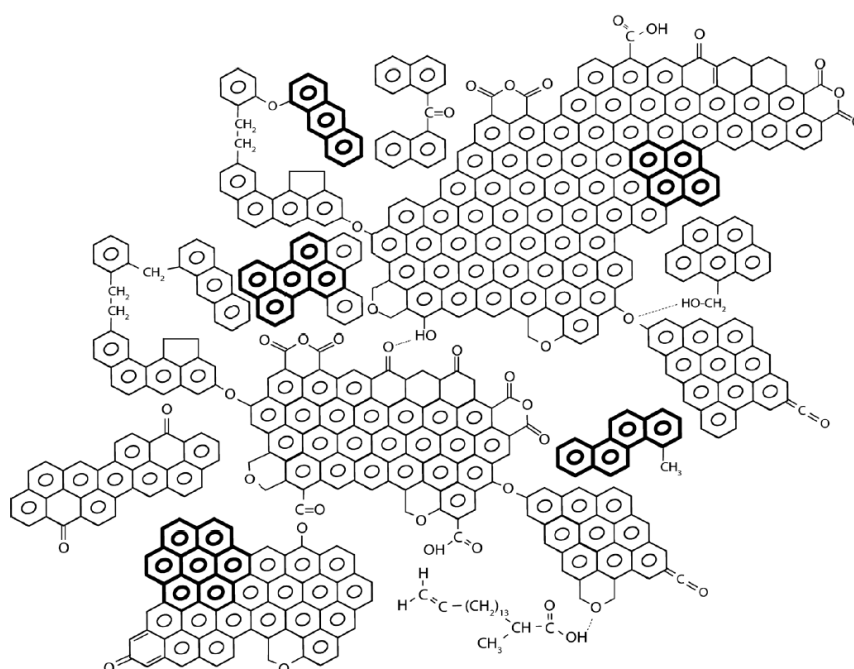


Figure 1-3 (a) The BC continuum as function of pyrolysis temperature. Aromatic ratios H/C and O/C decrease with increasing temperature, while particle size decreases from cm scale to μm scale. Aromaticity, degree of condensation as well as resistance to oxidation increases, while surface reactivity decreases. Particle size relation has exceptions, smoke for example can form under low temperature and contains extremely fine particles. (b) Example for a possible structural molecular representation of black carbon, from Ziolkowski et al. (2011). Highlighted in bold are benzene-polycarboxylic acids (BPCAs); for more details on BPCA please refer to the text (p. 22).

1.3 Motivation

Riverine biogeochemical processes as well as land-ocean coupling in the Arctic; and in the Mackenzie River system in particular; are important parts of the carbon cycle and the climate system. The main question underlying this work lies on the geochemical characteristics of different grain size fractions of sediment in the Mackenzie River system. First off it is important to assess the magnitude of the total flux of organic matter in the Mackenzie River system for 2017. Since organic matter was further analyzed for its BC content, this can be extended to the size of the BC flux in 2017. The amount of C_{org} and BC in different grain size fractions then becomes a main topic of interest. How do mineralogical and geochemical characteristics change with particle size? Are C_{org} and BC preferentially associated with certain grain size fractions? Are they associated with the same particles, or are they attracted to differently sized particles?

Furthermore, the grain size distribution in different rivers is of interest because certain grain size fractions might be more likely deposited in the delta than others. Which particles consequentially provide a sink and which a source for organic matter (C_{org} , BC)?

Based on the hydrodynamic properties, larger particles ($> 63 \mu\text{m}$) should be more prone to sediment out in the delta than smaller particles ($< 63 \mu\text{m}$). If in turn the amounts of C_{org} and BC found for these larger particles are not negligibly small, then this could provide a sink of organic matter important to the global climate.

Organic substances are attracted to and stabilized by particle surfaces, minerals, pores and aggregates (Blair and Aller, 2012). In consequence both C_{org} and BC should increase with an increase in surface area and mineral content, something that is usually associated with smaller particles (Walling et al., 2000).

This detailed look at the grain size distribution and its geochemical properties in suspended sediment will further our understanding of the fate of organic matter in this major river system. It will furthermore allow to look at black carbon dynamics by highlighting the amount and type of BC in suspended sediment of the most important tributaries of the Mackenzie River. The findings will contribute to better constrain the export of organic matter to the delta and ultimately to the Arctic Ocean. Thereby also refining the understanding of the Mackenzie River sediment transport and its consequences for the global climate by remineralization or burial of organic matter and black carbon.

1.4 Research Questions

The aforementioned questions can be grouped into two main research topics. The first set is concerned with differences in the geochemical characteristics between grain size fractions and between rivers:

- Do grain size fractions show differences in geochemical characteristics?
- Do observed differences exhibit a trend or relationship to grain size?
- How do differences between rivers and grain size fractions compare?

And the second set is motivated by the fluxes of C_{org} and BC for the year 2017:

- How large was the total flux?
- How large was the grain size specific flux?

The findings can be used to answer the question whether certain grain size fractions present a sink or a source of CO_2 and what this implies for the global carbon cycle and climate.

2 Study Setting and Riverine Sediment Transport

2.1 Study Setting

2.1.1 Mackenzie River Basin

The Mackenzie River basin spreads over British Columbia, Alberta, Saskatchewan, the Northwest Territories and eastern Yukon and comprises seven major rivers as well as three major lakes and three major deltas (Figure 2-1, Dumont et al., 1986). Since Great Slave Lake acts as a sediment trap, inputs from upstream rivers are not very important for the sediment budget (Vonk et al., 2015a). The Mackenzie River ultimately drains into the Beaufort Sea via the Mackenzie Delta (Figure 2-2), which is the most extensive and important delta in North America (Dumont et al., 1986).

In total the Mackenzie River system drains a watershed of 1.787×10^6 km² (Vonk et al., 2015a). According to Gareis and Lesack (2017) 62 % of the total suspended sediment export in the Mackenzie River is exported during the freshet (May to late June). The period from May to October furthermore accounts for about 99 % of the total sediment export (Carson et al., 1998). This illustrates that sampling timing is very important (Vonk et al., 2015a).

At the measurement station for the Mackenzie River in Tsiigehtchic, the total suspended sediment is estimated to be 96 Mt yr⁻¹ (Carson et al., 1998). This early estimate was recently updated by Gareis and Lesack (2017), who measured suspended sediment over four years (2007 – 2010), yielding an estimate of 51 Mt yr⁻¹. It is not clear why these estimates differ so much (Gareis and Lesack, 2017). At any rate, the rivers Mackenzie (at Tsiigehtchic), Arctic Red and Peel are also referred to as the delta-head rivers and they are the most important sediment contributors for the delta (Figure 2-2, Table 2-1).

Table 2-1 Fine sediment load for the delta-head rivers. Mackenzie River wash load (< 0.125 mm), Arctic Red and Peel Rivers suspended load, additionally added is the relative contribution of the respective load to the total found at Mackenzie / Inuvik, data from (a) Gareis and Lesack (2017) and (b) Carson et al. (1998).

Mackenzie / Tsiigehtchic	Arctic Red / Tsiigehtchic	Peel / Fort McPherson	Mackenzie / Inuvik
51 ^a – 96 ^b Mt	7.3 ^b Mt	20.8 ^b Mt	79.1 ^a - 124.1 ^b Mt
0.65 – 0.77	0.06 – 0.09	0.17 – 0.26	1.0

2.1.2 Carbon Export

Hilton et al. (2015) estimate a total particulate C_{org} flux of 2.2 (+ 1.3, - 0.9) Tg yr⁻¹ from the Mackenzie River. The most up-to-date estimate for POC from Mackenzie River is from McClelland et al. (2016) and is at 0.758 Tg yr⁻¹ ± 0.066 Tg yr⁻¹. Hilton et al. (2015) further suggest an efficient burial of C_{org} off-shore (65 % ± 27 %). Additionally, Vonk et al. (2015a)

also find an efficient burial of C_{org} on the shelf. 55 % of what arrives at the delta head is buried on the shelf (Vonk et al., 2015a). The export of organic material transfers C_{org} from a temporary and vulnerable sink (soils, permafrost) to a reservoir that is stable over geologic timescales, which might represent a long-term sink for CO_2 (Hilton et al., 2015). The DOC flux from the Mackenzie River is estimated at about 1.4 Mt yr^{-1} (Raymond et al., 2007; McClelland et al., 2016).

2.1.3 Geology and Climate

The drainage basin consists of three geologic units. The Precambrian Shield, the Interior Plains and the Western Cordillera (Figure 2-1). Only minor glacial and alluvial sediments cover the bedrock and the rivers and streams do not cut deep into the ground on the Precambrian Shield. The thin soils and the bedrock have low solubility and the vegetation is dominated by bogs and small trees. Permafrost thickness varies from 10 m at Lake Athabasca up to 90 – 375 m at Great Bear Lake (Dumont et al., 1986).

The Interior Plains follow west of the Precambrian Shield. The terrain is mostly flat and interspersed by ranges of smaller mountains and hills. The bedrock comprises a host of different rock formations, including sandstones, limestones and dolomites as well as alluvial and glacial deposits where rivers can cut several tens of meters into the surroundings (Dumont et al., 1986). But overall the erosion is limited by the low gradient and vegetation cover. Soils here are deep and can contain large quantities of water and ice. About 25 % to 75 % of the region is wetland and the vegetation ranges from grass and sedge dominated meadows, over forests comprising mostly the same trees as on the Precambrian Shield, to extensive wetlands (bogs, swamps, fens, Dumont et al., 1986). Permafrost thickness varies from 12 m at Fort Simpson over 60 m at Norman Wells, up to more than 800 m at the Mackenzie Delta (Dumont et al., 1986).

Lastly, the Western Cordillera lies to the west of the Interior Platform. The tectonically active mountain range (Vonk et al., 2015a) is between 2'000 to 2'500 m higher than the Mackenzie River and harbors amongst others the headwaters of the Liard, Arctic Red and Peel Rivers (Dumont et al., 1986). Here rivers cut deep into the bedrock and form mountain valleys. About 40 % – 70 % of the precipitation becomes runoff in this region, which is more than twice the amount found in the Precambrian Shield or the Interior Platform (Dumont et al., 1986). Rocks and soils in the Western Cordillera are well soluble and thus the runoff carries large sediment loads (Dumont et al., 1986). The subalpine and alpine vegetation zones provide habitat for black spruce and tamarack in wetter areas and balsam poplar and white spruce occur in the river valleys. When going northwards, trees are replaced by alpine tundra vegetation.

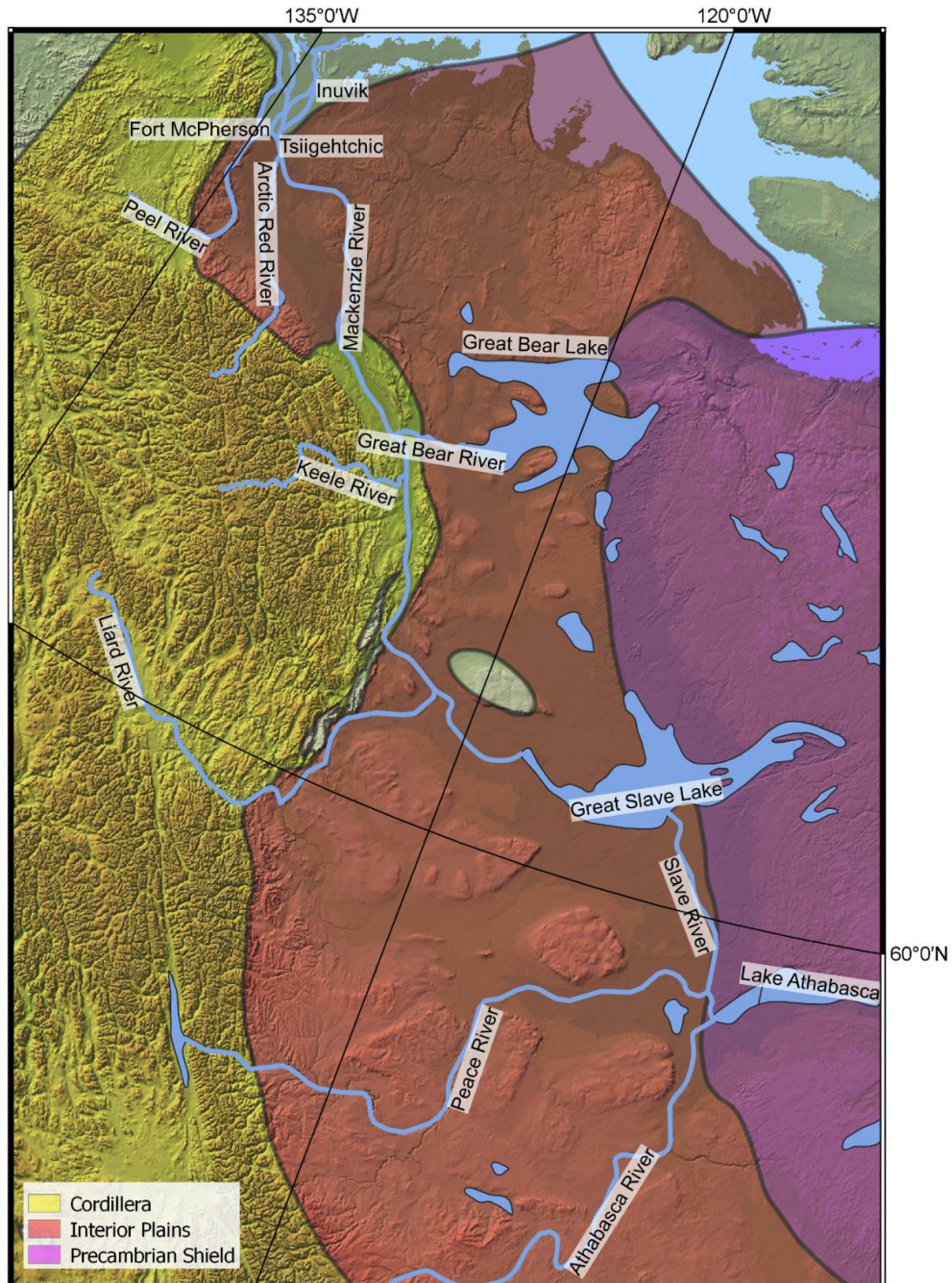


Figure 2-1 Map depicts Canada along 60 degrees latitude. Indicated are the large rivers and lakes of the Mackenzie River system, as well as the main physiographic regions. Map created using QGIS software (QGIS Development Team, 2019) and publicly available data from Natural Resources Canada (Natural Resources Canada, 2016) as well as with Natural Earth, free vector and raster map data @ naturalearthdata.com. Projection is Canada Lambert Conformal Conic (CLCC, EPSG:102002). Shaded relief based on NWT Centre for Geomatics (2015).

Annual Precipitation varies from 250 mm – 400 mm east of the Mackenzie River to 500 mm – 1'600 mm in the mountains west of the river. The winter lasts about 175 to 250 days depending on location and snow cover varies between 500 mm to 1'520 mm. Surface albedo varies from 10 % – 20 % in summer to 60 % – 70 % in winter.

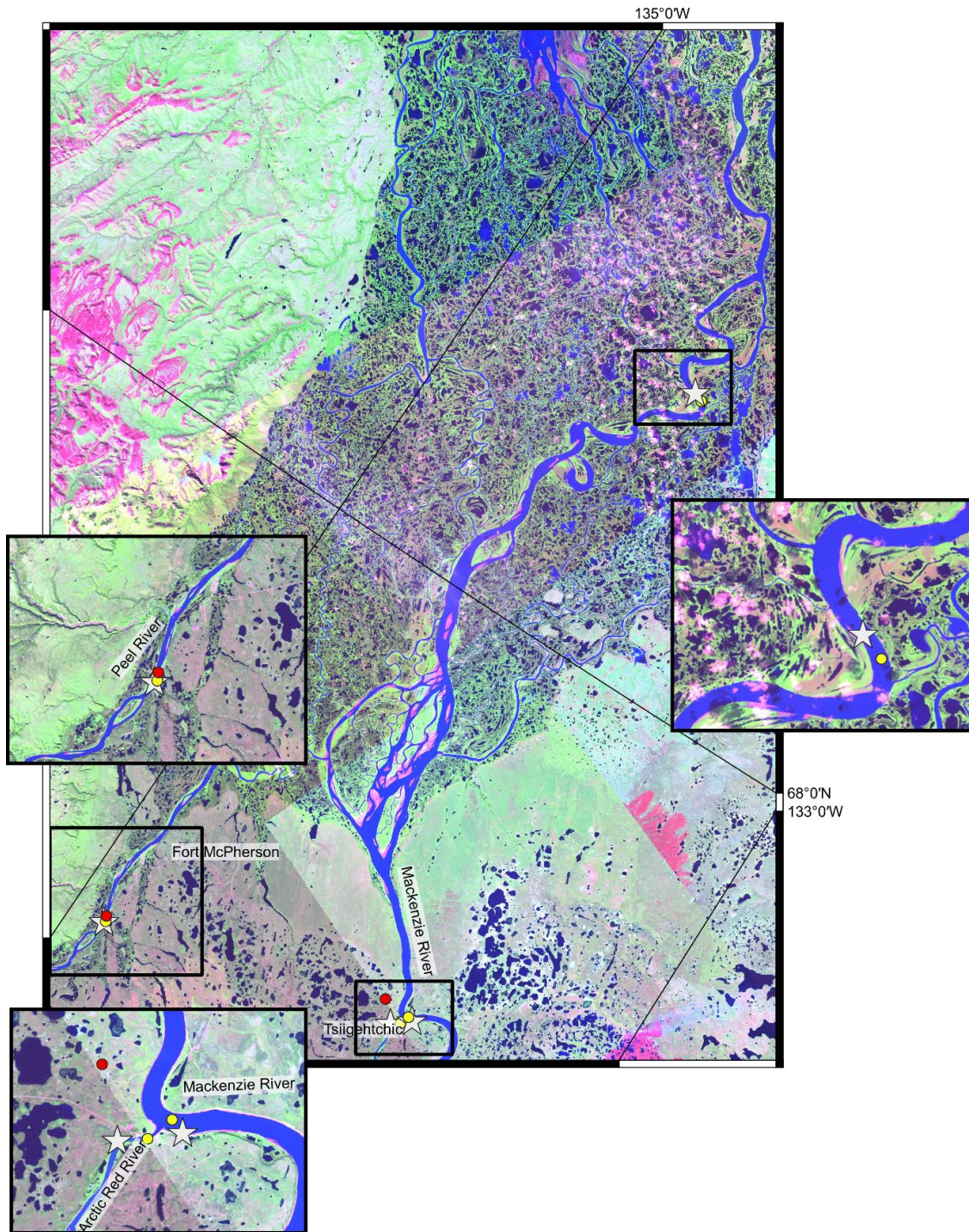


Figure 2-2 Satellite imagery (false color: thermal IR, green and blue) of the section of the Mackenzie Basin relevant to the study. Highlighted are the confluence of Arctic Red and Mackenzie River at Tsiigehtchic, the sampling location on the Peel River as well as on Mackenzie River at Inuvik. Star symbols indicate samples from 2017 analyzed in this thesis, whereas circles indicate samples from other authors (red = Vonk et al., 2015a, yellow = Hilton et al., 2015). Map created using QGIS (QGIS Development Team, 2019) and free satellite orthoimages (geo-referenced) from Natural Resources Canada (2016).

2.1.4 Fire History

With fires being a frequent and integral disturbance in the earth system, they are also affecting boreal forests to a large extent (Power, 2013; Flannigan et al., 2009; Scott et al., 2014). Each year around 100'000 km² – 150,000 km² of forests are burnt (Flannigan et

al., 2009) with about 20'000 km² in Canada (Stocks et al., 2003). With BC being primarily produced in fires, the Mackenzie River also exports large amounts. The Mackenzie River system is estimated to export 296 Gg yr⁻¹ of PBC, which makes it the third largest exporter of PBC globally (Coppola et al., 2018). BC as mass-% of total SOC in boreal soils is reported by Reisser et al. (2016) in a range from about 4 % up to about 7 % – 9 %. In combination with an expected increase in release of SOC from permafrost thaw in the Mackenzie region (Guo et al., 2007) with increased warming, a large amount of BC will also be susceptible to be released in the boreal regions. This will especially affect POC release (Guo et al., 2007). Overall large quantities of BC are produced and transported and there is a clear need to further our understanding of the BC cycle as a compartment of the global carbon cycle (Bird et al., 2015; Coppola et al., 2018).

2.2 Sediment

2.2.1 Transport and Erosion

Erosion of terrestrial land forms in combination with the production of organic matter is the main contributor to river sediment (Heininger and Cullmann, 2015). This sediment (mineral and organic material) is transported either in particulate (particle diameter > 0.1 µm – 1.0 µm) or in dissolved form (particle diameter < 0.1 – 1.0 µm, Table 2-2, Figure 2-3 a). Particulate sediment is divided into suspended sediment and bed load (Viers et al., 2009).

The bed load consists of larger grain size particles that move through the river in contact with the bed by saltation and rolling (Gilvear, 2016; Sly and Hart, 1989). The suspended sediment is further divided into suspended bed material, that is locally mobilized from the river bed, and wash load, that is fine material that has its origin further upstream (Figure 2-3 b) and rapidly moves through the channel (Gilvear, 2016; Sly and Hart, 1989). The differentiation between the two compartments (bed load and suspended load) is a function of the water velocity (Grotzinger and Jordan, 2010).

Kuhnle (2013) highlight that much more than 50 % of the total load a river carries is in the form of suspended load (total sediment load = bed load + suspended load, Sly and Hart, 1989). Generally, the larger the drainage basin, the higher the share of the suspended load is (Kuhnle, 2013).

Sediment is further divided into cohesive and non-cohesive sediment (Figure 2-3 a, Table 2-2). Cohesive sediment, with particles < 62 µm and non-cohesive sediment, starting with particles > 62 µm, are put into and held in suspension by different mechanisms. The behavior and transport of cohesive particles in a river is not yet well understood (Williams et al., 2008). Important to note is that silt sized particles (4 – 62 µm) are regarded as being both cohesive and non-cohesive, and that cohesion gradually becomes more important

towards the clay sized fraction, which is considered dominated by cohesive forces (Kuhnle, 2013).

(a)

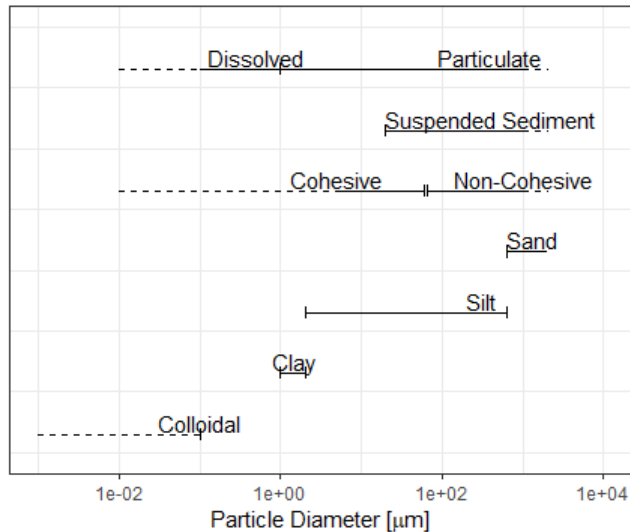


Table 2-2 Particle size classes and their respective particle diameter in μm , (Turnewitsch et al., 2007; Owens, 2008; Viers et al., 2009; Kuhnle, 2013)

Class	Particle diameter [μm]
Particulate	> 0.1 – 1.0
Dissolved	< 0.1 – 1.0
Suspended	> 0.20 – 0.45
Cohesive	< 62
Non-Cohesive	> 62
Sand	2'000 – 625
Silt	625 – 2.0
Clay	2.0 – 0.2

(b)

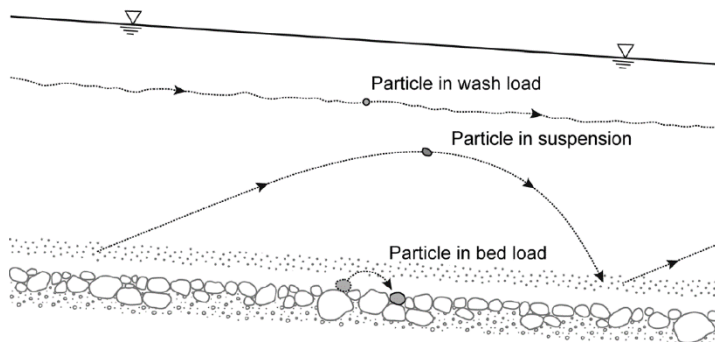


Figure 2-3 (a) different size classes used to describe sediment, (Table 2-2, note the logarithmic scale). (b) sketch of the particle transport in a river, including the common terminology used for the description of different particles transported in a river (Parsons et al., 2015)., please note the logarithmic scale.

The erodibility of the river bed surface is influenced by sediment properties such as the bulk density and water geochemistry, organic matter content and substances produced by sediment-dwelling organisms (e.g. bacteria) called extracellular polymeric substances (EPS, Grabowski et al., 2012). In consequence of the interplay between erosive (shear stress, turbulence) and resisting forces (gravity, friction), once the water reaches a critical flow velocity and erosive forces are higher than resisting forces, particles begin to move (Grabowski et al., 2011; Grabowski et al., 2012). First only by rolling, but with increased flow velocity also by saltation (Kuhnle, 2013). If the water velocity further increases, particles can be carried into the main body of the stream (Kuhnle, 2013). On its

way through the continuum, sediment therefore constantly undergoes transport, deposition and remobilization based on the balance between erosional and resisting forces (Koiter et al., 2013; Grabowski et al., 2012; Gilvear, 2016).

2.2.2 Effective Particle Size

Suspended fine sediments, especially those in the cohesive range (Droppo, 2001), are mostly transported as flocculated material, also called composite particles (Droppo, 2001; Woodward and Walling, 2007; Gilvear, 2016). The effective particle size is thus not found in the laboratory using traditional sampling and analysis methods, which chemically and physically alter and destroy flocs and aggregates (Gilvear, 2016). A floc can be orders of magnitude larger than the primary particles it is made up of (Woodward and Walling, 2007, Figure 2-4). Composite particles constitute a matrix of microbes, organic material such as EPS and cellular debris, inorganic particles such as clays and silts and a considerable pore volume (Droppo, 2001).

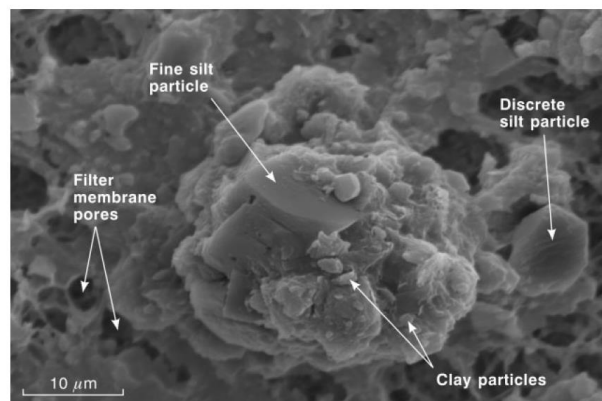


Figure 2-4 Image of a composite particle (Woodward and Walling, 2007).

2.2.3 Further Considerations

Elucidating the origin of sediment by analyzing key physical and chemical characteristics is called sediment source fingerprinting (Gilvear, 2016) and is a powerful tool for the further interpretation of sampled sediment. For this approach to be successful, it is important to know the processes and mechanisms that sediment undergoes from its source up until the measurement station (Koiter et al., 2013).

Overall it can be assumed that the longer the transit time of a sediment through a river is, the less it will resemble its source (Koiter et al., 2013). As a result Koiter et al. (2013) note that it might not be possible to determine the source of sediments in large river basins (which includes the Mackenzie River).

The differentiation between suspended and non-suspended sediment is ultimately not given by a clear boundary with physical differences (Parsons et al., 2015). Parsons et al. (2015) and (2018) found that suspended sediment does – on average – not move with the

velocity of the flowing water body and that suspended sediments are in a constant cycle of suspension and deposition.

It is thus important to keep in mind that the sediment taken from the suspended or bed load or from the river banks at a certain measurement station has experienced a myriad of saltation cycles. Consequently, the sampling locations in this thesis represent the average sediment exported by the selected rivers.

3 Methods

3.1 Sampling

The river bank and bedload samples used in this study were collected in 2017 by Melissa Schwab. The samples were collected in June, shortly after the freshet, from fresh deposits close to the channel. Table 3-1 gives an overview of the samples used in this study. In this thesis samples are often referred to by their working code (WC). The working code uniquely identifies a certain river and sampling station as well as a grain size fraction (Table 3-1). From the collected sediments (CAN17-XX) seven size fractions were filtered. Sieves of the sizes 250 μm , 150 μm and 63 μm were previously used by e.g. Hilton et al. (2015). The sieves of sizes 32 μm and 20 μm were used to get even smaller size fractions, approaching the dissolved pool.

Table 3-1 Sample overview. River bank and bedload material sampled in 2017 (Schwab, 2016). The first column (sample code) refers to the code used in other work. The second column (laboratory code) refers to the code attached for the present work in the laboratory and the third column (WC, working code) is a more convenient version for this specific text. MT refers to Tsiigehtchic / Mackenzie, AR to Tsiigehtchic / Arctic Red, PR to Fort McPherson / Peel and MD to Inuvik / Mackenzie, the number refers to the particle size, with 1 being associated with bulk and 8 with < 20 μm . GFR denotes the respective grain size fraction in [μm].

Sample Code	Lab. Code	WC	Lat.	Long.	Date	River	Location	Type	GFR
CAN17-31	186B18AC36	AR1	67.4308	133.7820	6/5/2017	Arctic Red	Tsiigehtchic	Bank	Bulk
—	186B18AC1	AR2	"	"	—	"	"	"	> 250
—	186B18AC2	AR3	"	"	—	"	"	"	150 - 250
—	186B18AC3	AR4	"	"	—	"	"	"	63 - 150
—	186B18AC4	AR5	"	"	—	"	"	"	< 63
—	186B18AC5	AR6	"	"	—	"	"	"	32 - 63
—	186B18AC6	AR7	"	"	—	"	"	"	20 - 32
—	186B18AC7	AR8	"	"	—	"	"	"	< 20
CAN17-24	186B18AC37	MT1	67.4503	133.7208	6/5/2017	Mackenzie	Tsiigehtchic	Bank	Bulk
—	186B18AC8	MT2	"	"	—	"	"	"	> 250
—	186B18AC9	MT3	"	"	—	"	"	"	150 - 250
—	186B18AC10	MT4	"	"	—	"	"	"	63 - 150
—	186B18AC11	MT5	"	"	—	"	"	"	< 63
—	186B18AC12	MT6	"	"	—	"	"	"	32 - 63
—	186B18AC13	MT7	"	"	—	"	"	"	20 - 32
—	186B18AC14	MT8	"	"	—	"	"	"	< 20

Table 3-2 Continuation of Table 3-1.

Sample Code	Lab. Code	WC	Lat.	Long.	Date	River	Location	Type	Fr
CAN17-11	186B18AC38	MD1	68.4136	134.1153	6/3/2017	Mackenzie	Delta	Bedload	Bulk
—	186B18AC15	MD2	"	"	—	"	"	"	> 250
—	186B18AC16	MD3	"	"	—	"	"	"	150 - 250
—	186B18AC17	MD4	"	"	—	"	"	"	63 - 150
—	186B18AC18	MD5	"	"	—	"	"	"	< 63
—	186B18AC19	MD6	"	"	—	"	"	"	32 - 63
—	186B18AC20	MD7	"	"	—	"	"	"	20 - 32
—	186B18AC21	MD8	"	"	—	"	"	"	< 20
CAN17-42	186B18AC39	PR1	67.3311	134.8642	6/7/2017	Peel	Fort McPherson	Bank	Bulk
—	186B18AC22	PR2	"	"	—	"	"	"	> 250
—	186B18AC23	PR3	"	"	—	"	"	"	150 - 250
—	186B18AC24	PR4	"	"	—	"	"	"	63 - 150
—	186B18AC25	PR5	"	"	—	"	"	"	< 63
—	186B18AC26	PR6	"	"	—	"	"	"	32 - 63
—	186B18AC27	PR7	"	"	—	"	"	"	20 - 32
—	186B18AC28	PR8	"	"	—	"	"	"	< 20

3.2 Mineral specific Surface Area

The Brunauer, Emmet and Teller (BET, Brunauer et al., 1938) method was used for the determination of the mineral-specific surface area (SA). Nitrogen vapour at very low temperatures (77.350 K) adsorbs onto the surface of the sample. This induces a change in the relative pressure (p/p_0 , where p the pressure and p_0 the saturation pressure) corresponding to the amount of gas adsorbed onto the sample surface (van Erp and Martens, 2011). For the cross-sectional area (σ_{N_2}) of nitrogen, 0.162 nm² were assumed, which is the present standard (van Erp and Martens, 2011; Lange et al., 2014). The adsorption isotherm for nitrogen is close to linear in the range $0.05 < p/p_0 < 0.35$. The relative pressure range from 0.048 to 0.3022 used here agrees with this linear range.

To remove organic components, 1 g of the freeze-dried samples were heated to 350 °C (12 h) and then transferred into pre-weighed sample cells. Organic matter was removed because its low surface area offsets the measured mineral specific SA. To determine the sample amount, the cells were again weighed. Finally, a glass rod was added to the sample cell. Before analyzing the samples, the sample cells were degassed using a Quantachrome Instruments FloVac degasser (Quantachrome Instruments, 2018a) at 350 °C for about 8 hours (or at 150 °C overnight). The sample cells were flushed with helium and removed from the degasser when the pressure reached a stable value (at around 2 Pa). The degassed cells were put onto the Quantachrome NOVA 4000e Surface Area Analyzer (Quantachrome Instruments, 2018b). The Quantachrome NovaWin software was used to

derive a 5-point BET measurement of relative pressure (p/p_0). The values of the correlation coefficient for all samples are $r > 0.9998$.

Mineral specific surface area (SA) is often used to normalize C_{org} , to indicate particle size or the amount of clay, or to differentiate supply and decomposition scenarios (Blair and Aller, 2012; Vonk et al., 2015a). The reported SA for the marine standard SRM 1941b (NIST, 2015) will be compared to the result for the same standard in the current samples. The difference between the two results will be used as an error estimate.

3.3 Homogenization

For all subsequently used techniques sample homogeneity was important. Thus roughly 6 g of each size fraction was milled for 2 minutes at 30 Hz using a horizontal Retsch Mixer Mill (MM 400, Retsch, 2018a) with two tungsten carbide balls.

3.4 Elemental Composition

Selected elements can give further insight into the cycling of substances, about the type and amount of minerals and about the processing of sediment. Aluminum is mainly associated with secondary minerals while silicon is associated with primary minerals (Viers et al., 2009). Furthermore the ratio between Al and Si (Al/Si) is often used to differentiate the environmental conditions and the processing of the sediment (Vonk et al., 2015a; Viers et al., 2009). Calcium on the other hand serves as a good proxy for carbonates present in a sample. All selected elements (Si, Al, Ca and Ti) are furthermore major elements in rocks and minerals, while Al, Si and Ti are only trace elements in river water (Gaillardet et al., 2014, Viers et al., 2009).

The elemental composition of the samples was determined using X-Ray Fluorescence (XRF). The method relies on the principle of interactions between X-rays and matter. The number of photons absorbed by an atom increases with the atomic number (Z). The measured beam of radiation leaving the sample is a function of the element distribution in the sample (Jenkins, 2012). The sensitivity of the XRF methods is generally in the ppm range (Jenkins, 2012). Jenkins (2012) notes that it is rather unlikely to receive error-prone results from an XRF device.

Five grams of milled sample were transferred into XRF cups and analyzed using an energy-dispersive XRF spectrometer (AMETEK Spectro) under helium gas flush. The lower atomic number limit for this device is $Z = 11$ (sodium). Each batch of 7 samples was run with an additional standard of known composition (chernozem soil standard, prepared in Spring 2018).

The uncertainty estimates ΔZ were derived using the standard deviation (Eq. III-1), where ΔZ is the uncertainty on the element with order Z , x are individual measurements

of the element Z in the reference soil matrix (chernozem), or of Z in replicates (if available).

$$\Delta Z = \sqrt{\sum_{i=1}^n \frac{(x_i - \bar{x})^2}{n-1}} \quad (III - 1)$$

The uncertainty ΔR (uncertainty propagation, Eq. III-2) for subsequent calculations based upon the elements with orders $Z_x \dots Z_y$ (e.g. ratio of Al/Si) were derived as follows.

$$\Delta R = \sqrt{\left(\frac{\Delta Z_x}{Z_x}\right)^2 + \left(\frac{\Delta Z_y}{Z_y}\right)^2} \quad (III - 2)$$

The measurements were affected by some problems with accuracy and reproducibility due to the use of powdered samples. A good estimate of the measurement error is very important. This issue was treated by a set of repeat measurements and can be found in the supplemental material (p. 78).

3.5 Diffuse Reflectance Infrared Fourier Transform

DRIFT (Diffuse Reflectance Infrared Fourier Transform) better referred to as diffuse reflectance (DR) spectrometry (Griffiths and Haseth, 2007) is a technique that allows to derive information about structure and composition of a sample on the molecular level (Chen et al., 2015). It is based on the absorption and excitation of polar molecular bonds by infrared radiation (IR, Vogel et al., 2008). Diffuse reflection means that radiation is scattered by reflection, refraction and diffraction upon interaction with a (powdered) sample (Griffiths and Haseth, 2007). A certain fraction of the incoming radiation will then reemerge from the sample, and due to scattering it is termed diffusely reflected radiance (Figure 3-1).

The infrared radiation produces molecular vibrations (such as stretching, bending and others, see Chen et al., 2015). A diatomic linear molecule for example has only a single way of vibration. Nonlinear molecules, however, can further vibrate in different ways (Griffiths and Haseth, 2007). The difference of energy between the non-excited or ground state and the first excited state corresponds (in most vibrational modes) to the emission of radiation in the mid-infrared (mid-IR) spectrum (400 – 4'000 cm^{-1} , Griffiths and Haseth, 2007). Thus, as noted in McKelvy (2000) the mid-IR is the most useful region for a general assessment of compounds. The far-infrared (10 – 400 cm^{-1}) is less often used but contains

information about inorganic compounds and hydrogen bonds (Griffiths and Haseth, 2007).

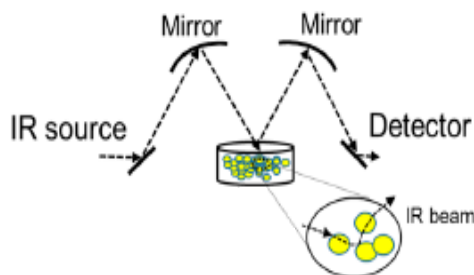


Figure 3-1 Schematic illustration of the methodology used in diffuse reflectance spectrometry, modified from Chen et al. (2015). IR denotes Infrared radiation. A source emits infrared radiation that is redirected by a mirror onto the sample, where it is scattered by the particles. Scattering can be due to reflection, refraction and diffraction. A sensor can finally measure the beam of IR that reemerges from the sample. Analysis of the signal yields information about molecules present in the sample.

The central unit used in DR-spectrometry is the so-called wavenumber ($\frac{1}{\lambda}$, in cm^{-1}) – the number of waves observed per cm (thus cm^{-1} , Che and Védérine, 2012). For quantitative purposes the spectra are reported in the dimensionless absorbance parameter (A, reported as absorbance unit, AU), since absorbance is proportional to concentration (Griffiths and Haseth, 2007; Stuart, 2004). Absorbance is defined as:

$$A = -\log\left(\frac{I}{I_0}\right) \quad (\text{III} - 3)$$

with I being the intensity of light transmitted and measured by the sensor. As an example at an absorption of 1.0, 90 % of the light is absorbed or only 10 % is transmitted ($-\log(x/100) = 1.0 \rightarrow x = 10$, see Stuart, 2004).

The observed spectral signal has regions which are often suggestive to chemical functional groups in a molecule (Chen et al., 2015). Consequently, there exist large tables that correlate spectral features with compounds and functional groups (e.g. LibreTexts, 2019; Sigma-Aldrich, 2019). Due to a relationship between absorbance and concentration, it is possible to do a quantitative analysis of spectral data (McKelvy, 2000). The amount of a specific functional group, determined by its spectral response and hence its vibrational band in the spectrum is given by the area between peak and baseline (Chen et al., 2015).

A quick overview of the sample can be gained by looking at the overall appearance of the spectrum and subsequently by looking at diagnostic wavenumber bands (Table 3-3). Testing for aromatic substances is conducted in a region with well-defined absorptions from $1'615 \text{ cm}^{-1} - 1'495 \text{ cm}^{-1}$ in combination with aromatic C-H stretching bands from $3'150 - 3'000 \text{ cm}^{-1}$ and some other indicative bands (Table 3-3, Coates, 2000).

In DR-spectrometry and for powdered, non-KBr diluted samples containing a large amount of unknown components, the previously introduced relation between absorbance and concentration is no longer clearly defined (Che and Védérine, 2012; McKelvy, 2000;

Griffiths and Haseth, 2007 and Stuart, 2004). A more advanced analysis is thus required. Partial least squares regression (PLSR) is the most common method (Stuart, 2004). PLSR allows to find spectral loadings that contribute to the observed concentrations. As Griffiths and Haseth (2007) note, PLSR is very robust and able to analyze complex mixtures. Furthermore, PLSR was already successfully tested on its potential to gain insight on black carbon (Bornemann et al., 2008) or other biogeochemical properties of sediments and soils (e.g. Vogel et al., 2008; Egli et al., 2015).

Table 3-3 Specific spectral bands for the determination of aromatic structures in a sample, from Coates (2000). Further the table shows bands of further importance (LibreTexts, 2019).

Wavenumber [cm ⁻¹]	Function
1'615 – 1'580	Aromatic ring stretch
1'510 – 1'450	Aromatic ring stretch
3'130 – 3'070	Aromatic C-H stretch
1'225 – 950 (several)	Aromatic C-H in-plane bend
900 – 670 (several)	Aromatic C-H out-of-plane bend (medium-to-strong absorptions, more than one)
2'000 – 1'660 (several)	Aromatic combination bands (simple aromatic compounds)
3'700	Alcohol (O-H stretching)
2'400	CO ₂ (O=C=O stretching)

The milled samples were placed in the sample holder cups and measured using a Bruker Tensor FTIR spectrometer (Bruker Tensor 27) from wavenumber 4'000 cm⁻¹ to 250 cm⁻¹ at a resolution of 6 cm⁻¹. The resulting spectra were water- and baseline corrected and smoothed using the device's software.

3.6 Black Carbon

For the determination of black carbon, the benzene polycarboxylic acid (BPCA) method was used (Wiedemeier et al., 2013). The method contains four steps (Figure 3-2 and Table 3-4) that allow to isolate marker compounds specific to fire-derived organic carbon.

Dry and homogenized samples (containing 1 – 10 mg of organic carbon) were digested based on an average C_{org} content of about 1 % – 3 % (based on POC values published in previous works, Hilton et al., 2015, Vonk et al., 2015a). About 800 mg were used for the sediment samples, 125 mg – 250 mg for the chernozem, about 20 mg for the chestnut wood-char, and about 200 mg for the marine sediment.

A pre-treatment using trifluoroacetic acid (TFA, C₂HF₃O₂) to remove polyvalent metals (Coppola et al., 2013; Brodowski et al., 2005) is required for sediment samples. This step

is omitted in the case of the chernozem soil standard (Schmidt et al., 1999; Wiedemeier et al., 2013) and chestnut wood standard (Hammes et al., 2006). It is omitted because Brodowski et al. (2005) found that pre-treating charred substances or soils with TFA can already produce BPCAs, which may result in an overestimation of BC content in the sample. The samples are placed in quartz tubes and 10 ml of 4 M TFA are carefully added.

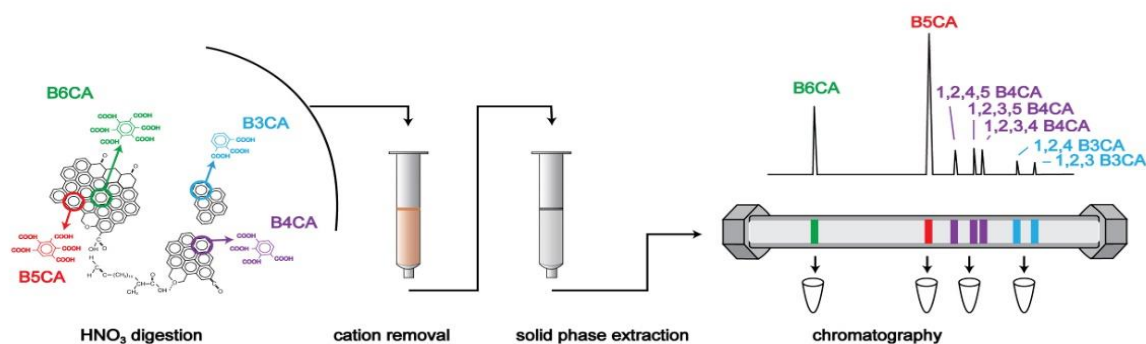


Figure 3-2 Sketch of the improved BPCA method with individual steps, (Wiedemeier et al., 2016).

The tubes are put into high pressure digestion chambers (Schramel et al., 1980) and put into a dry oven for 4 hours at 105 °C (see Brodowski et al., 2005). After recovery from the oven the samples are filtered using Chromabond glass fiber filters (< 0.7 µm) placed into glass syringes. Then the samples are dried overnight at 60 °C.

Table 3-4 Overview of the BPCA method steps and reference material. TFA stands for Trifluoroacetic acid, C/R denotes Cation Removal, SPE denotes Solid Phase Extraction (removal of apolar compounds).

Type	Reference	Pretreatment			Oxidation			C / R	SPE
		Time	Temp	Acid	Time	Temp	Acid		
Chernozem (30B00GW8)	Schmidt et al. (1999)	—	—	—	8 h	170 °C	HNO ₃	Yes	Yes
Chestnut (125B16MH23)	Hammes et al. (2006)	—	—	—	"	"	"	"	"
Marine (124B16MH4)	Hammes et al. (2007)	4 h	105 °C	TFA	"	"	"	"	"
Sample		"	"	"	"	"	"	"	"

The first step of the BPCA method is the nitric acid (HNO₃) digestion (Figure 3-2). The samples are again placed into quartz tubes and 2 ml of nitric acid are added. Samples previously treated with TFA are transferred from the glass syringes, carrying over the Chromabond glass fiber filter. The quartz tubes are then placed into the high pressure chambers and put into a drying oven at 170° for 8 hours (Wiedemeier et al., 2016). The quartz tubes are then recovered from the pressure chamber and the samples are filtered with Milli-Q water into 25 ml volumetric flasks using glass syringes, Chromabond filters and a vacuum chamber (Wiedemeier et al., 2016).

Once the samples are collected in the volumetric flasks, the cations need to be removed with a cation exchange resin (a synthetic resin with all sites being negatively charged to remove cations; Encyclopaedia Britannica, 2009). The conditioning involves rinsing it with 2 columns of water, 1 column of 2 M NaOH, again 3 columns of water, then 1 column of 2 M HCl and finally, 2 columns of water.

The quality of the resin is controlled by checking the conductivity of water collected after rinsing, it should be below 2 μ S. For standards, an aliquot of 10 ml is applied to the resin and subsequently rinsed five times with 10 ml ultrapure water. For samples, the whole 25 ml were applied to the resin, rinsed with 4 times 10 ml of ultrapure water. The solution is collected in 100 ml conical flasks and frozen at - 25 °C. Freezing with liquid nitrogen ("snap freezing") was omitted because of the higher nitric acid content posing a risk for the breaking of the conical flasks. The frozen samples were then freeze-dried at - 80 °C and 100 Pa (Christ, 2018).

The dry samples are then re-dissolved in 3 ml of a methanol / water (1:1, v:v) solution and applied to Supelco LC 18 SPE cartridges (Supelco, 1998). Here the sample solution is split into A and B for later reproducibility checks. Onto each SPE cartridge 1.5 ml of sample solution are added and rinsed with 1 ml of MeOH/H₂O solution (1:1, v:v) and collected in 2.5 ml test tubes. The test tubes are then dried in a vacuum concentrator for 4.5 hours at 45 °C and 500 Pa.

Finally, the dried samples are dissolved using 0.5 ml of ultrapure water and dissolution is supported using a shaker. This procedure is repeated once again, so that 1 ml of sample solution is produced. Now the samples are ready for chromatographic analysis and can be stored in a refrigerator for up to three months (Wiedemeier et al., 2016).

The chromatography was done using high pressure liquid chromatography (HPLC, Agilent technologies, Infinity). For solvent A 20 ml of 85 % orthophosphoric acid (H₃PO₄) were diluted in 980 ml of ultrapure water. The solution was filtered using a glass fiber filter under vacuum. The pH of this solution should be between 1.23 and 1.27. For solvent B pure HPLC grade acetonitrile was used (Wiedemeier et al., 2016).

Standard solutions, consisting of commercially available BPCAs were used to produce a standard series with known concentrations of BPCAs (5 μ g, 20 μ g, 60 μ g, 100 μ g, 150 μ g and 250 μ g of each BPCA dissolved in 1 ml of ultrapure water, see Wiedemeier et al., 2016). The BPCAs in the external standard series are: hemimellitic (B3CA), trimellitic (B3CA), pyromellitic (B4CA), pentacarboxylic (B5CA) and mellitic acid (B6CA, see also Figure 2-3 a).

The five BPCAs have distinct retention times and are thus quantitatively distinguishable (Figure 2-3 b). The area under the curve (of a certain peak) is representative of the concentration. Thus, extracting the correct retention time and the corresponding peak area yields the amount of a certain compound. In order to extract the correct peak from

the noisier chromatogram of a sample, the relative retention time can be used ($RRT = t_2/t_1$). It is a better measure than the absolute retention time (M. Hilf, personal communication, 2018). The exact retention time is not constant across multiple HPLC runs and is a function of the sample as well as the solvent and the age of the column, thus the absolute retention time of the sampled BPCAs is not exactly comparable to e.g. results found in other literature (such as Wiedemeier et al., 2013). The distribution of the different BPCAs indicates the degree of aromatic condensation of BC (Wiedemeier et al., 2016).

The BPCA method suffers from the disadvantage of underestimating the amount of BC in the sample because the actual overarching structure (Figure 1-3 for an example) of the condensed BC is lost during the breakdown into marker compounds (Wiedemeier et al., 2016). Several conversion factors from the measured amount of BPCAs to the actual BC have been proposed, ranging from 2.27 (Glaser et al., 1998) to 4.5 (Brodowski et al., 2005). Most recently the conversion factor was estimated at 4 ± 1 (Ziolkowski et al., 2011).

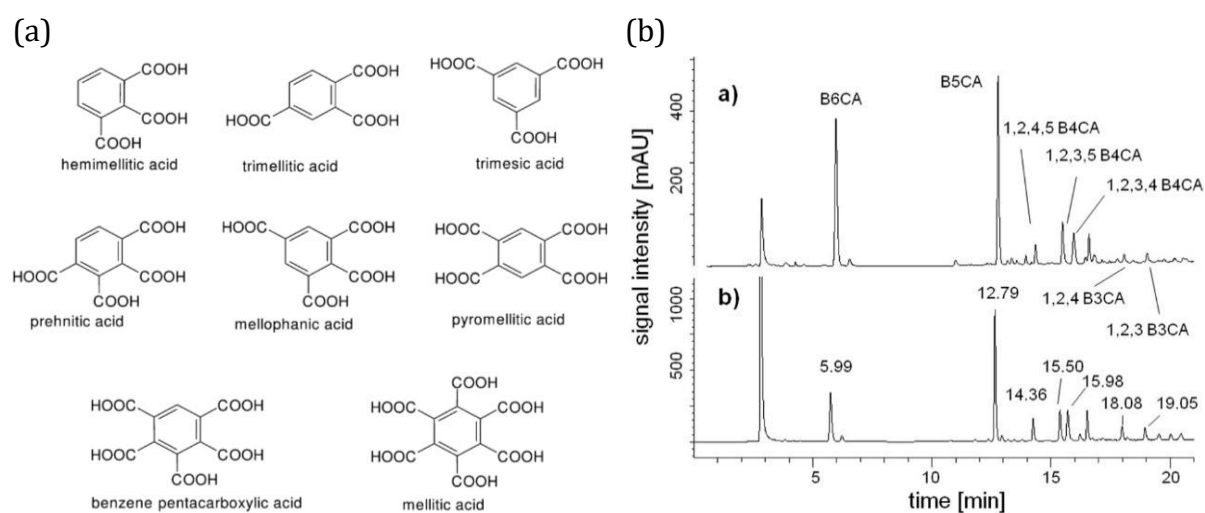


Figure 3-3 (a) Molecular structure of the marker compounds (benzene polycarboxylic acids, BPCAs) isolated in the BPCA method, figure adapted from Brodowski et al. (2005). (b) Illustrating the approximate retention time in the HPLC for BPCA marker compounds (Wiedemeier et al., 2013). In (b) The specific samples used were (a) a soil sample (chernozem) and (b) grass charcoal (*Oryza Sativa*).

3.7 Carbon and Stable Isotopes

3.7.1 Isotope Ratio Mass Spectrometry

For the determination of organic carbon and the stable organic carbon isotopes, about 15 mg – 20 mg of the milled and freeze-dried samples were weighed into analytical silver capsules (Säntis Analytical AG, 2019). The capsules were placed in a desiccator and fumigated with HCl at 60 °C for three days. NaOH pellets were added to remove residual acid. The capsules were then closed and measured using an elemental analyzer isotope ratio mass spectrometer (IRMS) at the Department of Earth Sciences of the ETH Zürich.

Isotopic signals are presented in the δ -notation, which is the ratio of the heavier isotope (H) to the lighter isotope (L, Table II-6) in a ratio between the sample and a standard (Eq. III-4).

$$\delta^{Mass}Element = \left[\frac{R_{sample}}{R_{standard}} - 1 \right] \times 1000 \text{ ‰} \quad (III - 4)$$

Isotopic differences express themselves in kinetic reactions, where the weight difference between the two isotopes is the driver when it comes to mixing and fractionation. The lighter isotope is usually faster in kinetic reactions. In chemical equilibrium reactions, the heavier isotope concentrates in the state with the higher bonding strength (Fry, 2006).

Different behavior in kinetic reactions arises due to the different mass of the two isotopes. Kinetic energy is defined as:

$$E_{kin} = kT = \frac{1}{2}mv^2 \quad (III - 5)$$

with k = Boltzmann constant, T = temperature, m = mass, v = velocity. Kinetic energy depends only on temperature (kT = constant) and thus heavier isotopes ($m_{heavy} > m_{light}$) are less mobile (Mook, 2001).

Table 3-5 Isotopes of carbon (C) and nitrogen (N) and their relative attribution to the total, from Fry (2006).

Element	Isotope Abundance			
		Light (L) %		Heavy (H) %
Carbon	12C	98.89	13C	1.11
Nitrogen	14N	99.64	15N	0.36

For some samples it was not possible to directly measure C_{org} by means of IRMS. In these cases, the amount of C_{org} was approximated by means of a partial least squares regression using data obtained by DR-spectrometry. A discussion of this procedure can be found in the supplements (p. 85).

3.7.2 Cavity Ring-Down Spectrometry

The total carbon stable isotopic signature ($\delta^{13}C_{tot}$) and carbon content (%) was determined with a PICARRO G2131-I Cavity Ring-Down Spectrometer (CRDS) concentration analyzer (PICARRO, 2017). In CRDS a single-frequency laser beam is inserted into a cylindrical chamber with three mirrors. These three mirrors continuously re-direct the laser

beam. The reflectivity of the PICARRO mirrors is 99.999 % and thus the laser beam gradually loses light intensity as soon as the incoming laser is shut off. This decay, also called ring-down is measured by a photodetector. This leads to up to 100'000 cycles and a path length of up to 20 kilometers (PICARRO, 2019). Using an empty cavity (no sample gas injected) the ring-down time is only dependent on the reflectivity of the mirrors, however once a sample gas is introduced, further intensity loss occurs and the ring-down time is shortened (Berden and Engeln, 2009).

CO₂ has a well-defined absorption spectrum in the near-infrared, which is used in CRDS to calculate the concentration of carbon. The strength of the absorption can be precisely measured with CRDS, which in turn relates directly to the concentration (PICARRO, 2019). Since the sample is burned and converted into CO₂, the measured amount of CO₂ corresponds directly to the carbon content in the sample. Furthermore, the precision of CRDS in combination with different but well-constrained absorption spectra of ¹²CO₂ and ¹³CO₂ allows to determine the isotopic signature δ¹³C.

For the measurement around 10 mg – 15 mg of the milled samples were weighed into analytical tin capsules (Säntis Analytical AG, 2019), which were then measured using a PICARRO G2131-i concentration analyzer (PICARRO, 2017).

3.8 Mixing Model and Export Fluxes

The transport behavior of particles can be studied with a mixing model (Eq. III-6). The measured contribution of a certain grain size fraction at Inuvik / Mackenzie should result from the input of the three main rivers (Mackenzie, Arctic Red, Peel). For this the fraction (f) of each river in the total sediment flux measured at Inuvik is used (Table 2-1). Where θ refers to the measured fraction of a certain grain size in a specific river, and x refers to a certain sampling site ($x_1 \dots x_4$, with x_1 = Tsiigehtchic / Mackenzie, x_2 = Tsiigehtchic / Arctic Red, x_3 = Fort McPherson / Peel, and x_4 = Inuvik / Mackenzie).

$$f_{x_1} * \theta_{x_1} + f_{x_2} * \theta_{x_2} + f_{x_3} * \theta_{x_3} = \theta_{x_4} \quad (III - 6)$$

The fluxes for the different grain size fractions are based on three assumptions. Firstly, the measured grain size composition represents a temporally averaged and representative distribution in the sampled rivers. Secondly, the averaged suspended sediment yield reported by others is representative both in time and space. Finally, suspended sediment, river bank sediment and bedload sediment are regarded as being identical. Based on this, a flux is calculated as follows:

$$Flux_{\theta} = TSS \times f \times \theta \quad (III - 7)$$

Where TSS denotes total suspended sediment in [Mt yr⁻¹] and f is the fraction of the total a certain size fraction is accounting for. θ represents a certain measure, here either C_{org} , relative to the sampled sediment [%], or BPCA-C in [g BPCA-C / kg sample].

4 Results

4.1 Mass Balance

The samples were size fractioned, and the results are thus represented as particle size ranges. And since the size fraction $< 63 \mu\text{m}$ was further sieved down, the results can be put into different size-classes (Table 4-1). This essentially means that “bulk” is an average of what is found in the sample (no sieving). Then what is called “first sieving” entails particles with diameters larger than $63 \mu\text{m}$ and what is called “second sieving” encompasses particles with diameters smaller than $63 \mu\text{m}$.

Table 4-1 Overview of the presentation scheme for the sampled results.

Size-Class	Particle size range
Bulk	Bulk sample, as mixture of all particle sizes
first sieving / larger particles	$> 250 \mu\text{m}$, $150 - 250 \mu\text{m}$, $63 - 150 \mu\text{m}$, $< 63 \mu\text{m}$
second sieving / smaller particles, pseudo-dissolved	$32 - 63 \mu\text{m}$, $20 - 32 \mu\text{m}$, $< 20 \mu\text{m}$

The rivers show different distributions in the larger particles (Figure 4-1, first sieving). The largest particles ($> 250 \mu\text{m}$) have the lowest share in all four sites. The second lowest contribution is found for the next smaller grain size fraction ($150 - 250 \mu\text{m}$). The Mackenzie River at Inuvik shows a lower value (5 %) than the incoming rivers (15 %, 11 %, 10 %, same order as presented in Figure 4-1).

The range of particles between 63 and $150 \mu\text{m}$ comes next in importance for the distribution, with 34 % in Tsiigehtchic / Mackenzie, 21 % in Arctic Red, 40 % in Peel, and 60 % in Inuvik / Mackenzie. Particles smaller than $63 \mu\text{m}$ account for 48 % and 62 % of the total mass in Tsiigehtchic / Mackenzie, respectively Tsiigehtchic / Arctic Red. Peel River shows a different distribution, with particles smaller than $63 \mu\text{m}$ only accounting for 21 % of the mass. Inuvik / Mackenzie shows the second lowest contribution of this grain size fraction (29 %).

When looking at the smaller particles, the distributions look more similar. Highest in all four rivers is the contribution of particles in the range of $32 - 63 \mu\text{m}$. It is at 59 % (relative to $< 63 \mu\text{m}$) for Tsiigehtchic / Mackenzie, at 41 % for Arctic Red River and at 53 % for Peel River. In Inuvik / Mackenzie this grain size fraction accounts for 48 % of the particles $< 63 \mu\text{m}$.

Particles below $< 20 \mu\text{m}$ are next in importance, with 22 % in Tsiigehtchic / Mackenzie, 31 % and 30 % in Arctic Red, respectively Peel River and 34 % in Inuvik / Mackenzie. This grain size fraction accounts for less mass in the delta with only a contribution of about 20 %.

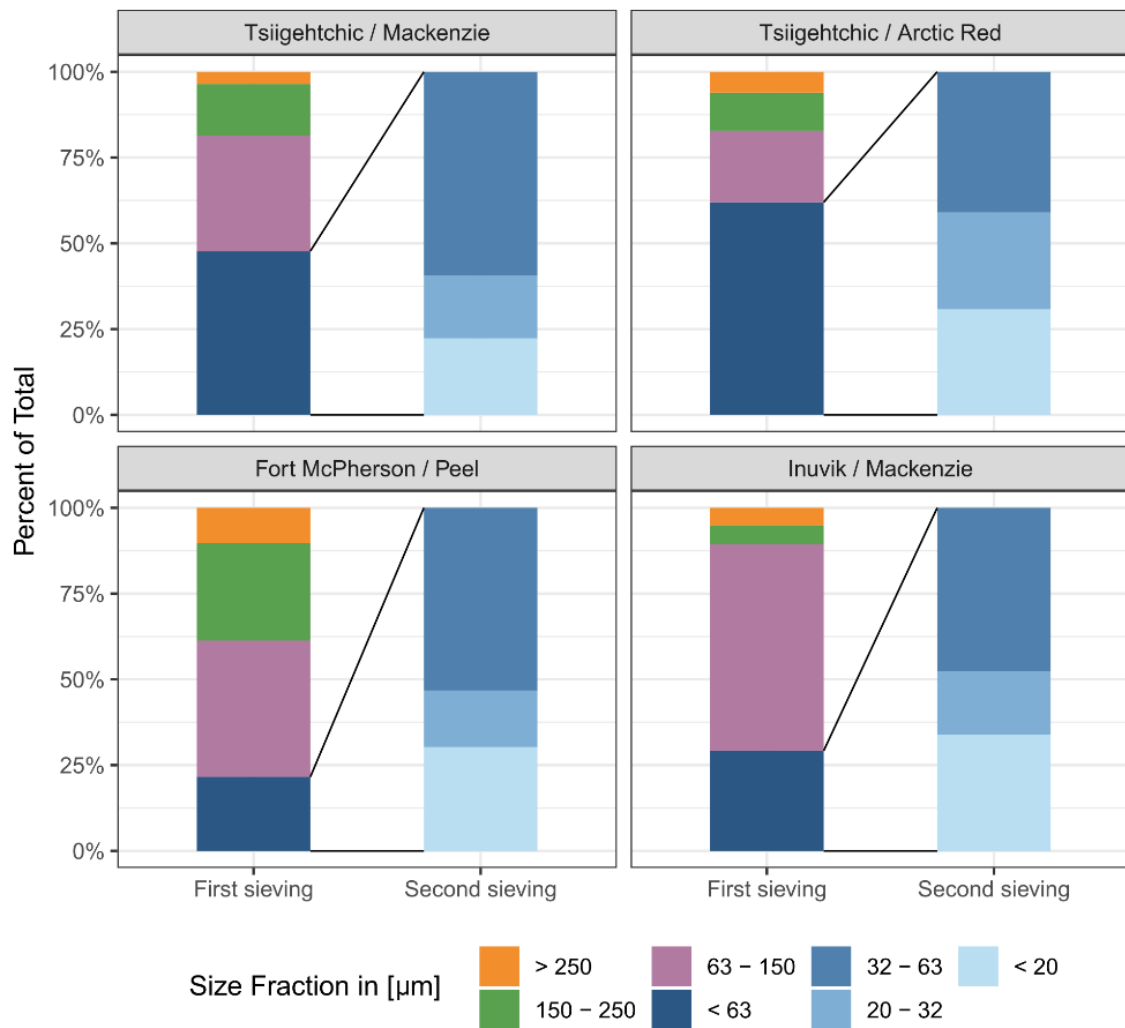


Figure 4-1 Mass balance for the four different sampling locations and rivers (Station / River). Particle sizes were determined by two consecutive rounds of sieving, more info in Table 4-1.

The mixing model is subsequently demonstrated based on sediment discharge data from Carson et al. (1998) and the 32 – 63 µm grain size fraction (Eq. IV-1). The theoretical 57 % contribution at Inuvik / Mackenzie is contrasted with a measured contribution of 48 % for the 32 – 63 µm grain size fraction.

$$0.77 * 59 \% + 0.06 * 41 \% + 0.17 * 53 \% = 57 \% \neq 48 \% \quad (IV - 1)$$

Overall intermediate sized particles (63 – 150 µm) as well as very small particles (< 20 µm) are enriched in the deltaic environment, whereas the other particles experience either little change (32 – 20 µm) or are being deposited (bulk, > 250 µm, < 63 µm, 32 – 63 µm, Table 4-2).

Table 4-2 Results of the simple mixing model, values in [%] of total or in [%] of the grain size fraction < 63 μm , where indicated with a star (*). Calculated using data from (a) Gareis and Lesack (2017) and (b) Carson et al. (1998) and equation III-6. The last column gives the measured contribution (m).

Grain Size Fraction	Inuvik / Mackenzie ^a	Inuvik / Mackenzie ^b	Inuvik / Mackenzie ^m
> 250 μm	6	5	5
150 – 250 μm	18	17	5
63 – 150 μm	34	34	60
< 63 μm	42	44	29
32 – 63 μm	56*	57*	48*
20 – 32 μm	19*	19*	18*
< 20 μm	25*	24*	34*

4.2 Elemental Composition

Aluminum (Figure 4-2, a) is higher in Tsiigehtcic / Arctic Red (average of 7.1 ± 0.4 %) and Fort McPherson / Peel (6.3 ± 0.4 %) compared to Mackenzie River. Mackenzie River at Tsiigehtcic shows lower values (average 5.3 ± 0.4 %) than at Inuvik (5.8 ± 0.4 %). Which is reasonable due to the input of sediment with higher Al content from Arctic Red and Peel Rivers (mixing model tested). Also noticeable is a lower Al content in > 250 μm (average $4.9\% \pm 0.4$ %) compared to < 20 μm (8.2 ± 0.4 %) in all four rivers. This trend is most pronounced in Mackenzie River, both at Tsiigehtcic and Inuvik. With Tsiigehtcic / Mackenzie increasing from 3.7 ± 0.4 % (> 250 μm) up to 8.2 ± 0.4 % (< 20 μm) and Inuvik / Mackenzie increasing from 3.8 ± 0.4 % up to 8.5 ± 0.4 %. As both the bulk as well as the < 63 μm size fraction are mixtures of the respectively smaller size fractions, it is obvious why they show values in the middle of the distribution.

Silicon content is generally high compared to the other elements, with values rarely below the range of 30 % – 40 %. The highest values are on average found in Peel River (40.3 ± 2.6 %), with Arctic Red (37.5 ± 2.6 %) and Tsiigehtcic / Mackenzie (36.6 ± 2.6 %) having lower values. Inuvik / Mackenzie has on average the smallest Si content (33.1 ± 2.6 %). The low values of Si in Inuvik / Mackenzie (bulk: 29.6 ± 3.3 %, > 250 μm : 22.6 ± 2.6 %, 150 – 250 μm : 28.5 ± 3.3 %) and in the bulk of Tsiigehtcic / Mackenzie (30 ± 7.0 %) might be affected by measurement problems. In contrast to aluminum, silicon does not show a trend or relationship between size fraction and content. The ratio of Al/Si (Figure 4-2, b) shows a trend for the correlation between Al/Si and particle size. Al/Si increases with decreasing particle size.

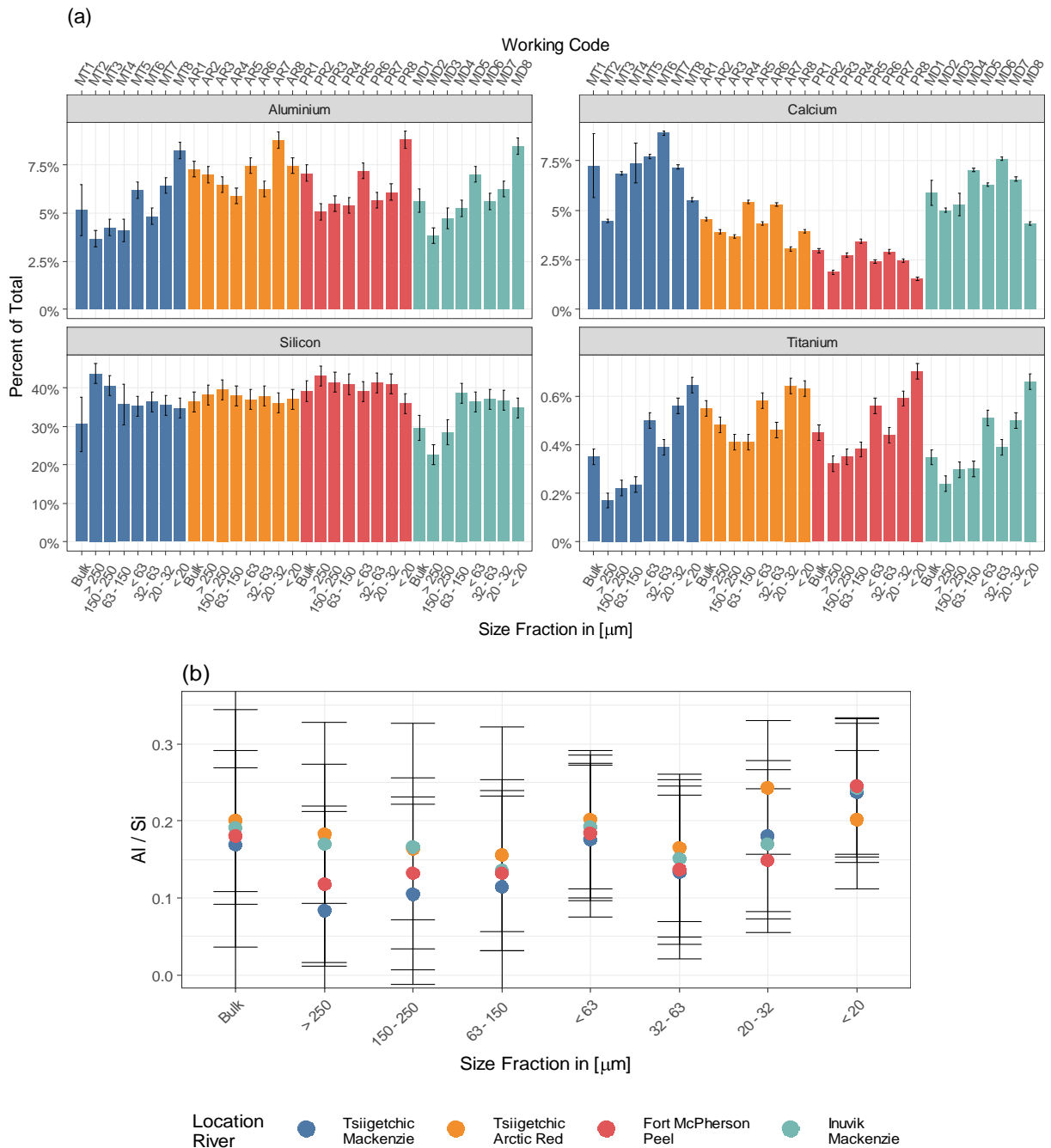


Figure 4-2 (a) Overview of selected elemental shares. Black bars indicate the error range for a specific measurement. The working code is a unique code identifying each sample. MT refers to Tsiigehtchic / Mackenzie, AR to Tsiigehtchic / Arctic Red, PR to Fort McPherson / Peel and MD to Inuvik / Mackenzie, the number refers to the particle size, with 1 being associated with bulk and 8 with $< 20 \mu\text{m}$ (more details in Table 3-1). (b) Particle size (grain size fraction) vs. Al/Si ratio.

Calcium is the lowest in Peel River (average of $2.5 \pm 0.1 \%$), followed by the Arctic Red River ($4.3 \pm 0.1 \%$). Tsiigehtchic / Mackenzie has on average $6.9 \pm 0.4 \%$ of Ca, spanning a range from $4.5 \pm 0.1 \%$ ($> 250 \mu\text{m}$) up to $8.9 \pm 0.1 \%$ ($32 - 63 \mu\text{m}$). Inuvik / Mackenzie has on average about $6 \pm 0.2 \%$ Ca, ranging from $4.3 \pm 0.1 \%$ ($< 20 \mu\text{m}$) up to $7.6 \pm 0.1 \%$ ($32 - 63 \mu\text{m}$). Then it decreases again towards the smallest size fractions.

The difference between Tsiigehtchic / Mackenzie and Inuvik / Mackenzie is attributable to a dilution with low-Ca water from Arctic Red and Peel Rivers. For the bulk, the mixing model suggests a Ca-content of 6.33 % for Inuvik / Mackenzie. Measured for the bulk is 5.9 ± 0.62 . Ca in Inuvik / Mackenzie is thus diluted by the lower Ca-containing sediment from Arctic Red and Peel Rivers.

$$0.77 * 7.2 + 0.06 * 4.6 + 0.17 * 3.0 = 6.33 \approx 5.9 \pm 0.62 \quad (IV - 2)$$

The only exception is the > 250 grain size fraction, where Ca is increased compared to the inputs (Figure 4-2).

Titanium is mainly associated with minerals (Viers et al., 2009; Bouchez et al., 2011). It is highest in Tsiigehtchic / Arctic Red (0.4 ± 0.03 %), followed by Fort McPherson / Peel (0.32 ± 0.03 %), Inuvik / Mackenzie (0.24 ± 0.03 %) and Tsiigehtchic / Mackenzie (0.17 ± 0.03 %). Ignoring the mixed samples (bulk and $< 63 \mu\text{m}$) shows a clear trend from large particles with lower Ti ($> 250 \mu\text{m}$ average of 0.17 ± 0.03 %) to small particles with higher Ti ($< 20 \mu\text{m}$ 0.63 ± 0.03 %).

4.3 Surface Area

The measurement conducted here for the marine standard (SRM 1941b, NIST, 2015), resulted in $27.9 \text{ m}^2/\text{g}$. Hammes et al. (2007) measured $28.6 \text{ m}^2/\text{g}$. The difference of $0.7 \text{ m}^2/\text{g}$ or about 2.5 % is used as an estimate for the measurement uncertainty.

Tsiigehtchic / Arctic Red has on average the highest value of SA ($10.6 \pm 0.7 \text{ m}^2/\text{g}$), followed by Fort McPherson / Peel ($8.1 \pm 0.7 \text{ m}^2/\text{g}$), Inuvik / Mackenzie ($6.6 \pm 0.7 \text{ m}^2/\text{g}$) and Tsiigehtchic / Mackenzie ($3.9 \pm 0.7 \text{ m}^2/\text{g}$, Figure 4-3).

When leaving the bulk and the $< 63 \mu\text{m}$ aside, as they represent mixtures of the other grain size fractions, a clear increase of SA from larger to smaller particles is found in Tsiigehtchic / Mackenzie. This trend is not as well pronounced in the other rivers. A certain increase in surface area can further be noted for smaller size fractions, where especially the size fraction $< 20 \mu\text{m}$ shows high values of up to $23 \pm 0.7 \text{ m}^2/\text{g}$.

Surface area is significantly correlated with Al content, which in turn is a proxy for clay mineral content ($R^2 = 0.83$, highly significant, $p = 3.5 * 10^{-13}$, Figure 4-4).



Figure 4-3 Mineral specific surface area for the 2017 samples (BET method, see methods, p. 18). Colors indicate different measurement sites. The working code is a unique code identifying each sample. MT refers to Tsiigetchic / Mackenzie, AR to Tsiigetchic / Arctic Red, PR to Fort McPherson / Peel and MD to Inuvik / Mackenzie, the number refers to the particle size, with 1 being associated with bulk and 8 with < 20 μm (more details in Table 3-1).

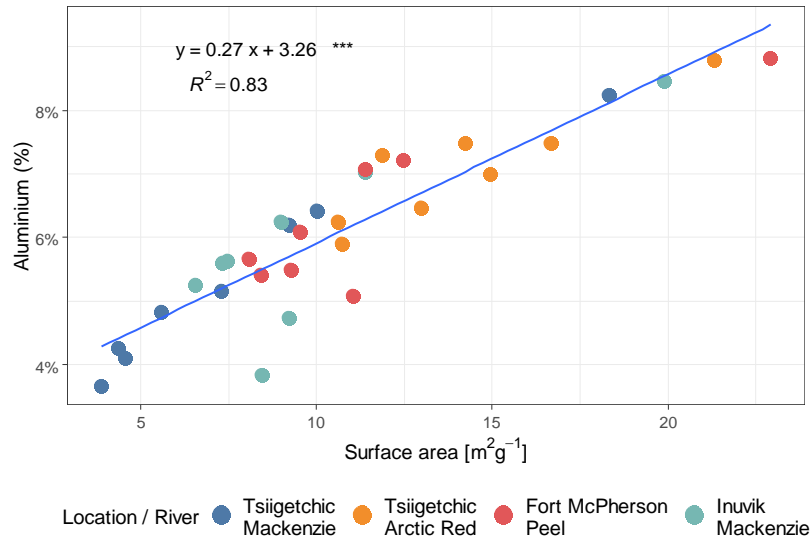


Figure 4-4 Relationship between aluminum and surface area. Linear regression significance levels (* 0.05, ** 0.01, *** 0.001) and R^2 . Colors indicate the different measurement sites (Location / River). Aluminum was determined using XRF (p. 19), mineral specific surface area was determined using BET (p. 18).

4.4 Carbon Content

4.4.1 Total Carbon

The total carbon amount (Figure 4-5) can be used as a proxy for carbonate content and to constrain the C_{org} measurement and predictions. Carbon is lowest in Fort McPherson / Peel (average 2.1 % C) and highest in Inuvik / Mackenzie (4.8 %). Tsiigehtchic / Mackenzie with an average of 3.5 % and Tsiigehtchic / Arctic Red (3.3 %) fall in between. Inuvik / Mackenzie being a good portion higher (1.3 %) than Tsiigehtchic / Mackenzie means that the two other rivers contribute to the total C found in the samples at Inuvik. Two large values of carbon are present in the Inuvik / Mackenzie larger size fractions (> 250 μm and 150 – 250 μm). Here the carbon content is 10.3 % respectively 6.9 %. These two values contrast with other samples.

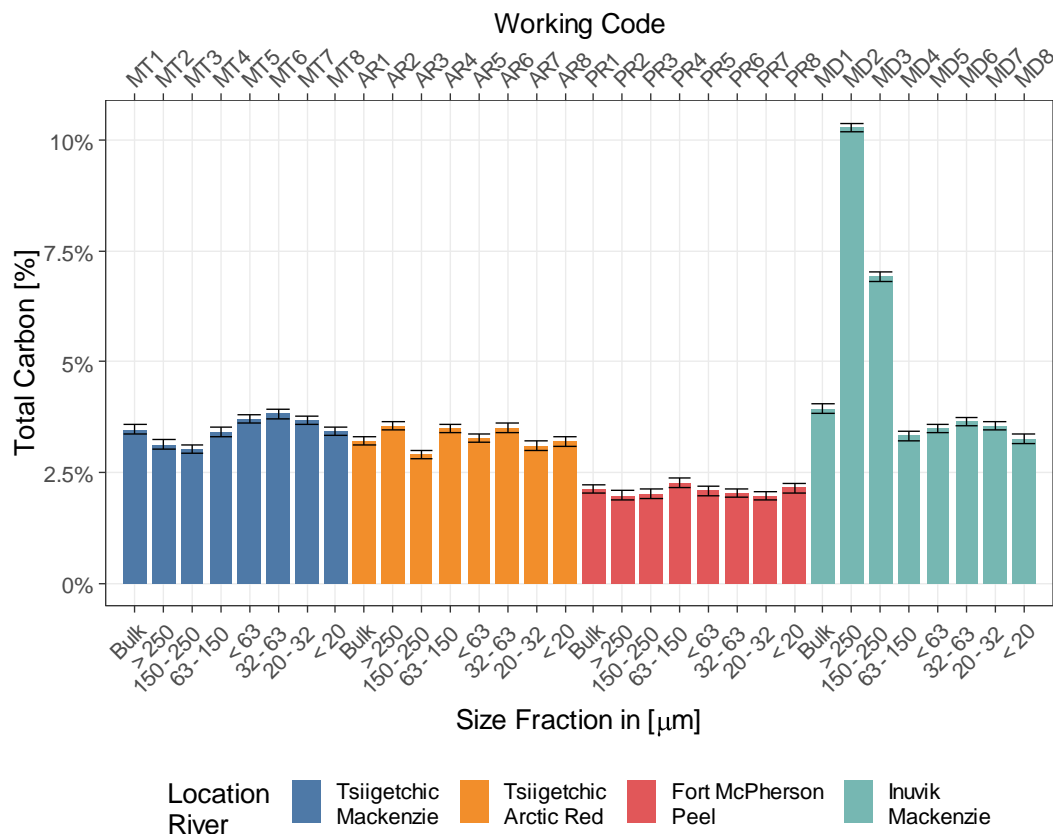


Figure 4-5 Amount of total carbon (% C). Colors indicate different measurement sites. The working code is a unique code identifying each sample. MT refers to Tsiigehtchic / Mackenzie, AR to Tsiigehtchic / Arctic Red, PR to Fort McPherson / Peel and MD to Inuvik / Mackenzie, the number refers to the particle size, with 1 being associated with bulk and 8 with < 20 μm (more details in Table 3-1).

The influence of carbonates on the total carbon content can be estimated by looking at the Ca content in the samples (Figure 4-6). The correlation between total carbon and calcium is low (Pearson's $r = 0.35$, Figure 4-6 a) when using the full dataset, but high when

ignoring the two extreme values (Pearson's $r = 0.83$, Figure 4-6 b) found for Inuvik / Mackenzie grain size fractions $> 250 \mu\text{m}$ and $150 - 250 \mu\text{m}$. The significance of the relationship could not be assessed since regression conditions were not met (auto-correlation).

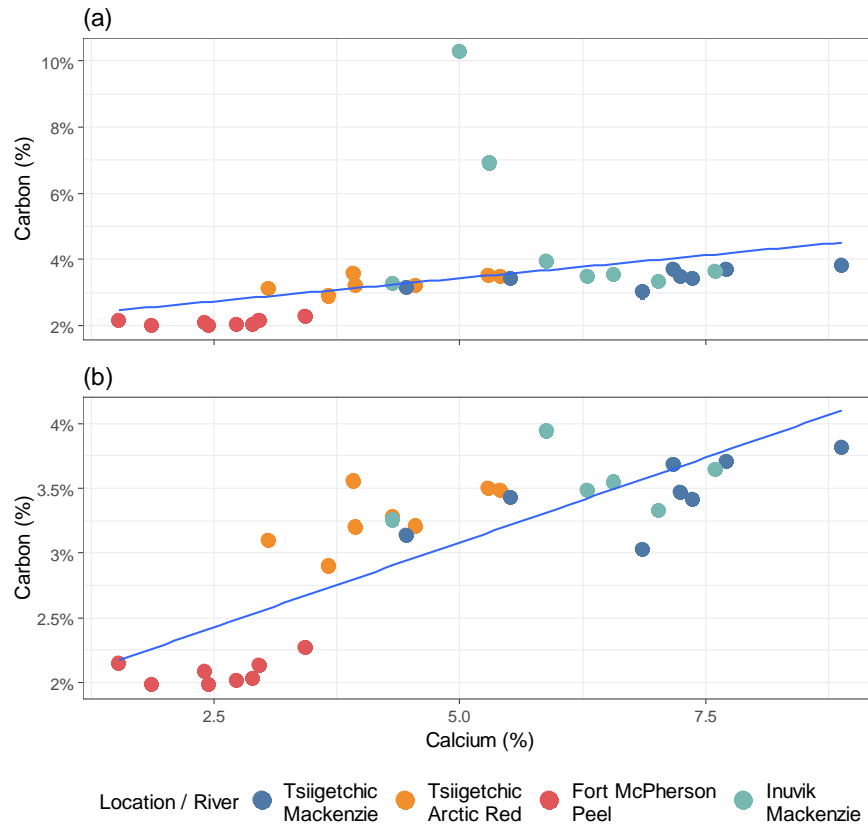


Figure 4-6 Relationship between calcium and carbon. The upper panel (a) includes the extreme values found in Inuvik / Mackenzie (Pearson's $r = 0.35$), while the lower panel (b) ignores these two (Pearson's $r = 0.83$).

4.4.2 Organic Carbon

Using total carbon as a constraint for C_{org} (Figure 4-7) shows that no single value can be regarded as unrealistic. This is clear because no value shows higher organic carbon than total carbon.

C_{org} in the samples ranges from as low as 0.4 % for the $32 - 63 \mu\text{m}$ particles of Fort McPherson / Peel up to more than 6 % for the $>250 \mu\text{m}$ particles in Inuvik / Mackenzie (Figure 4-7). More variation is found for C_{org} than for total carbon. On average Fort McPherson / Peel and Tsiigetichic / Mackenzie have the lowest C_{org} content (0.9 %). The highest value of C_{org} (on average) is in Inuvik / Mackenzie (2.2 %) followed by Tsiigetichic / Arctic Red (1.6 %). On average the size fraction $> 250 \mu\text{m}$ has the highest C_{org} content (2.9 %) followed by the $150 - 250 \mu\text{m}$ size fraction (1.9 %). This can be explained with plant residues (roots, leaves, etc.). The two smallest size fractions come next in average C_{org} content. Particles between $20 - 32 \mu\text{m}$ have on average 1.1 % of C_{org} and particles $< 20 \mu\text{m}$ have about 1.6 %. This indicates that C_{org} is associated with larger fragments of

biomass (as in bulk and the larger size fractions) and is again increasing towards the very small particles.



Figure 4-7 Organic carbon (C_{org}) in the samples. Colors indicate different measurement sites. The Working code is a unique code identifying each sample. MT refers to Tsiigehtchic / Mackenzie, AR to Tsiigehtchic / Arctic Red, PR to Fort McPherson / Peel and MD to Inuvik / Mackenzie, the number refers to the particle size, with 1 being associated with bulk and 8 with $< 20 \mu\text{m}$ (more details in Table 3-1).

4.4.3 Black Carbon

Evaluating BPCA based on sample mass (Figure 4-8, a) yields on average the lowest amount for Tsiigehtchic / Mackenzie (0.56 ± 0.14 g BPCA-C /kg sample), followed by Fort McPherson / Peel (0.93 ± 0.14 g BPCA-C /kg sample) and Inuvik / Mackenzie (0.99 ± 0.14 g BPCA-C /kg sample). Arctic Red River has the highest amount of BPCA per kilogram of sample (1.26 ± 0.14 g BPCA-C /kg sample). The two peaks in the larger particles of Inuvik / Mackenzie ($>250 \mu\text{m}$ and $150 - 250 \mu\text{m}$) are also present for total carbon (Figure 4-5) and organic carbon (Figure 4-7).

Comparing the individual measurements across the different particle sizes (Figure 4-8, b) illustrates that the sites show some distinct features. For instance, Tsiigehtchic / Arctic Red and Fort McPherson / Peel follow a similar pattern with Arctic Red having just slightly higher values (except for $< 20 \mu\text{m}$, where they are the same). Furthermore, a clear (although small) difference between the Mackenzie River and both Arctic Red and Peel Rivers is evident. Overall no clear relationship or trend can be found between particle size and BPCA. However, looking only at the smallest particles ($32 - 63 \mu\text{m}$, $20 - 32 \mu\text{m}$ and $< 20 \mu\text{m}$) shows an increase of BPCA with decreasing particle size.

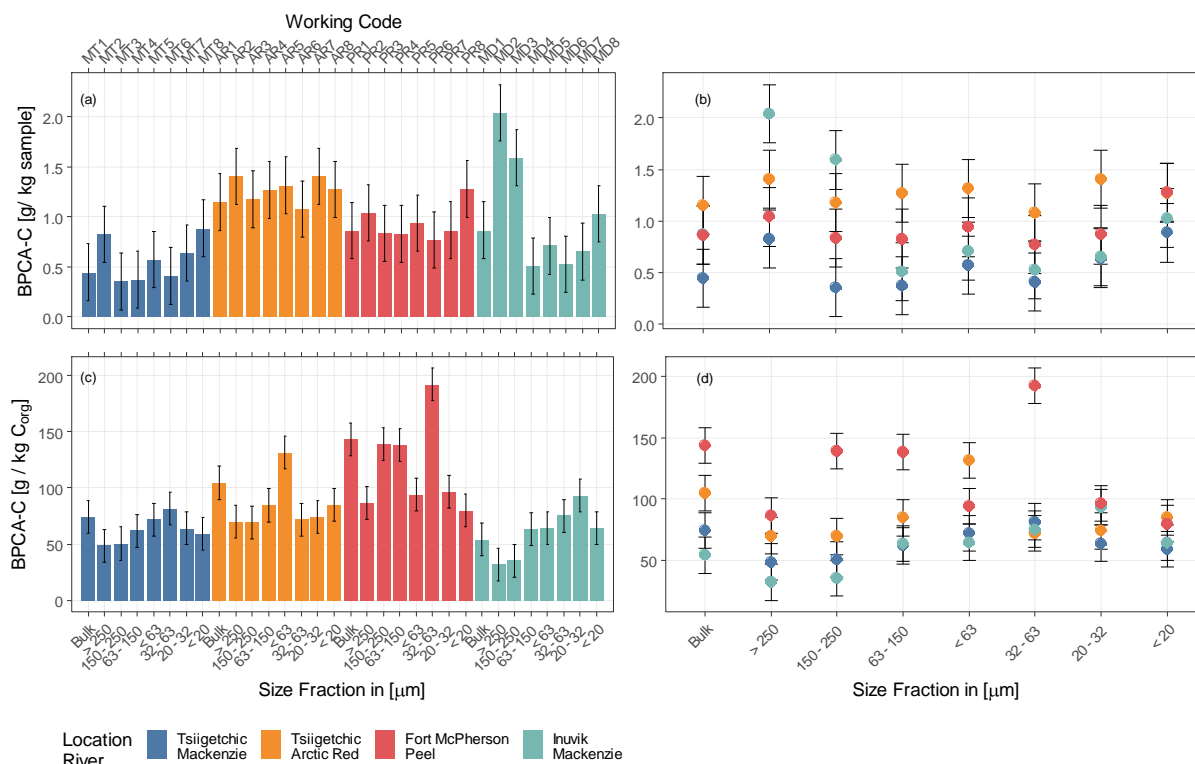


Figure 4-8 Compilation of the measured BPCA in the samples. (a) Overview by location, giving all size fractions individually, BC in [g BPCA-C / kg sample] is independent of the amount of C_{org} . (b) Overview by particle size, location indicated by the same colors as in (a), same units as (a). (c) same as (a) but BC reported in [g BPCA-C / kg C_{org}]. (d) same as (b) but in units of (c). The working code is a unique code identifying each sample. MT refers to Tsiigehtchic / Mackenzie, AR to Tsiigehtchic / Arctic Red, PR to Fort McPherson / Peel and MD to Inuvik / Mackenzie, the number refers to the particle size, with 1 being associated with bulk and 8 with $< 20 \mu\text{m}$ (more details in Table 3-1).

Normalizing the measured BPCA values to the amount of organic carbon found in the samples changes the situation (Figure 4-8, c). Here the lowest average values are in Inuvik / Mackenzie (60 ± 14 g BPCA-C /kg C_{org}) and Tsiigehtchic / Mackenzie (64 ± 14 g BPCA-C /kg C_{org}). Arctic Red River follows next with about 86 ± 14 g BPCA-C /kg C_{org} . The most amount of BC is present in samples from Peel River (121 ± 14 g BPCA-C /kg C_{org}). Both the Arctic Red and Peel Rivers have on average higher values than the Mackenzie River. Thus, it is surprising to find the lowest overall value of BC in the Mackenzie River at Inuvik.

Again, the two rivers Arctic Red and Peel show different values in the size fractions (Figure 4-8, d), however the pattern is not the same as for the non-normalized values. For the Mackenzie River (Tsiigehtchic and Inuvik) an increase of BC from $48 (\pm 14)$ g BPCA-C /kg C_{org} , respectively $32 (\pm 14)$ g BPCA-C/kg C_{org} , at $> 250 \mu\text{m}$, to about $81 (\pm 14)$ g BPCA-C /kg C_{org} , respectively 75 , at $32 - 63 \mu\text{m}$ is visible. Then Inuvik / Mackenzie further increases to $93 (\pm 14)$ g BPCA-C /kg C_{org} and subsequently decreases drastically to $64 (\pm 14)$ g BPCA-C /kg C_{org} . Mackenzie decreases directly after $20 - 32 \mu\text{m}$. The variability of BPCA per particle size narrows down from large particles to the smallest, with especially $20 - 32 \mu\text{m}$ and $< 20 \mu\text{m}$ exhibiting little variation.

As with C_{org} , BC may be primarily associated with particle surfaces and mineral aggregations, thus assessing the relationship between SA and BC is important (Figure 4-9). When ignoring the outliers found in the samples from Inuvik / Mackenzie (as done earlier for total carbon) there is a strong correlation (Pearson's $r = 0.75$) between SA and BC on the level of [g BPCA-C / kg sample] (Figure 4-9 a). The correlation is low when looking at BC as a portion of C [g BPCA-C / kg C_{org}] (Pearson's $r = 0.04$, Figure 4-9 b).

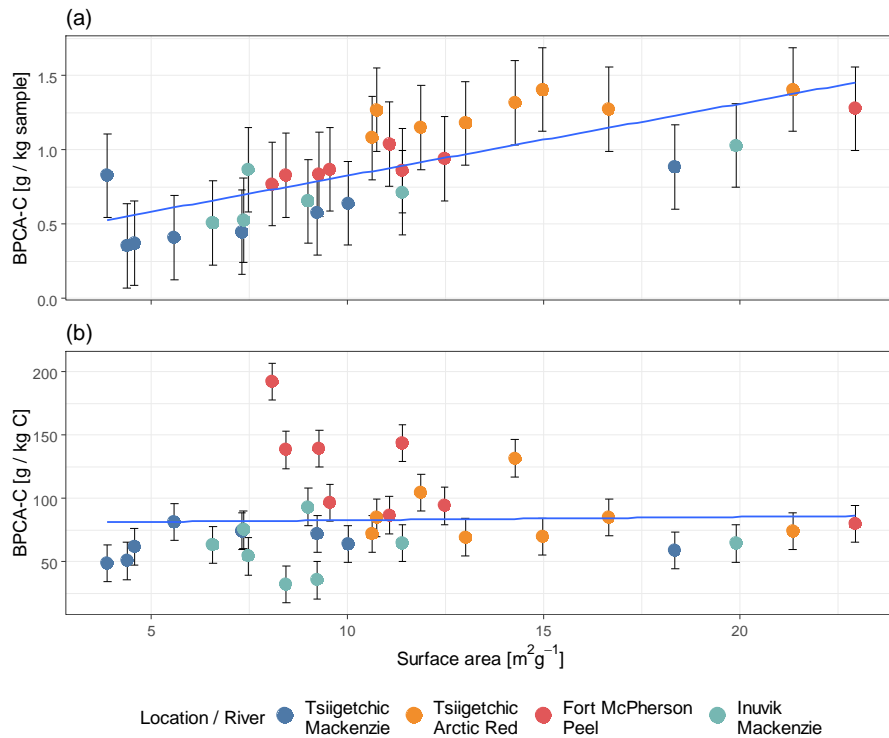


Figure 4-9 Mineral specific surface area vs. BPCA-C. (a) C_{org} independent measurement in [g BPCA-C / kg sample], (b) BPCA-C as portion of C_{org} in [g BPCA-C / kg C]. Linear regression significance levels (* 0.05, ** 0.01, *** 0.001) and R^2 . Colors indicate the different measurement sites (Location / River). BPCA-C determined using the method introduced by Wiedemeier et al. (2013) (p.22), mineral specific surface area was determined using BET (p. 18).

The distribution of the different BPCAs (B3CA, B4CA, B5CA, B6CA) gives an indication of the quality, structure and polycyclic aromatic condensation of BC (Figure 4-10). Across all samples (Figure 4-10, a) the distribution shows some variation. B3CA has the lowest share across all samples (6.7 ± 0.3 %), followed by B5CA (27.9 ± 1.7 %) and B6CA (30.0 ± 3.3 %). The highest average share across all samples has B4CA with 35 ± 3.2 %.

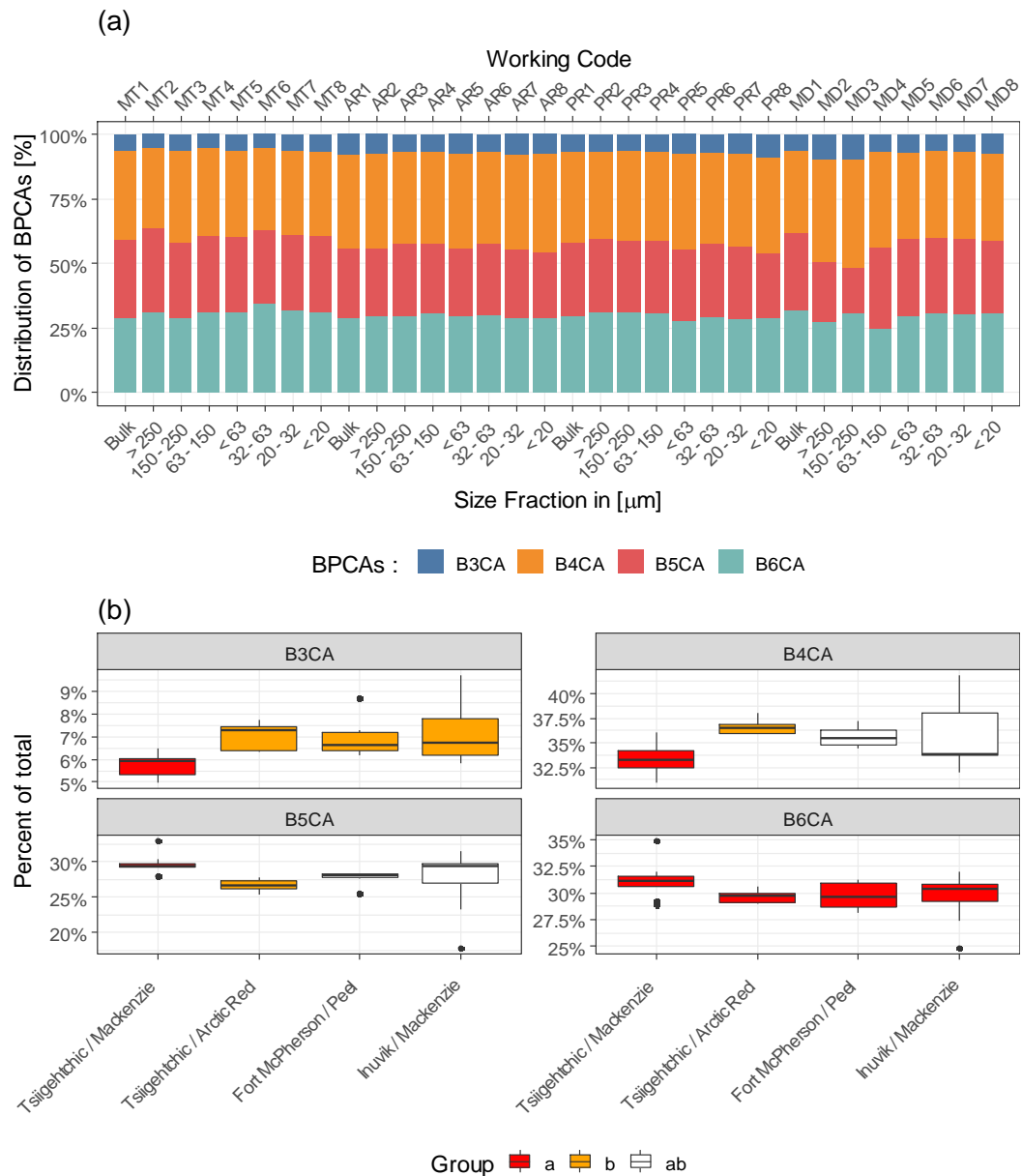


Figure 4-10 Distribution of the different BPCAs. (a) all samples individually, stacked distribution of the BPCAs. (b) shows the distribution of the different BPCAs between sites. Here the grouping colors indicate statistically significant different groups. For each of the four BPCAs a test for normal distribution was conducted by using the Shapiro method, subsequently a Levene test was used to test for equal variances and finally either a Kruskal-Wallis (K-W.) or an analysis of variance (ANOVA; AOV) was conducted to see if measurement sites have significantly different BPCA distribution. A Dunn post-hoc test, using the Bonferroni method, was used to find the different groups. The working code is a unique code identifying each sample. MT refers to Tsiigehtchic / Mackenzie, AR to Tsiigehtchic / Arctic Red, PR to Fort McPherson / Peel and MD to Inuvik / Mackenzie, the number refers to the particle size, with 1 being associated with bulk and 8 with < 20 μm (more details in Table 3-1).

Differences become more apparent when comparing BPCAs between sites (Figure 4-10, b). B3CA in Tsiigehtchic / Mackenzie is significantly lower ($r = 1.18$, large effect, Cohen, 1992) than in the other three sites. For B4CA the distribution in Tsiigehtchic / Mackenzie is lower than in Tsiigehtchic / Arctic Red ($r = 1.15$, large effect), while both are no different from the distribution at Fort McPherson / Peel and Inuvik / Mackenzie. Furthermore, the distribution of B5CA is higher in the Mackenzie River than in the Arctic Red

River at Tsiigehtchic, while they are no different from Peel and Mackenzie (at Inuvik). Finally, B6CA is statistically the same across all sites.

These results indicate that the three delta-head rivers transport BC of slightly different quality. These differences are especially apparent between the rivers Mackenzie and Arctic Red. With Arctic Red exporting, on average, less condensed BC, as B3CA and B4CA are higher and B5CA is lower than in Mackenzie River (at Tsiigehtchic).

4.5 Stable Isotopes

The signal of total stable carbon shows a group of less negative $\delta^{13}\text{C}$ values for Tsiigehtchic / Mackenzie ($\sim -7.3 \pm 0.1 \text{ ‰}$ to $10.3 \pm 0.1 \text{ ‰}$) and overall more negative $\delta^{13}\text{C}$ values for most of the other samples ($-14.2 \pm 0.1 \text{ ‰}$ to $-24.4 \pm 0.1 \text{ ‰}$, Figure 4-11, a). Four samples show even lower (i.e. more ^{13}C depleted relative to standard) values. The lowest (i.e. most negative) value is that of the size fraction $< 20 \text{ }\mu\text{m}$ in Fort McPherson / Peel with $-24.4 \pm 0.1 \text{ ‰}$. This is followed by Inuvik / Mackenzie, $> 250 \text{ }\mu\text{m}$ with $-23.6 \pm 0.1 \text{ ‰}$ and Fort McPherson / Peel, $> 250 \text{ }\mu\text{m}$ with $-21.5 \pm 0.1 \text{ ‰}$. Then there is the size fraction of particles within $150 \text{ }\mu\text{m}$ to $250 \text{ }\mu\text{m}$ in Inuvik / Mackenzie with $-21.2 \pm 0.1 \text{ ‰}$.

Higher (less negative) ^{13}C (values close to 0.0 ‰) is attributable to higher calcium content, while biological processes result in a ^{13}C depletion and lower (more negative) $\delta^{13}\text{C}$. The values with the least negative $\delta^{13}\text{C}$ signal, as described above at around -7.3 to $10.3 \pm 0.1 \text{ ‰}$, show the highest Ca content (Figure 4-11, b). While values with more negative $\delta^{13}\text{C}$ values show less Ca content ($R^2 = 0.84$, highly significant, $p = 1.1 \cdot 10^{-12}$). In this regression the two outliers in Inuvik / Mackenzie were again ignored.

Stable organic carbon is distributed over a narrow range (Figure 4-12). The differences between the sites as well as the particles sizes are not further explored because of limitations in the laboratory. Overall the values fall into the range of terrestrial C3-plant origin (-30 ‰ to -25 ‰).

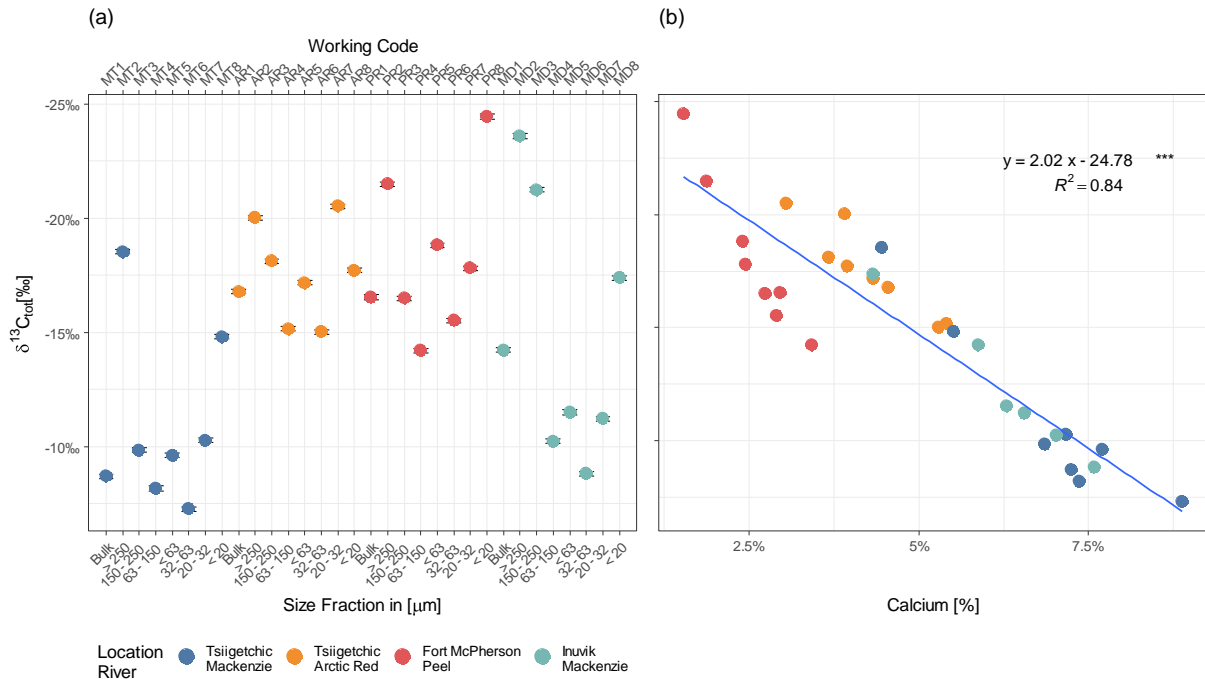


Figure 4-11 Stable carbon isotopes (total carbon, C_{tot} , organic + inorganic C) in (a) the different size fractions and the different sampling sites, and in (b) relative to calcium content. Significance levels * $p < 0.05$, ** $p < 0.01$, *** $p < 0.001$. The working code is a unique code identifying each sample. MT refers to Tsiigehtchic / Mackenzie, AR to Tsiigehtchic / Arctic Red, PR to Fort McPherson / Peel and MD to Inuvik / Mackenzie, the number refers to the grain size fraction, with 1 being associated with bulk material and 8 with $< 20 \mu m$ (more details in Table 3-1).

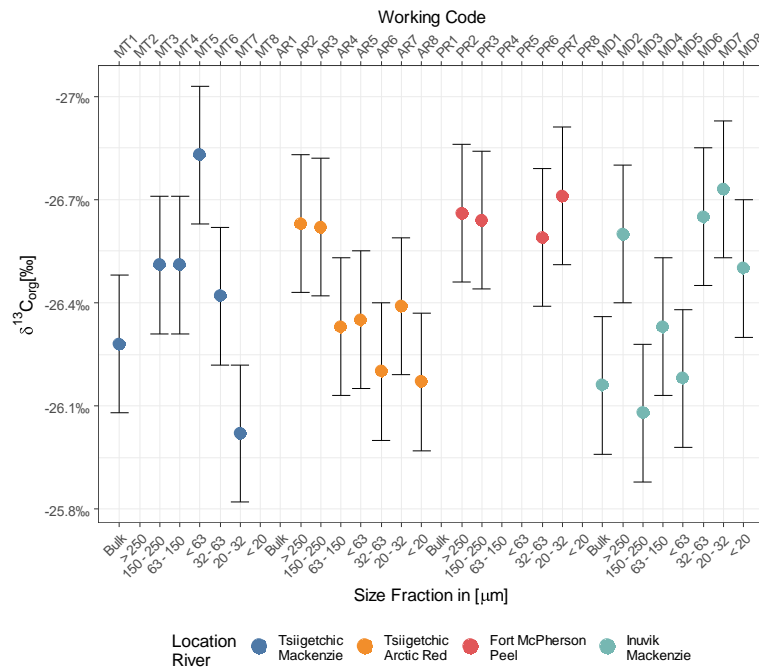


Figure 4-12 Stable carbon isotopes in the different size fractions, determined using isotope ratio mass spectrometry (p. 25). The Working Code is a unique code identifying each sample. MT refers to Tsiigehtchic / Mackenzie, AR to Tsiigehtchic / Arctic Red, PR to Fort McPherson / Peel and MD to Inuvik / Mackenzie, the number refers to the grain size fraction, with 1 being associated with bulk material and 8 with $< 20 \mu m$ (more details in Table 3-1).

4.6 Mid-infrared spectrometry

The inspection of all absorbance spectra in a single view highlights dominant features across samples, sites and particle sizes (Figure 4-13). First off, this is a rather complex situation, with a lot of signals, and more than a few peaks. A strong peak at around 3600 cm^{-1} is visible for all samples. Another clear peak around 2600 cm^{-1} is also found in all samples, albeit it is not as well pronounced everywhere (see e.g. $< 20\text{ }\mu\text{m}$ at Fort McPherson / Peel). The signature from around 2000 cm^{-1} down to 400 cm^{-1} shows the strongest differences both between as well as across sites and size fractions. A closer look at this region can only be successful when looking at the results with a higher resolution. This is exemplarily done for a single site (Figure 4-14). Spectra for the other samples are found in the supplementary figures (p. 82).

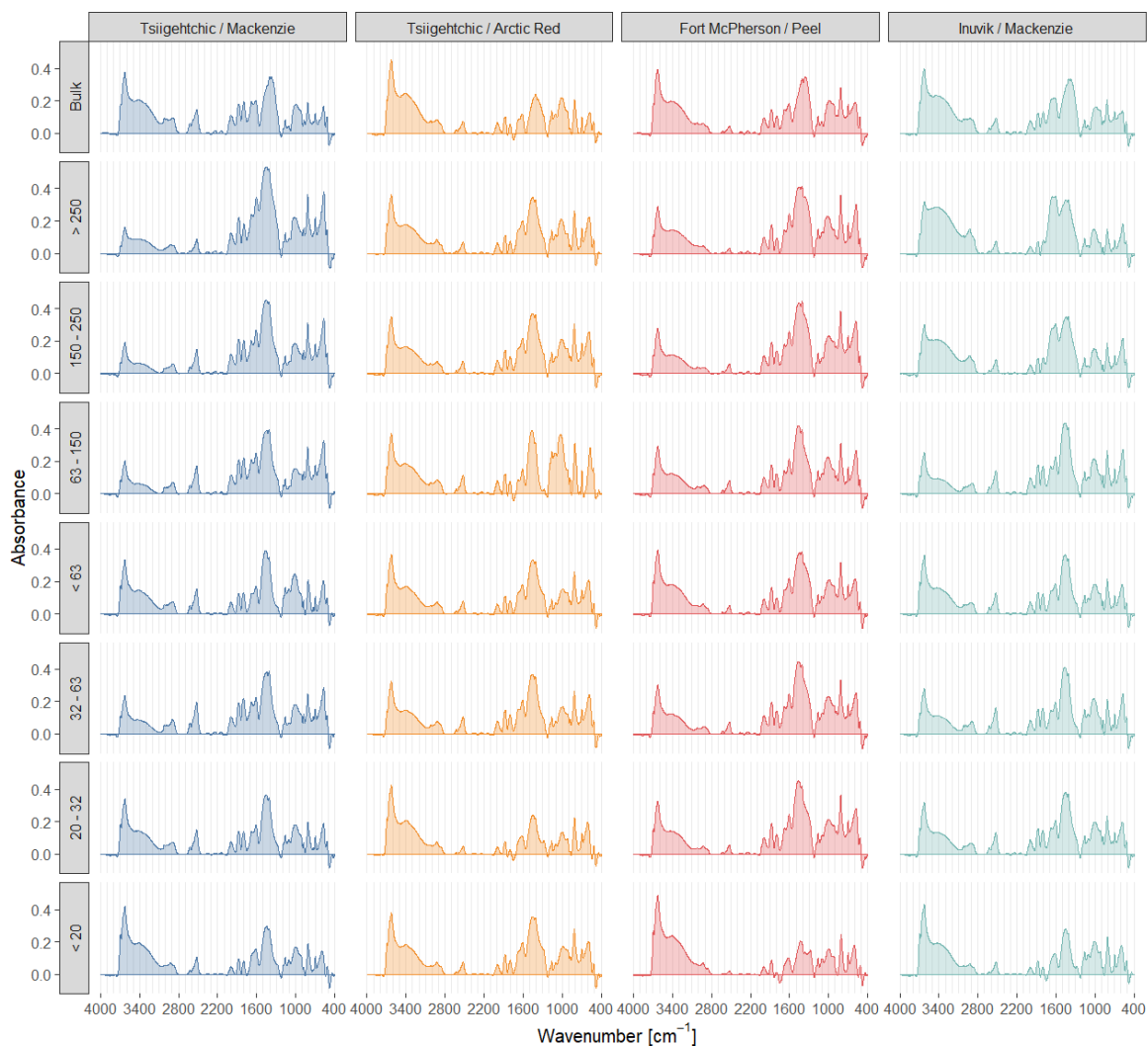


Figure 4-13 Overview of the mid-infrared spectral data from diffuse reflectance spectrometry across all samples and all sites. Colors highlight sites, individual spectra represent samples. From top to bottom the particle sizes decrease. Absorbance is a unitless ratio defined as $A = -\log\left(\frac{I}{I_0}\right)$, where I is the measured light intensity and I_0 is the initial intensity.

Bands resulting from aromatic structures are highlighted in different colors, based on Table 3-3. Starting with the region indicating aromatic C-H stretching (shaded red, 3'130 – 3'070 cm^{-1}) no clear peaks can be observed and absorbance is close to 0.1. A peak is however visible near 3'700 cm^{-1} , which corresponds to alcohol functional groups (O-H stretching). A very clear peak is visible at around 2'400 cm^{-1} , this corresponds to CO_2 (O=C=O stretching).

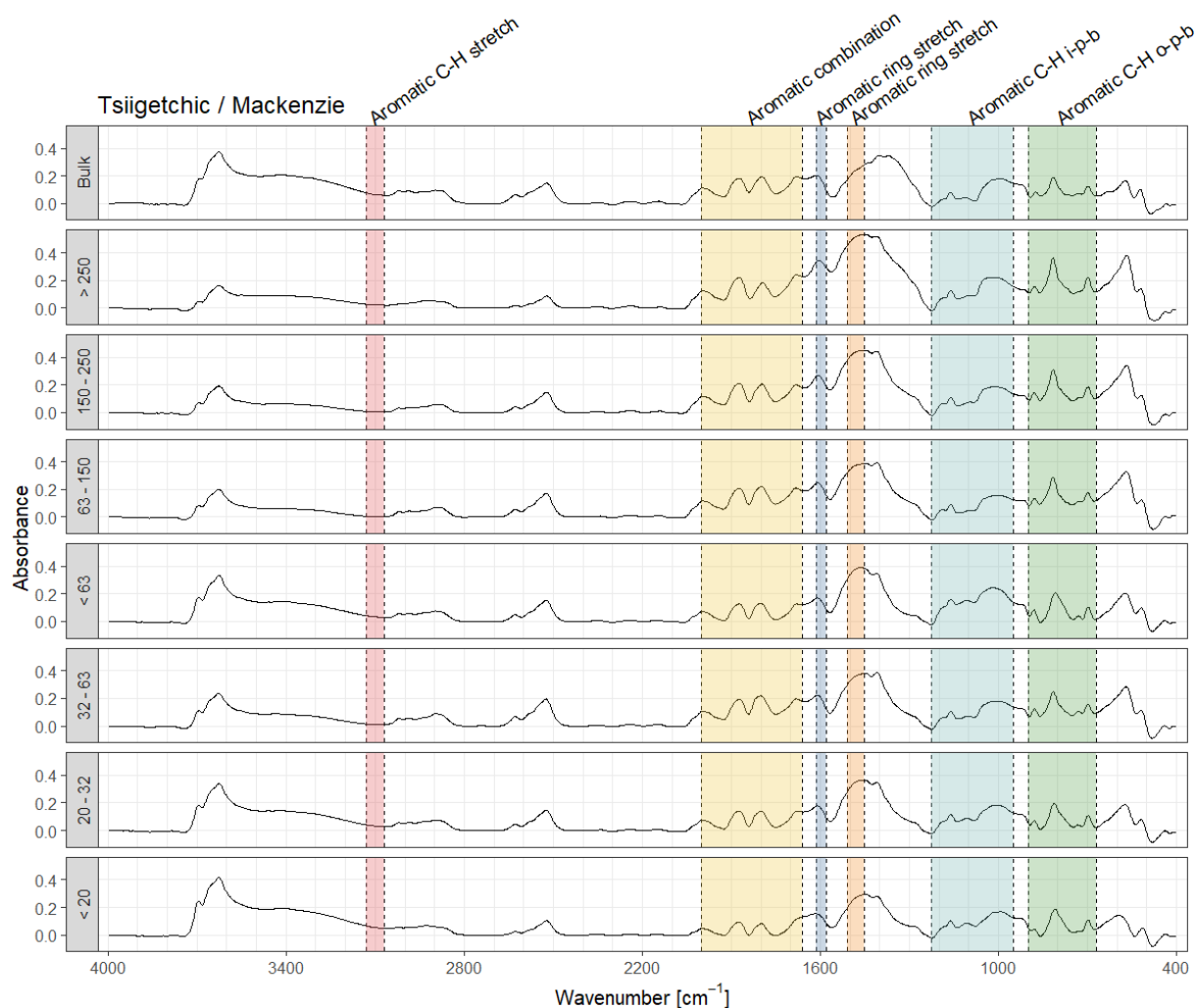


Figure 4-14 Mid-infrared spectral data from diffuse reflectance spectrometry for the site Tsiigetichic / Mackenzie. Dashed lines indicate absorption bands of compounds related to aromatic structures. Aromatic C-H i-p-b refers to aromatic C-H in-plane bending. Aromatic C-H o-p-b denotes aromatic C-H out-of-plane bending. For more details about the bands and the spectra refer to the text and Table 3-3. Absorbance is a unitless ratio defined as $A = -\log\left(\frac{I}{I_0}\right)$, where I is the measured light intensity and I_0 is the initial intensity.

Naturally this is atmospheric CO_2 . In the aromatic combination band (shaded yellow, 2'000 – 1'600 cm^{-1}) two peaks are visible. Absorbance in this region indicates simple aromatic compounds (therefore maybe indicative of BC). Two peaks are also present for the aromatic ring stretch bands (shaded in dark blue and orange, 1615 – 1580 cm^{-1} , respectively 1510 – 1450 cm^{-1}), indicating benzene ring stretching. The band for aromatic C-H in-plane-bending (1225 – 950 cm^{-1} , shaded in light green) shows one small peak and one

large peak, that extends beyond the boundaries of the band. The band for aromatic C-H out-of-plane bending ($900 - 670 \text{ cm}^{-1}$, shaded in dark green) shows two distinctive peaks at 700 cm^{-1} and 600 cm^{-1} and a small peak at around 900 cm^{-1} .

The correspondence between the area under the curve (AUC, or the integral) of a certain band and the concentration of BPCA-C is only significant for AUC-3 (aromatic C-H stretch, $R^2 = 0.66$, Figure 4-15). The individual AUC values are found in Table 4-3. Again, the relationship is only significant for BPCA-C in relation to sample mass (Figure 4-15 b) and not in relation to C_{org} (Figure 4-15 b).

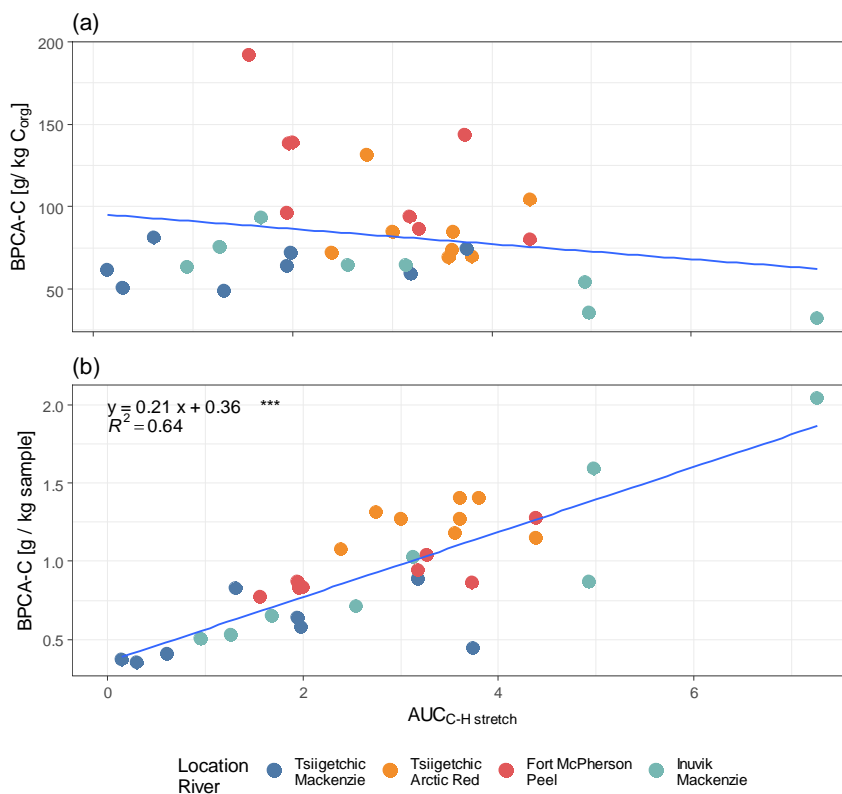


Figure 4-15 C-H stretch absorbance area under curve vs. BPCA-C. (a) AUC vs. g BPCA-C / kg C, no significant relationship (b) AUC vs. g BPCA-C / kg sample showing a significant relationship. Levels of significance * $p < 0.05$, ** $p < 0.01$, *** $p < 0.001$.

Table 4-3 Area under the curve (AUC) for the samples and the different NIR bands important for aromatic compounds.

Sample	AUC-1 Aromatic ring stretch (blue)	AUC-2 Aromatic ring stretch (orange)	AUC-3 Aromatic C-H stretch	AUC-4 Aromatic C-H in-plane bend	AUC-5 Aromatic C-H out-of-plane bend	AUC-6 Aromatic combina- tion	AUC-tot
MT1	5.5	13.7	3.7	22.7	19.5	41.0	106.2
MT2	10.8	29.5	1.3	35.0	37.9	46.0	160.6
MT3	8.0	25.0	0.3	29.2	32.4	44.3	139.2
MT4	7.2	21.3	0.1	23.1	31.5	47.2	130.4
MT5	4.8	21.4	2.0	43.0	15.6	22.7	109.5
MT6	6.3	20.6	0.6	28.1	27.4	44.1	127.2
MT7	5.0	19.9	1.9	29.1	15.9	25.6	97.5
MT8	4.3	15.3	3.2	25.8	14.2	14.7	77.5
AR1	3.1	9.2	4.4	35.7	12.6	10.2	75.1
AR2	6.1	18.6	3.8	35.1	20.7	18.1	102.4
AR3	6.5	20.2	3.6	34.3	31.1	25.2	120.8
AR4	4.3	21.4	3.6	67.5	20.0	12.5	129.3
AR5	5.3	17.9	2.7	22.4	25.4	17.7	91.4
AR6	6.1	20.2	2.4	26.3	25.3	25.6	106.0
AR7	3.1	12.2	3.6	18.9	16.1	6.4	60.3
AR8	5.8	19.1	3.0	23.7	29.3	19.0	100.0
PR1	5.3	12.9	3.7	27.9	31.9	27.5	109.3
PR2	7.5	22.5	3.3	39.7	32.3	26.4	131.6
PR3	7.9	23.8	2.0	36.2	43.7	37.1	150.8
PR4	6.4	23.2	2.0	38.0	29.2	29.4	128.2
PR5	6.6	20.0	3.2	32.8	33.1	26.3	121.9
PR6	7.5	24.7	1.6	39.0	35.6	36.1	144.6
PR7	7.4	25.1	1.9	35.4	38.9	31.2	140.0
PR8	2.7	8.1	4.4	24.2	16.6	4.5	60.4
MD1	6.4	13.7	4.9	21.3	22.6	31.5	100.5
MD2	11.1	17.8	7.3	21.2	10.8	30.7	98.8
MD3	9.5	18.6	5.0	22.1	15.6	28.4	99.2
MD4	6.7	24.2	0.9	35.2	24.5	34.8	126.3
MD5	5.4	20.0	2.6	29.9	18.4	23.5	99.7
MD6	5.6	22.8	1.3	37.4	17.2	29.5	113.7
MD7	6.0	20.7	1.7	31.3	24.5	30.4	114.6
MD8	3.6	14.4	3.1	34.2	16.0	7.8	79.2

Table 4-4 Overview of the results from the different measurements. Individual samples are referred to by their working code (WC). WC is a unique code identifying each sample. MT refers to Tsiigehtchic / Mackenzie, AR to Tsiigehtchic / Arctic Red, PR to Fort McPherson / Peel and MD to Inuvik / Mackenzie, the number refers to the grain size fraction, with 1 being associated with bulk material and 8 with < 20 µm (more details in Table 3-1). L/R denotes the sampling location (L) and the corresponding river (R), GFR denotes the grain size fraction, S1 denote the share of a certain GFR to the total. S2 denotes the share of a certain GFR to < 63 µm. SA denotes mineral specific surface area, C_{org} denotes organic carbon, C_{pred} denotes C_{org} predicted from a partial least squares regression on diffuse reflectance spectrometry data, C_{tot} gives the total carbon content measured with cavity ring-down spectrometry. BPCA denotes benzene poly-carboxylic acid and is the sum of the individual marker compounds (B3CA, B4CA, B5CA and B6CA). BPCA is given in % of C_{org}, in g / kg C_{org} as well as in g / kg S, where S denotes sample mass. Al denotes aluminum, Si denotes silicon, Ca denotes calcium and Ti denotes titanium.

WC	L/R	GFR [µm]	S1 [%]	S2 [%]	SA m ² g ⁻¹	δ ¹³ _{tot}	δ ¹³ _{org} [‰]	C _{org}	C _{pred} [%]	C _{tot}	BPCA			B3CA	B4CA	B5CA	B6CA	Al	Si	Ca	Ti
											[%-C _{org}]	[g / kg C _{org}]	[g / kg S]								
MT1	Tsiigehtchic / Mackenzie	Bulk			7.31	-8.7	-26.3 ± 0.2	0.61		3.5	7.4 ± 1.46	74.1 ± 14.6	0.4 ± 0.28	5.9 ± 0.31	34.7 ± 3.18	30.3 ± 1.69	29.2 ± 3.26	5.2 ± 1.32	30.5 ± 7.04	7.2 ± 1.60	0.3 ± 0.03
MT2		> 250	4		3.88	-8.5			1.7	3.1	4.9 ± 1.46	48.6 ± 14.6	0.8 ± 0.28	5.0 ± 0.31	31.0 ± 3.18	32.9 ± 1.69	31.1 ± 3.26	3.7 ± 0.42	43.8 ± 2.61	4.5 ± 0.10	0.2 ± 0.03
MT3		150 - 250	15		4.38	-9.8	-26.5 ± 0.2	0.66		3.0	5.1 ± 1.46	50.5 ± 14.6	0.4 ± 0.28	6.0 ± 0.31	36.1 ± 3.18	29.1 ± 1.69	28.8 ± 3.26	4.3 ± 0.42	40.6 ± 2.61	6.9 ± 0.10	0.2 ± 0.03
MT4		63 - 150	34		4.57	-8.2	-26.5 ± 0.2	0.55		3.4	6.2 ± 1.46	61.7 ± 14.6	0.4 ± 0.28	5.3 ± 0.31	34.0 ± 3.18	29.4 ± 1.69	31.2 ± 3.26	4.1 ± 0.58	35.7 ± 5.35	7.4 ± 0.99	0.2 ± 0.03
MT5		< 63	48		9.23	-9.6	-26.8 ± 0.2		0.8	3.7	7.2 ± 1.46	71.7 ± 14.6	0.6 ± 0.28	6.0 ± 0.31	33.5 ± 3.18	29.4 ± 1.69	31.1 ± 3.26	6.2 ± 0.42	35.3 ± 2.61	7.7 ± 0.10	0.5 ± 0.03
MT6		32 - 63		59	5.59	-7.3	-26.4 ± 0.2	0.54		3.8	8.1 ± 1.46	81.4 ± 14.6	0.4 ± 0.28	5.3 ± 0.31	31.8 ± 3.18	27.9 ± 1.69	34.9 ± 3.26	4.8 ± 0.42	36.4 ± 2.61	8.9 ± 0.10	0.4 ± 0.03
MT7		20 - 32		18	10.01	-0.3	-26.0 ± 0.2	0.96		3.7	6.4 ± 1.46	63.9 ± 14.6	0.6 ± 0.28	6.1 ± 0.31	32.7 ± 3.18	29.2 ± 1.69	32.0 ± 3.26	6.4 ± 0.42	35.5 ± 2.61	7.2 ± 0.10	0.6 ± 0.03
MT8		< 20		22	18.34	-4.8			1.5	3.4	5.9 ± 1.46	59.0 ± 14.6	0.9 ± 0.28	6.5 ± 0.31	33.0 ± 3.18	29.2 ± 1.69	31.4 ± 3.26	8.2 ± 0.42	34.8 ± 2.61	5.5 ± 0.10	0.6 ± 0.03
AR1	Arctic Red	Bulk			11.87	-16.8			1.1	3.2	10.4 ± 1.46	104.5 ± 14.6	1.1 ± 0.28	7.6 ± 0.31	36.5 ± 3.18	26.9 ± 1.69	29.0 ± 3.26	7.3 ± 0.42	36.4 ± 2.61	4.6 ± 0.10	0.6 ± 0.03
AR2		> 250	6		14.96	-20.0	-26.6 ± 0.2	2.13		3.6	7.0 ± 1.46	69.9 ± 14.6	1.4 ± 0.28	7.4 ± 0.31	36.6 ± 3.18	26.0 ± 1.69	30.0 ± 3.26	7.0 ± 0.42	38.2 ± 2.61	3.9 ± 0.10	0.5 ± 0.03
AR3		150 - 250	11		13	-18.1	-26.6 ± 0.2		1.7	2.9	6.9 ± 1.46	69.2 ± 14.6	1.2 ± 0.28	6.4 ± 0.31	36.0 ± 3.18	27.7 ± 1.69	29.9 ± 3.26	6.5 ± 0.42	39.6 ± 2.61	3.7 ± 0.10	0.4 ± 0.03
AR4		63 - 150	21		10.74	-15.2	-26.3 ± 0.2	1.47		3.5	8.5 ± 1.46	84.6 ± 14.6	1.3 ± 0.28	6.3 ± 0.31	36.0 ± 3.18	27.1 ± 1.69	30.6 ± 3.26	5.9 ± 0.42	38.0 ± 2.61	5.4 ± 0.10	0.4 ± 0.03
AR5		< 63	62		14.26	-17.2	-26.4 ± 0.2		1.5	3.3	13.1 ± 1.46	131.5 ± 14.6	1.3 ± 0.28	7.2 ± 0.31	36.9 ± 3.18	26.2 ± 1.69	29.7 ± 3.26	7.5 ± 0.42	37.0 ± 2.61	4.3 ± 0.10	0.6 ± 0.03
AR6		32 - 63		41	10.63	-15.0	-26.2 ± 0.2	1.5		3.5	7.2 ± 1.46	71.9 ± 14.6	1.1 ± 0.28	6.3 ± 0.31	35.9 ± 3.18	27.7 ± 1.69	30.1 ± 3.26	6.2 ± 0.42	37.9 ± 2.61	5.3 ± 0.10	0.5 ± 0.03
AR7		20 - 32		28	21.34	-20.5	-26.4 ± 0.2	1.92		3.1	7.4 ± 1.46	73.9 ± 14.6	1.4 ± 0.28	7.7 ± 0.31	36.8 ± 3.18	26.3 ± 1.69	29.1 ± 3.26	8.8 ± 0.42	36.1 ± 2.61	3.1 ± 0.10	0.6 ± 0.03
AR8		< 20		31	16.66	-17.7	-26.2 ± 0.2		1.5	3.2	8.5 ± 1.46	84.8 ± 14.6	1.3 ± 0.28	7.4 ± 0.31	38.1 ± 3.18	25.4 ± 1.69	29.1 ± 3.26	7.5 ± 0.42	37.1 ± 2.61	3.9 ± 0.10	0.6 ± 0.03
PR1	Fort McPherson / Peel	Bulk			11.4	-16.5			0.6	2.1	14.3 ± 1.46	143.3 ± 14.6	0.9 ± 0.28	6.6 ± 0.31	35.2 ± 3.18	28.3 ± 1.69	30.0 ± 3.26	7.1 ± 0.42	39.2 ± 2.61	3.0 ± 0.10	0.5 ± 0.03
PR2		> 250	10		11.06	-21.5	-26.7 ± 0.2	1.2		2.0	8.7 ± 1.46	86.5 ± 14.6	1.0 ± 0.28	6.3 ± 0.31	34.4 ± 3.18	28.1 ± 1.69	31.3 ± 3.26	5.1 ± 0.42	43.1 ± 2.61	1.9 ± 0.10	0.3 ± 0.03
PR3		150 - 250	28		9.28	-16.5	-26.6 ± 0.2		0.6	2.0	13.9 ± 1.46	139.2 ± 14.6	0.8 ± 0.28	6.2 ± 0.31	34.8 ± 3.18	27.8 ± 1.69	31.2 ± 3.26	5.5 ± 0.42	41.5 ± 2.61	2.7 ± 0.10	0.4 ± 0.03
PR4		63 - 150	40		8.43	-14.2			0.6	2.3	13.8 ± 1.46	138.1 ± 14.6	0.8 ± 0.28	6.4 ± 0.31	34.7 ± 3.18	28.0 ± 1.69	30.9 ± 3.26	5.4 ± 0.42	41.0 ± 2.61	3.4 ± 0.10	0.4 ± 0.03
PR5		< 63	22		12.47	-18.8			1	2.1	9.4 ± 1.46	93.9 ± 14.6	0.9 ± 0.28	7.2 ± 0.31	37.2 ± 3.18	27.5 ± 1.69	28.1 ± 3.26	7.2 ± 0.42	39.1 ± 2.61	2.4 ± 0.10	0.6 ± 0.03
PR6		32 - 63		53	8.08	-15.5	-26.6 ± 0.2		0.4	2.0	19.2 ± 1.46	192.2 ± 14.6	0.8 ± 0.28	6.7 ± 0.31	35.8 ± 3.18	28.2 ± 1.69	29.2 ± 3.26	5.7 ± 0.42	41.4 ± 2.61	2.9 ± 0.10	0.4 ± 0.03
PR7		20 - 32		16	9.55	-17.8	-26.7 ± 0.2		0.9	2.0	9.6 ± 1.46	96.3 ± 14.6	0.9 ± 0.28	7.3 ± 0.31	36.1 ± 3.18	28.3 ± 1.69	28.3 ± 3.26	6.1 ± 0.42	41.0 ± 2.61	2.5 ± 0.10	0.6 ± 0.03
PR8		< 20		30	22.93	-24.4			1.6	2.1	8.0 ± 1.46	79.8 ± 14.6	1.3 ± 0.28	8.7 ± 0.31	37.1 ± 3.18	25.5 ± 1.69	28.7 ± 3.26	8.8 ± 0.44	35.9 ± 2.61	1.5 ± 0.10	0.7 ± 0.03

Table 4-5 Continuation of Table 4-4.

WC	L/R	GFR [µm]	S1 [%]	S2 [%]	SA m ² g ⁻¹	δ ¹³ _{tot}	δ ¹³ _{org} [‰]	C _{org}	C _{pred} [%]	C _{tot}	BPCA			B3CA	B4CA	B5CA	B6CA [%]	Al	Si	Ca	Ti
											[%-C _{org}]	[g / kg C _{org}]	[g / kg S]								
MD1	Inuvik / Mackenzie	Bulk			7.47	-14.2	-26.2 ± 0.2	1.57		3.9	5.4 ± 1.46	54.1 ± 14.6	0.9 ± 0.28	5.8 ± 0.31	32.0 ± 3.18	30.2 ± 1.69	32.0 ± 3.26	5.6 ± 0.60	29.6 ± 3.31	5.9 ± 0.62	0.3 ± 0.03
MD2		> 250	5		8.44	-23.6	-26.6 ± 0.2		6.4	10.3	3.2 ± 1.46	31.9 ± 14.6	2.0 ± 0.28	9.4 ± 0.31	39.9 ± 3.18	23.3 ± 1.69	27.4 ± 3.26	3.8 ± 0.42	22.6 ± 2.61	5.0 ± 0.10	0.2 ± 0.03
MD3		150 - 250	5		9.22	-21.2	-26.1 ± 0.2	4.47		6.9	3.5 ± 1.46	35.4 ± 14.6	1.6 ± 0.28	9.7 ± 0.31	41.9 ± 3.18	17.7 ± 1.69	30.7 ± 3.26	4.7 ± 0.53	28.5 ± 3.27	5.3 ± 0.57	0.3 ± 0.03
MD4		63 - 150	60		6.57	-10.2	-26.3 ± 0.2	0.77		3.3	6.3 ± 1.46	63.3 ± 14.6	0.5 ± 0.28	6.3 ± 0.31	37.5 ± 3.18	31.5 ± 1.69	24.8 ± 3.26	5.3 ± 0.42	38.7 ± 2.61	7.0 ± 0.10	0.3 ± 0.03
MD5		< 63	29		11.4	-11.5	-26.2 ± 0.2	1.05		3.5	6.5 ± 1.46	64.5 ± 14.6	0.7 ± 0.28	6.8 ± 0.31	33.8 ± 3.18	29.6 ± 1.69	29.9 ± 3.26	7.0 ± 0.42	36.4 ± 2.61	6.3 ± 0.10	0.5 ± 0.03
MD6		32 - 63		48	7.35	-8.8	-26.7 ± 0.2	0.72		3.6	7.5 ± 1.46	75.2 ± 14.6	0.5 ± 0.28	6.0 ± 0.31	33.9 ± 3.18	29.3 ± 1.69	30.8 ± 3.26	5.6 ± 0.42	37.1 ± 2.61	7.6 ± 0.10	0.4 ± 0.03
MD7		20 - 32		18	9	-11.2	-26.7 ± 0.2		0.7	3.5	9.3 ± 1.46	93.2 ± 14.6	0.7 ± 0.28	6.7 ± 0.31	33.7 ± 3.18	29.4 ± 1.69	30.2 ± 3.26	6.2 ± 0.42	36.8 ± 2.61	6.6 ± 0.10	0.5 ± 0.03
MD8		< 20		34	19.89	-17.4	-26.5 ± 0.2		1.6	3.3	6.4 ± 1.46	64.3 ± 14.6	1.0 ± 0.28	7.2 ± 0.31	33.8 ± 3.18	28.1 ± 1.69	30.8 ± 3.26	8.5 ± 0.42	34.9 ± 2.61	4.3 ± 0.10	0.7 ± 0.03

5 Discussion

5.1 Geochemical Characteristics of Grain Size Fractions

The driving question for the present work is: “Do grain size fractions show differences in geochemical characteristics?”.

Depending on the hydrodynamic sorting of particles, river suspended sediment has a different grain size distribution (Walling et al., 2000). Furthermore, a large river on a passive margin is different from a steep river on an active continental margin (Blair and Aller, 2012). The geochemical characteristics of different grain size fractions in suspended sediment from the Mackenzie River as well as the fluxes of organic matter and black carbon are discussed in the following.

5.1.1 Grain Size Distribution

The three delta-head rivers, as well as the delta middle channel, exhibit different grain-size distributions (Figure 4-1). What Mackenzie, Arctic Red and Peel Rivers bring into the delta does however not correspond to what is found there (Inuvik / Mackenzie).

Considering the particle size distribution there are three main observations. First, there seems to be a loss of particles in the range of 150 – 250 μm . These particles account for very little mass in the delta (5 %) but are considerably higher in Arctic Red (11 %), Peel (28 %) and Mackenzie (15 %). This is interesting because the even larger particles (> 250 μm) are transported conservatively. Secondly, there is a loss of particles smaller than 63 μm . In the delta these particles account for 29 % of the mass, whereas they account for 62 % in the Arctic Red River, 22 % in the Peel River and 48 % in the Mackenzie River at Tsiigehtchic. Thirdly, there is an increase of particles in the range of 63 – 150 μm . In the delta they account for 60 % of the mass.

This clearly demonstrates that the delta dynamics in combination with arctic hydrology (freshet) create a unique sedimentological setting. Both large (150 – 250 μm) and small particles (< 63 μm) are lost, while the very large particles (> 250 μm) are kept in suspension and medium sized particles (63 – 150 μm) become the dominant particle size.

During the freshet, the Mackenzie River transports the most material, and the timing can influence the results discussed here. Temporal differences in discharge could thus account for these differences to some extent. From a hydrodynamic point of view, it is less likely that both small and large particles are lost, while medium sized particles become the dominant mode of transport. But the delta gets flooded massively during the freshet,

with almost half of the whole discharge being distributed over lakes and floodplains (Emmerton et al., 2007). This could potentially remobilize medium sized particles from river or channel banks, closed lakes and floodplains.

Studies have shown that overbank sediment close to the river channel is sand dominated and that sediment gets progressively finer with increasing distance to the channel (Lecce and Pavlowsky, 2004; Walling et al., 1997). Walling et al., 1997 found that more than 50 % of particles from overbank deposits fell into the range of 112 μm – 346 μm . At the same time the grain size fraction < 63 μm accounted for about 13.4 % – 36.8 % of the total (Walling et al., 1997), similar to the Peel River (22 %) and the Mackenzie River (29 %) in the delta. According to Walling et al. (1997) the overbank sediment was substantially more coarse than actual river suspended sediment. However, they were only able to compare their results to river suspended sediment sampled during non-flooding conditions. Interestingly Yamada et al. (2016) found fine grained overbank deposits during a flooding event, and argue that coarser grains are being deposited at the channel margin and cannot be transported into newly formed overflow-channels. Differences between river suspended sediment samples and riverbank, overbank and bedload samples are thus very likely influencing the grain size distribution.

The observed composition of the delta-head rivers represents their respective drainage basin quite well. Arctic Red River has its source in the Western Cordillera, however at the measurement station it already passed several hundred kilometers of the Interior Plains. The Mackenzie River on the other hand flows out of Great Bear Lake, where the Liard River contributes the largest amount of sediment, shortly after the outflow from Great Bear Lake (at Fort Simpson). After this, the Mackenzie River gradually flows down towards the Delta, draining mostly the Interior Plains. In consequence of similar hydrodynamics, it is reasonable that these rivers show similar particle size distributions. Even more so since Liard River also has its source in the Western Cordillera. Carson et al. (1998) found a similar grain size distribution between the Mackenzie River and the Arctic Red River and a clearly different distribution for Peel River – at least during the sampling time May to June. The Peel River finally has its source also in the Western Cordillera; however, its source is far more up north than that of the other rivers. It may thus be even more affected by seasonal forcing, with large parts of the snow-cover mobilizing massive amounts of bedrock during the melting period. Furthermore, the passage of the Peel River over the flat Interior Plains is shorter and thus provides less time and place for the settling out of larger particles. This would explain the shift towards larger particles in this river.

It was not possible to account for composite particles in this work. Particles in the cohesive range (< 62 μm) can form large aggregates with huge pores (Droppo, 2001; Droppo et al., 2015). This implies that the grain size fractions 32 – 63 μm , 20 – 32 μm and < 20 μm might have been transported as aggregates, bringing them towards the relative size of the

larger grain size fractions. Aggregates in the range of several 100 μm are well possible (Droppo, 2001). This suggests that it might be more reasonable to sample suspended sediment and riverbank material based on a bulk sample, with known grain size distribution, rather than on a filtered sample (of any filter size).

5.1.2 Geochemical Characteristics

Aluminum is higher in the two tributaries Arctic Red and Peel than in the Mackenzie River. They likely transport more minerals in suspension because they are closer to their drainage basin, where they can mobilize material from soils and bedrock. Calcium on the other hand seems to peak at medium sized particles and is lowest in the Peel River and highest in the Mackenzie River. The Al/Si ratio, as an indicator for relative grain size and clay content, shows an increase with smaller particles (Figure 4-2 b). This suggests that the ratio, commonly used to reflect mineral content as well as grain size, is also suitable for grain size fractions. It shows however, that Al/Si is not a site-specific indicator for mineral content and sediment processing, but rather that it is grain size dominated.

Inorganic elements are frequently used in the assessment of weathering strength in the catchment (Guo et al., 2018). Since many minerals are enriched in finer grain size fractions, it is important to know the grain size distribution and the corresponding geochemical and mineral compositions (Guo et al., 2018). Otherwise weathering will be assessed too strong, simply by the higher amount of minerals in finer material (Guo et al., 2018). In the samples analyzed here, titanium clearly increases with decreasing particle size (lowest in $> 250 \mu\text{m}$ and highest in $< 20 \mu\text{m}$). This enrichment of Ti is reasonable as it is primarily associated with high-density secondary minerals (Guo et al., 2018; Viers et al., 2009). For instance Viers et al. (2009) report on average 0.44% of Ti in the world's rivers. The average Ti content in the sampled rivers ranges from $0.17 \pm 0.03 \%$ to $0.4 \pm 0.03 \%$ and one could thus think that the weathering is below or near the average. However, Ti can be as high as 0.63 % for the smallest grain size fraction, which would then result in much stronger weathering. Of course weathering indices are not solely based on a single element (Guo et al., 2018), but it still demonstrates the magnitude of variability between grain size fractions.

The relationship between minerals, indicated by high aluminum content, and surface area is significant ($R^2 = 0.83$). This illustrates that the two tributaries Arctic Red and Peel export higher amounts of clay minerals than the Mackenzie River (Figure 4-4). The Mackenzie River has the higher surface area at Inuvik than at Tsiigehtchic, which is attributable to the inputs of the tributaries.

The bulk surface area for Tsiigehtchic / Mackenzie measured here is $7.31 \pm 0.7 \text{ m}^2/\text{g}$, which is lower than the $12 \text{ m}^2/\text{g}$ measured by Vonk et al. (2015a) for the middle channel, however their value for the east channel is the same ($7.3 \text{ m}^2/\text{g}$). For the Peel River they

report 11 m²/g which is in good agreement to the value of 11.40 m²/g measured here (Table 5-2). Interestingly the mineral specific surface area shows little variability between years. This could indicate export of similar minerals and consequently similar weathering and hydrodynamic conditions in the catchments.

5.1.3 Carbon in the Mix

Total carbon is on average lowest in the Peel River (2.1 %), followed by the Arctic Red River (3.3 %) and the Mackenzie River at Tsiigehtchic (3.5 %, Figure 4-5). It is highest in Mackenzie at Inuvik (4.8 %). There is no clear relationship with particle size. However, total carbon and calcium are related (Figure 4-6) and clearly group the four rivers, with Fort McPherson / Peel exhibiting low calcium and low carbon, Tsiigehtchic / Arctic Red exhibiting high C and intermediate Ca and the two Mackenzie River sites falling into the high carbon / high calcium range.

Organic carbon shows variability between both sites and size fractions. Differences between sites are larger than differences between size fractions. High organic carbon contents are present in the smallest grain size fraction (< 20 µm). This is likely due to the higher surface area and higher mineral content that allows for more C_{org} to attach to the surface or inter-particle areas (Blair and Aller, 2012).

In 2015, Hilton et al. also investigated C_{org} in different grain size fractions (Table 5-2). The reported value for the grain size fraction 150 – 250 µm of Tsiigehtchic / Mackenzie is about 2.0 % in the year 2009. The same fraction shows 0.7 % C_{org} in 2017. The fraction of particles between 63 – 150 µm is reported with 1.0 % C_{org} in 2009. This was measured at about 0.6 % in 2017. Lastly for particles < 63 µm, Hilton et al. (2015) report about 1.0 % C_{org} in 2009. This corresponds to about 0.8 % in 2017. The comparison shows that C_{org} is variable between grain size fractions and to some extent also between different years.

The relationship between surface area and C_{org}, referred to as C_{org} loading, gives information about the sedimentological setting but also about the supply and preservation of organic matter (Figure 4-1). The three main regimes defined by different loadings are: 0.4 – 1.0 C_{org} / m², < 0.4 C_{org} / m² and > 1.0 C_{org} / m² (Blair and Aller, 2012).

The region between 0.4 C_{org} / m² and 1.0 C_{org} / m² describes river suspended and non-deltaic shelf sediments that are in balance between composition and supply. Many values fall into this range. The smallest particles (20 – 32 µm and < 20 µm), with high surface area, are mostly distributed in this range. This is reasonable as the higher amount of minerals likely has a stabilizing effect on C_{org}. At the same time very high amounts of C_{org} would be required to bring these particles into the high-productivity zones (> 1.0 C_{org} / m²). Intermediately sized particles as well as the bulk and < 63 µm size fractions mostly

fall into a zone between 5 m²/g and 12.5 m²/g. In Vonk et al. (2015a) the riverbank samples are also located in the same region with around 10 m²/g SA and around 1 % C_{org} (Table 5-2).

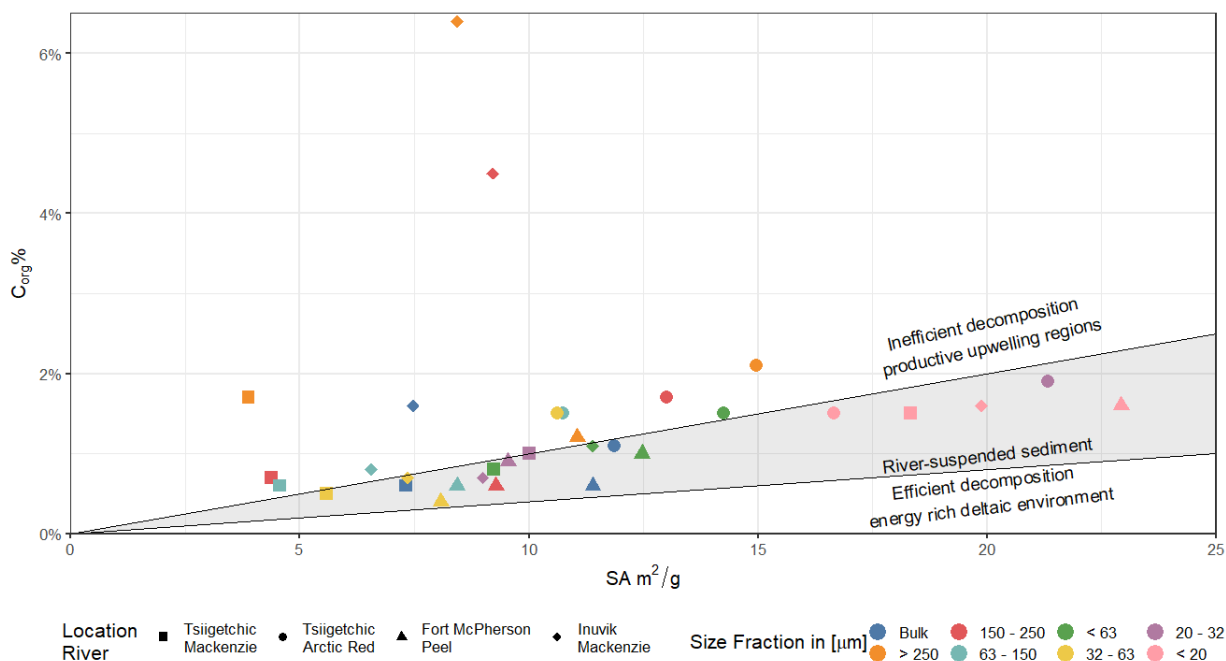


Figure 5-1 Relationship ($SA:C_{org}$), also referred to as C_{org} loading, between mineral specific surface area (SA) and organic carbon (C_{org}). Superimposed is the typical range for this relationship from 0.4 to 1.0 mg C_{org} / m² (gray area, calculation based on Blair and Aller, 2012; Mayer, 1994). Color indicates different grain size fractions, whereas shapes represent different sampling sites (Location / River).

Values above 1.0 C_{org} / m² mark regimes with inefficient decomposition (high productivity, upwelling regions; Blair and Aller, 2012). This region is mostly occupied by larger grain sizes, especially > 250 μm, but also 150 – 250 μm particles. This is reasonable due to inputs from plant litter. At the same time, the range of surface area values that the samples in this zone span is noticeably large (< 5 m²/g to ca. 15 m²/g). This indicates that there are multiple ways of stabilizing (or at least mobilizing from a point source) high amounts of organic carbon (Blair and Aller, 2012).

The zone below 0.4 C_{org} / m² describes regimes with efficient decomposition (energetic deltaic sediments and deep sea; Blair and Aller, 2012). No sample falls into this zone. According to the definition of the energetic deltaic sediment, samples from Inuvik / Mackenzie might have been expected to fall into this range. During the freshet, however, the supply of sediment might just be too high for an efficient decomposition.

Although an increase of POC through increased release of SOC from soils and thawing permafrost might have been expected (Vonk et al., 2015b), compared to previous years this is not directly visible in the amount of carbon found here. The age, type and isotopic signature of exported C_{org} can be used to identify material sourced from permafrost (Feng et al., 2013). Due to limited samples and measurement difficulties this is not possible for

the present data. According to Feng et al. (2013) permafrost C_{org} can be masked by other sources of organic material. Furthermore, during the freshet large parts of the sediment that is transported is mobilized from bank erosion and not yet from soils, as they might still be frozen (McClelland et al., 2016). In conclusion POC from permafrost could still be present but masked by other sources. However, it could also have not yet been released or it could also have been remineralized in soils or along the transport.

Overall the findings show different amounts of organic carbon both in size fractions but also in the different rivers. Some grain size fractions show ineffective decomposition, noticeably the largest particles. The particles $> 250 \mu\text{m}$ are furthermore likely to be exported beyond the sampling point in the delta.

Having looked at organic carbon, the black carbon portion that was also analyzed is discussed next. BC has the potential for being a reservoir for the longer-term storage of organic carbon and is thus of interest for the broader context of the riverine-oceanic-atmospheric coupling.

5.1.4 Black Carbon

Black carbon is clearly the lowest in the Mackenzie River prior to its confluence with the Arctic Red River (at Tsiigehtchic, Figure 4-8). The Arctic Red River in turn shows the highest absolute values of BC (normalized to sample mass, otherwise second highest amount). Overall the results indicate that no single grain size fraction dominates the others (except in Inuvik / Mackenzie). BPCA-C is high in all grain size fractions of Arctic Red and Peel Rivers and hints at an increase with decreasing particle size in Arctic Red. This trend is also evident in the Mackenzie River (both sites). This is consistent with the pattern of C_{org} and indicates that BC is associated with mineral surfaces. Which might be explained to some extent by surface area (Figure 4-9, Pearson's $r = 0.75$).

As the amount of BC is different between rivers, so is also its quality (Figure 4-10). Differences of BC quality between grain size fractions are present but not reasonably quantifiable (number of samples too low). Differences between sites are clearer. Here Arctic Red exports the least condensed BC. The amount of B6CA produced from pyrolyzing wood scales with the fire temperature, with almost exclusively B6CA at temperatures near $1000 \text{ }^\circ\text{C}$ (Schneider et al., 2010). From the work of Schneider et al. (2010), the BC found on average in the Mackenzie River might come from fires burning at $250 \text{ }^\circ\text{C}$ to $300 \text{ }^\circ\text{C}$. Different conditions during the formation of BC might be attributable to vegetation differences in the catchments. The Western Cordillera has different vegetation, different climate and higher elevations than the Interior Plains. Fire frequency and history is also different between the Western Cordillera and the Interior Plains (Flannigan et al., 2009). Furthermore, BC is processed on its journey from the site of formation to the sampling point in the river.

Black Carbon from Diffuse Reflectance Spectrometry

With the use of mid-infrared spectroscopy, a relationship between the amount of BPCAs and an aromatic band (aromatic C-H stretch) was uncovered (Figure 4-15, $R^2 = 0.64$). This relationship is important because it allows to quickly determine BC by using DR-spectrometry. It remains unclear how this relationship would shift if more condensed BC (i.e. more B6CA) were to be present in the samples. The more condensed the BPCA, the less C-H groups are present, with none at all for B6CA (Schneider et al., 2010). Consequently, the C-H stretch would not be possible. However, this would maybe produce a dip in absorbance in this band, which again could be diagnostic. Using a sampling approach similar to Schneider et al. (2010) with increasing pyrolysis temperature could elucidate the predictive power of the found relationship for a wider range of conditions.

In two specific samples the total and organic carbon as well as the black carbon content is drastically higher than in all other samples (Inuvik / Mackenzie, >250 μm and 150 – 250 μm), the sources and implications of these high amounts of carbon can now also be explored.

5.1.5 Identifying Sources for Higher C_{org} Content

The high carbon content found for two samples (Inuvik / Mackenzie of particles with sizes > 250 μm and 150 – 250 μm) could either be caused by large amounts of carbonates, by biomass litter (e.g. plant fragments, root or leaf litter, etc.), or both. Calcium content is however not able to explain these high C values (Figure 4-6). Furthermore, the high values are also found for organic carbon (Figure 4-7). This implies that they are the result of some organic material. The high values are likely from larger fragments of biomass, such as vascular plant debris, like roots or leaves.

Interestingly these two samples also exhibit high values of BPCA-C (Figure 4-8). Zimmerman and Mitra (2017) note that plants, fungi and pigments can yield BPCAs, and that during strong oxidation conditions (such as in the BPCA method), BPCA can be formed from non-BPCA substances. Additionally, it is also possible to have some charcoal or pre-aged soil organic matter with high BPCA content in these larger grain size fractions.

This shows that alongside the larger particles (250 – 63 μm) tiny fragments of organic residues (roots, leaves, etc.) can be transported. Which seems to be especially important in the deltaic environment, rather than under the flow conditions in the delta-head rivers. Such fragments of organic material in larger grain size fractions were also found by e.g. Hilton et al. (2010), where it was particularly apparent for the grain size fraction > 500 μm . In the case of Hilton et al. (2010) the C/N ratio, as well as stable carbon isotopes clearly indicated these plant fragments and they were further also visible to the naked eye.

These organic substances should be readily digestible by organisms and they should furthermore rapidly sediment out of the suspension. It seems thus not likely that these high values of C_{org} will be exported to the shelf or beyond. However, Schwab (2016) found values of C_{org} as high as 9.01 % in sediments collected in May in a sediment trap on the shelf. This demonstrates that during the freshet, with the large pulse of freshwater, even large particles and fragments of biomass can be transported through the delta and onto the shelf.

Having explored the amount and distribution of C_{org} and BC between grain sizes and sampling sites, as well as the transport through the basin, the flux for the year 2017 is of interest. Not only the total flux for POC and PBC, but also the flux for the individual grain size fractions.

5.2 Fluxes

The total export of POC in 2017 (1.7 ± 0.7 Mt, Table 5-1, Figure 5-2) is within the range reported by Hilton et al. (2015) of $2.1 + 1.3, - 0.9$ Mt and others (Table 5-2). The total export of PBC in 2017 (0.362 ± 0.090 Mt) is within the range presented by Coppola et al. (2018) based on samples from 2006 (0.296 Mt, Table 5-2). The fluxes for the individual rivers show that the Mackenzie River transports the most POC and BC, which was to be expected because of the higher sediment discharge.

The bulk and the $< 63 \mu\text{m}$ value were not integrated and thus not presented. The bulk represents all size fractions, whereas $< 63 \mu\text{m}$ represents the sum of $32 - 63 \mu\text{m}$, $20 - 32 \mu\text{m}$ and $< 20 \mu\text{m}$.

The fluxes calculated for the different rivers and sites clearly show that larger ($> 63 \mu\text{m}$) grain size fractions are also carriers for large amounts of C_{org} and BC. This is not surprising as these size fractions account for a large amount of the total mass. Evidently what the individual rivers transport does not add up to what is found in the delta. Differences can be attributed to assumptions, to measurement errors, to mobilization in the delta and to inputs by smaller rivers or lakes. But most importantly the high export in the Mackenzie River in the delta is attributable to the high C_{org} content in the two grain size fractions $> 250 \mu\text{m}$, $150 - 250 \mu\text{m}$. In Fort McPherson / Peel and Inuvik / Mackenzie the larger particles ($> 63 \mu\text{m}$) contribute more to the total, than the smaller particle sizes ($< 63 \mu\text{m}$). This is not so much the case in Tsiigehtchic / Mackenzie and Tsiigehtchic / Arctic Red. In general, this shows that the larger grains ($> 63 \mu\text{m}$) also carry a significant amount of the load.

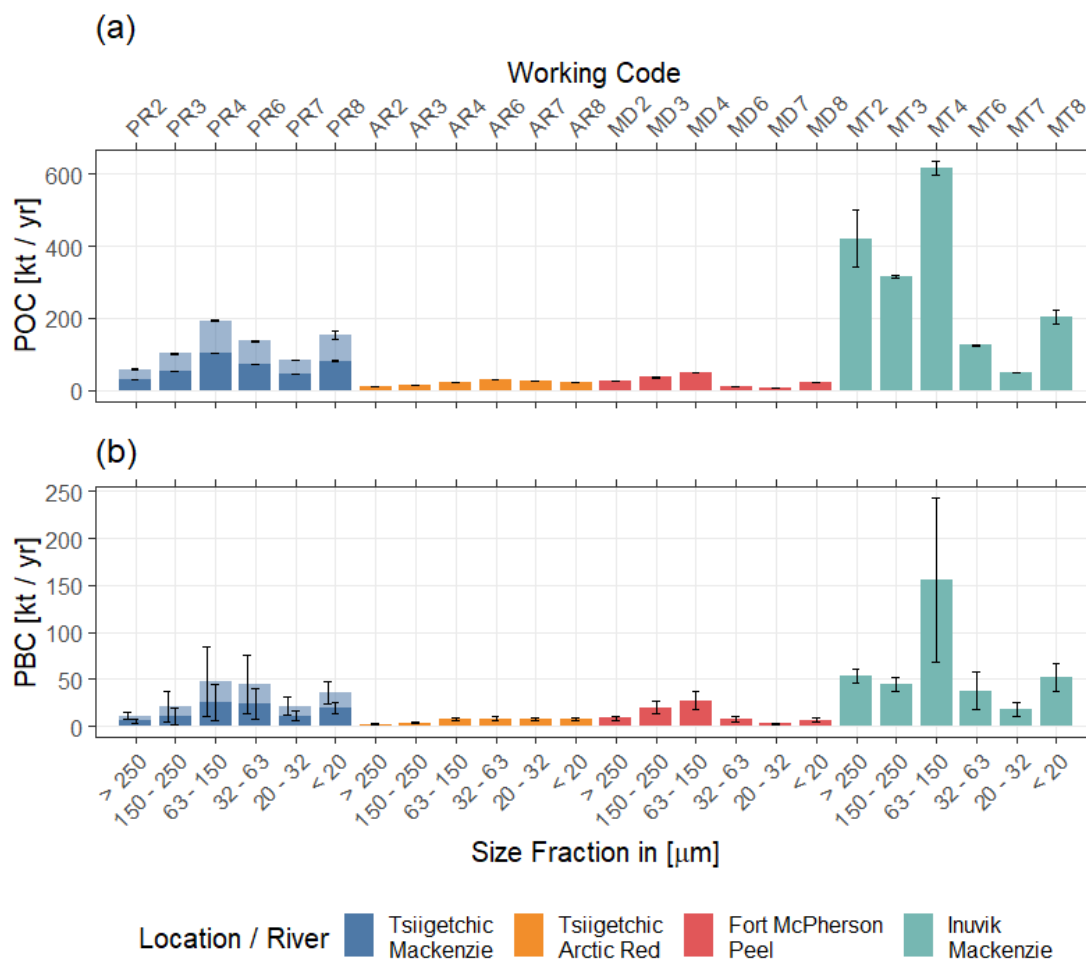


Figure 5-2 Flux of POC (C_{org} associated with particles) and PBC (black carbon associated with particles) for the year 2017 presented for the different rivers and the different grain size fractions. For Tsiigetichic / Mackenzie two different estimates for TSS were available, dark blue is the lower limit (51 Mt yr^{-1}) measured by Gareis and Lesack (2017), light blue is the upper limit (93 Mt yr^{-1}) estimated by Carson et al. (1998). Please note that the scale is in kt yr^{-1} ($10^{-3} \text{ Mt yr}^{-1}$). Results for the bulk as well as the $< 63 \mu\text{m}$ grain size fraction are intentionally not presented (see text). The working code is a unique code identifying each sample. MT refers to Tsiigetichic / Mackenzie, AR to Tsiigetichic / Arctic Red, PR to Fort McPherson / Peel and MD to Inuvik / Mackenzie, the number refers to the grain size fraction, with 1 being associated with bulk material and 8 with $< 20 \mu\text{m}$ (more details in Table 3-1).

The burial efficiency of organic carbon on the shelf is about 50 % – 65 % (Ward et al., 2017; Vonk et al., 2015a; Hilton et al., 2015). By assuming this burial efficiency to hold for all grain size fractions this could result in a sink of about $0.994 \pm 0.130 \text{ Mt}$ of POC in 2017. Of which $0.208 \pm 0.027 \text{ Mt}$ could be in the form of PBC. Converted to CO_2 this amounts to roughly $3.6 \pm 0.48 \text{ Mt CO}_2$. For reference, the cumulated emissions of Madagascar (3.2 Mt) or Iceland (3.5 Mt) were about of the same size in 2017 (Global Carbon Project, 2018). This illustrates that the Mackenzie River system and the adjacent shelf are important sites of carbon processing for the global climate.

The particle size range 63 – 150 μm shows the most impressive flux in the delta. It has previously been suggested that during the freshet a burst of sediment-laden water is pushed onto the shelf (Lalande et al., 2009), thus also explaining the extremely high C_{org} contents found in the Mackenzie Basin sediment traps (up to 9 %). If that would be the case, then the Mackenzie River would be a very efficient exporter of C_{org} during the freshet.

On the other hand, if these rather large particles were primarily deposited in the delta, in lakes and on floodplains, due to lower relative water velocities, then it could as well be, that the most part of the estimated flux of POC and PBC never reaches the ocean.

The important question is thus how are these particle sizes affected by hydrodynamic sorting further down into the delta? Clearly, they are found in the delta where the samples were taken, but this is only a single point. Furthermore, what happens to these particles at the terminus or on the shelf? Are they rapidly consumed? Or do they quickly deposit because they flocculate in salt water?

Table 5-1 W/C = Working Code, MT = Tsiigehtchic / Mackenzie, AR = Tsiigehtchic / Arctic Red, PR = Fort McPherson / Peel, MD = Inuvik / Mackenzie, L/R = Location / River, TSS = Total Suspended Sediment, * conversion factor = 4 ± 1 (Ziolkowski et al., 2011). ^a Hilton et al. (2015), ^b Coppola et al. (2018).

W/C	Size Fraction	L/R	TSS Flux	Flux			Reported	
				C _{org} [kt yr ⁻¹]	BPCA-C [kt yr ⁻¹]	PBC* [kt yr ⁻¹]	C _{org} [kt yr ⁻¹]	PBC [kt yr ⁻¹]
MT2	> 250 µm	Tsiigehtchic / Mackenzie	51 - 93	30.8 - 57.9	1.5 - 2.8	6.0 - 11.3		
MT3	150 - 250 µm			53.8 - 101.3	2.7 - 5.1	10.9 - 20.5		
MT4	63 - 150 µm			102.9 - 193.8	6.4 - 12.0	25.4 - 47.9		
MT6	32 - 63 µm			72.3 - 136.1	5.9 - 11.1	23.5 - 44.3		
MT7	20 - 32 µm			44.6 - 83.9	2.8 - 5.4	11.4 - 21.4		
MT8	< 20 µm			81.4 - 153.2	4.8 - 9.0	19.2 - 6.1		
Total						385.8 - 726.2	24.1 - 45.4	96.4 ± 24.1 - 181.5 ± 45.4
AR2	> 250 µm	Tsiigehtchic / Arctic Red	7.3	9.3	0.6	2.5		
AR3	150 - 250 µm			13.8	1.0	3.8		
AR4	63 - 150 µm			22.8	1.9	7.7		
AR6	32 - 63 µm			27.8	2.0	8.0		
AR7	20 - 32 µm			24.3	1.8	7.2		
AR8	< 20 µm			20.9	1.8	7.1		
Total						118.9	9.1	36.3 ± 9.1
PR2	> 250 µm	Fort McPherson / Peel	20.8	25.5	2.2	8.8		
PR3	150 - 250 µm			35.5	4.9	19.8		
PR4	63 - 150 µm			49.6	6.9	27.4		
PR6	32 - 63 µm			9.6	1.8	7.4		
PR7	20 - 32 µm			6.6	0.6	2.5		
PR8	< 20 µm			21.8	1.7	6.9		
Total						148.6	18.1	72.8 ± 18.1
MD2	> 250 µm	Fort McPherson / Peel	128	421.5	13.4	53.8		
MD3	150 - 250 µm			315.1	11.1	44.6		
MD4	63 - 150 µm			616.5	39.0	156.1		
MD6	32 - 63 µm			124.6	9.4	37.5		
MD7	20 - 32 µm			48.1	4.5	17.9		
MD8	< 20 µm			202.9	13.0	52.2		
Total						1'728.7	90.4	362.1 ± 90.4

Table 5-2 Overview of relevant results found in other work. MT = Mackenzie at Tsiigehtchic, AR = Arctic Red, PR = Peel River, MD = Mackenzie at Inuvik/Delta. SA = Surface Area, C_{org} = organic carbon, POC = Particulate Organic Carbon, DOC = Dissolved Organic Carbon, TSS = Total suspended sediment.

What	Where	Value	Reference
Al		8.72 %	
Si		25.4 %	
Ca	Suspended sediment	2.59 %	Viers et al. (2009)
Ti		0.44 %	
	Bank and channel sediment	0.15 – 0.22	Vonk et al. (2015a)
		MT, MD, PR	
Al/Si		MT 0.08 – 0.36	
	Suspended Load	AR 0.30 – 0.31	Hilton et al. (2015)
		PR 0.10 – 0.29	
		MD 0.15 – 0.40	
SA	Bank and channel sediment	MT 12 m ² /g	Vonk et al. (2015a)
		PR 11 m ² /g	
		MD 7.3 m ² /g	
	Bank and channel sediment	MT 1.24 %	Vonk et al. (2015a)
		PR 0.78 %	
		MD 1.1 %	
		0.16 – 1.62 %	
C_{org}		MT	
	Suspended Load	AR 1.95 – 2.17 %	Hilton et al. (2015)
		PR 0.75 – 2.27 %	
		MD 0.37 – 2.71 %	
		MT	
		Bulk 0.99 %	
		150 – 250 μ m 2.02 %	
C_{org}	Bank sediment, size fractions	MT, PR	Hilton et al. (2015)
		63 – 150 μ m 1.01 %	
		< 63 μ m 1.06 %	
		PR	
		Bulk 2.02 %	
		< 63 μ m 1.63 %	
POC	Flux	Mackenzie River	Hilton et al. (2015)
		0.758 ± 0.066 Tg yr ⁻¹	McClelland et al. (2016)
		0.317 Tg yr ⁻¹	Le Fouest et al. (2013)
		1.797 Tg yr ⁻¹	Gareis and Lesack (2017)
DOC	Flux	Mackenzie River	Le Fouest et al. (2013)
		1.575 Tg yr ⁻¹	Raymond et al. (2007)
		1.4 Tg yr ⁻¹	Carson et al. (1998)
		MT 96 Tg yr ⁻¹	
		MT 51 Tg yr ⁻¹	Gareis and Lesack (2017)
TSS	Flux	MT, AR, PR, MD	
		AR 7.3 Tg yr ⁻¹	Carson et al. (1998)
		PR 20.8 Tg yr ⁻¹	
		MD 128 Tg yr ⁻¹	

6 Conclusion

This study allowed to look at organic and black carbon on different spatial scales. Both, organic carbon and black carbon, are distributed differently across the rivers and across different grain size fractions. Generally, the differences between rivers are larger and more obvious than differences between grain size fractions. Having said that, some major differences between particle sizes were also uncovered. Firstly, results confirmed that C_{org} and BC are associated with high surface area particles, most likely secondary minerals (i.e. clay). But the larger particles also transport high amounts of C_{org} and BC mostly likely from larger fragments of plants and charcoaled material.

Interestingly it looks like they might be able to transport these high amounts of PBC and POC out onto the shelf and into sediments. The total flux of POC (1.7 ± 0.7 Mt) and PBC in 2017 (0.362 ± 0.090) was large and in agreement with assessments from previous years.

The mass balance provided information about the distribution of grain size fractions in the different rivers. It is now clear that the sedimentological setting in the delta is complex, as distribution of grain size fractions in the delta does not correspond to the inputs. This highlights the need to use bulk samples for suspended and riverbank sediments. This adds weight to the argumentation of Parsons et al. (2015), that there is no real reason for the differentiation between suspended sediment and bed load.

The initial research questions can now be answered:

- Do grain size fractions show differences in geochemical characteristics?
 - Yes, both the climate relevant substances (C_{org} , BC) as well as indicators for minerals and sediment processing (Al, Si, Ti, Ca) clearly show differences.
- Do observed differences exhibit a trend or relationship to grain size?
 - Yes, C_{org} and BC are high in the largest as well as the smallest grain size fraction, where they are sourced and stabilized by different mechanisms. In larger grain size fractions, they are sourced from plant biomass fragments and charcoal residues. In smallest grain size fractions, they are attached to minerals. Indicators for minerals show a trend towards higher values for smaller grain size fractions (Al, Si, Ti).
- How do differences between river and grain size fractions compare?
 - Differences between rivers are generally clearer than between grain size fractions. The rivers drain different catchments and they travel different distances across the Interior Plains. This results in different sediment budget and different composition. Titanium and mineral specific surface

area, as well as BC are higher in the Peel River and the Arctic Red River than in the Mackenzie River. Calcium is lower in the Peel River and the Arctic Red River than in the Mackenzie River. C_{org} is highest on average in the Arctic Red River.

- How large was the total flux of C_{org} and BC?
 - The total flux of POC was 1.7 ± 0.7 Mt and that of PBC was 0.362 ± 0.090 Mt in 2017.
- How large was the grain size specific flux?
 - The larger grain size fractions account for the largest part of the export, because they account for more mass of the sediment. Some evidence points at the possibility that these larger grains can also be exported through the delta.

In conclusion this implies that no single grain size fraction is evidently a sink for C_{org} and BC. The freshet seems to keep a large variety of grain sizes in suspension and can transport them into the delta and likely onto the shelf. However, the burial rate on the shelf is high and thus the potential sink is large.

7 Outlook

The observed variability between grain size fractions deserves more attention and should be explored in the future with an optimized setup. Replicates would be required to account for both spatial and temporal heterogeneity. This could be achieved by taking several samples from the same site, thereby creating real replicates. As also the timing affects the results, it is advisable to take samples on several days before, throughout and after the freshet. This would allow to draw statistically meaningful conclusions. By collecting both suspended and bed load sediment as well as riverbank sediment at the same time, it would be possible to further our understanding of differences and similarities between these two types of sediment.

Another interesting aspect would be to measure the age of the exported constituents in the different grain size fractions. It has already been shown that the Mackenzie River exports very old, potentially permafrost derived and pre-aged POC. The age and provenance of POC changes with the hydrology and thus a combination of the spatially and temporally improved sampling with dating techniques would be very interesting.

As research in the area is in the process of uncovering many more details about the Mackenzie Basin and especially the delta and shelf dynamics, this work adds valuable information about the amount and location of C_{org} and BC.

8 Limitations

The main drawbacks for the present work concern the variability and the precision of measurements. As the relatively large error ranges denote, the precision required to draw decisive results concerning the different grain size fractions are quite high. Therefore, improved methods would be highly beneficial. Some problems that caused these issues are clear. For instance more precise measurements could be achieved when pressing samples into pellets for x-ray fluorescence (Jenkins, 2012). Another matter for concern was the mid-IR spectrometry. Here it is highly advisable to dilute a powdered sample with KBr to reduce sources of interference. Then it needs to be stated that the approximation of C_{org} is not optimal. Although it is possible to derive information about C_{org} from mid-IR spectrometry, it should not be conducted with less than 50 samples. Finally, it would be important to have the stable carbon and stable nitrogen isotopic signature as well as absolute carbon and nitrogen amounts for more detailed analyses and provenance studies. This data was unfortunately not available for all samples (C_{org}), or not at all provided (nitrogen) and thus was only touched upon.

Finally, neither the hydrodynamic differences nor the geochemical differences are well enough established in the literature. For the present work this means that observed differences could also be influenced by differences in sediment type.

References

- AMETEK Spectro: XRF Spectrometer: <https://www.spectro.com/products/xrf-spectrometer>, last access: 28 April 2019.
- Aufdenkampe, A. K., Mayorga, E., Raymond, P. A., Melack, J. M., Doney, S. C., Alin, S. R., Aalto, R. E., and Yoo, K.: Riverine coupling of biogeochemical cycles between land, oceans, and atmosphere, *Frontiers in Ecology and the Environment*, 9, 53–60, doi:10.1890/100014, 2011.
- Battin, T. J., Luysaert, S., Kaplan, L. A., Aufdenkampe, A. K., Richter, A., and Tranvik, L. J.: The boundless carbon cycle, *Nature Geosci*, 2, 598–600, doi:10.1038/ngeo618, 2009.
- Berden, G. and Engeln, R.: Cavity ring-down spectroscopy: Techniques and applications, Wiley, Chichester U.K., xix, 322 [2] of plates, 2009.
- Bird, M. I. and Ascough, P. L.: Isotopes in pyrogenic carbon: A review, *Organic Geochemistry*, 42, 1529–1539, doi:10.1016/j.orggeochem.2010.09.005, 2012.
- Bird, M. I., Wynn, J. G., Saiz, G., Wurster, C. M., and McBeath, A.: The Pyrogenic Carbon Cycle, *Annu. Rev. Earth Planet. Sci.*, 43, 273–298, doi:10.1146/annurev-earth-060614-105038, 2015.
- Blair, N. E. and Aller, R. C.: The fate of terrestrial organic carbon in the marine environment, *Annual review of marine science*, 4, 401–423, doi:10.1146/annurev-marine-120709-142717, 2012.
- Bornemann, L., Welp, G., Brodowski, S., Rodionov, A., and Amelung, W.: Rapid assessment of black carbon in soil organic matter using mid-infrared spectroscopy, *Organic Geochemistry*, 39, 1537–1544, doi:10.1016/j.orggeochem.2008.07.012, 2008.
- Bouchez, J., Gaillardet, J., France-Lanord, C., Maurice, L., and Dutra-Maia, P.: Grain size control of river suspended sediment geochemistry: Clues from Amazon River depth profiles, *Geochem. Geophys. Geosyst.*, 12, n/a-n/a, doi:10.1029/2010GC003380, 2011.
- Box, J. E., Colgan, W. T., Christensen, T. R., Schmidt, N. M., Lund, M., Parmentier, F.-J. W., Brown, R., Bhatt, U. S., Euskirchen, E. S., Romanovsky, V. E., Walsh, J. E., Overland, J. E., Wang, M., Corell, R. W., Meier, W. N., Wouters, B., Mernild, S., Mård, J., Pawlak, J., and Olsen, M. S.: Key indicators of Arctic climate change: 1971–2017, *Environ. Res. Lett.*, 14, 45010, doi:10.1088/1748-9326/aafc1b, 2019.
- Brodowski, S., Rodionov, A., Haumaier, L., Glaser, B., and Amelung, W.: Revised black carbon assessment using benzene polycarboxylic acids, *Organic Geochemistry*, 36, 1299–1310, doi:10.1016/j.orggeochem.2005.03.011, 2005.
- Brunauer, S., Emmett, P. H., and Teller, E.: Adsorption of Gases in Multimolecular Layers, *J. Am. Chem. Soc.*, 60, 309–319, doi:10.1021/ja01269a023, 1938.

- Burt, T. P. and Allison, R. J. (Eds.): *Sediment cascades: An integrated approach*, Wiley, Chichester, West Sussex, Hoboken, NJ, 471 pp., 2010.
- Carpenter, S. R., Stanley, E. H., and Vander Zanden, M. J.: State of the World's Freshwater Ecosystems: Physical, Chemical, and Biological Changes, *Annu. Rev. Environ. Resour.*, 36, 75–99, doi:10.1146/annurev-environ-021810-094524, 2011.
- Carson, M. A., Jasper, J. N., and Conly, F. M.: Magnitude and Sources of Sediment Input to the Mackenzie Delta, Northwest Territories, 1974–94, *Arctic*, 51, 116–124, 1998.
- Chatterjee, S., Santos, F., Abiven, S., Itin, B., Stark, R. E., and Bird, J. A.: Elucidating the chemical structure of pyrogenic organic matter by combining magnetic resonance, mid-infrared spectroscopy and mass spectrometry, *Organic Geochemistry*, 51, 35–44, doi:10.1016/j.orggeochem.2012.07.006, 2012.
- Che, M. and Védrine, J. C.: *Characterization of solid materials and heterogeneous catalysts: From structure to surface reactivity / edited by Michel Che and Jacques C. Védrine*, Wiley-VCH; [Chichester John Wiley, Weinheim, 2012.
- Chen, Y., Zou, C., Mastalerz, M., Hu, S., Gasaway, C., and Tao, X.: Applications of Micro-Fourier Transform Infrared Spectroscopy (FTIR) in the Geological Sciences--A Review, *International journal of molecular sciences*, 16, 30223–30250, doi:10.3390/ijms161226227, 2015.
- Christ: Alpha 2-4 LSCbasic: <https://www.martinchrist.de/en/products/laboratory/product/p/pr/s/alpha-2-4-lscbasic/>, last access: 28 April 2019.
- Clark, J. M., Bottrell, S. H., Evans, C. D., Monteith, D. T., Bartlett, R., Rose, R., Newton, R. J., and Chapman, P. J.: The importance of the relationship between scale and process in understanding long-term DOC dynamics, *The Science of the total environment*, 408, 2768–2775, doi:10.1016/j.scitotenv.2010.02.046, 2010.
- Coates, J.: *Interpretation of Infrared Spectra, A Practical Approach*, in: *Encyclopedia of analytical chemistry: Applications, theory and instrumentation*, Meyers, R. A. (Ed.), Wiley, Chichester, 2000.
- Cohen, J.: A power primer, *Psychological Bulletin*, 112, 155–159, doi:10.1037//0033-2909.112.1.155, 1992.
- Cole, J. J., Prairie, Y. T., Caraco, N. F., McDowell, W. H., Tranvik, L. J., Striegl, R. G., Duarte, C. M., Kortelainen, P., Downing, J. A., Middelburg, J. J., and Melack, J.: Plumbing the Global Carbon Cycle: Integrating Inland Waters into the Terrestrial Carbon Budget, *Ecosystems*, 10, 172–185, doi:10.1007/s10021-006-9013-8, 2007.
- Coppola, A. I., Wiedemeier, D. B., Galy, V., Haghypour, N., Hanke, U. M., Nascimento, G. S., Usman, M., Blattmann, T. M., Reisser, M., Freymond, C. V., Zhao, M., Voss, B., Wacker, L., Schefuß, E., Peucker-Ehrenbrink, B., Abiven, S., Schmidt, M. W. I., and Eglinton, T. I.: Global-scale evidence for the refractory nature of riverine black carbon, *Nature Geosci*, 11, 584–588, doi:10.1038/s41561-018-0159-8, 2018.

- Coppola, A. I., Ziolkowski, L. A., and Druffel, E. R. M.: Extraneous Carbon Assessments in Radiocarbon Measurements of Black Carbon in Environmental Matrices, *Radiocarbon*, 55, 1631–1640, doi:10.1017/S0033822200048542, 2013.
- Droppo, I. G.: Rethinking what constitutes suspended sediment, *Hydrol. Process.*, 15, 1551–1564, doi:10.1002/hyp.228, 2001.
- Droppo, I. G., D’Andrea, L., Krishnappan, B. G., Jaskot, C., Trapp, B., Basuvaraj, M., and Liss, S. N.: Fine-sediment dynamics: Towards an improved understanding of sediment erosion and transport, *J Soils Sediments*, 15, 467–479, doi:10.1007/s11368-014-1004-3, 2015.
- Dumont, H. J., Davies, B. R., and Walker, K. F.: *The Ecology of River Systems*, 60, Springer Netherlands, Dordrecht, 1986.
- Egli, M., Lessovaia, S. N., Chistyakov, K., Inozemzev, S., Polekhovsky, Y., and Ganyushkin, D.: Microclimate affects soil chemical and mineralogical properties of cold alpine soils of the Altai Mountains (Russia), *J Soils Sediments*, 15, 1420–1436, doi:10.1007/s11368-013-0838-4, 2015.
- Emerson, S. and Hedges, J. I.: Processes controlling the organic carbon content of open ocean sediments, *Paleoceanography*, 3, 621–634, doi:10.1029/PA003i005p00621, 1988.
- Emmerton, C. A., Lesack, L. F. W., and Marsh, P.: Lake abundance, potential water storage, and habitat distribution in the Mackenzie River Delta, western Canadian Arctic, *Water Resour. Res.*, 43, 14,485, doi:10.1029/2006WR005139, 2007.
- Encyclopaedia Britannica: Ion-Exchange Resin: <https://academic.eb.com/levels/collegiate/article/ion-exchange-resin/42691>, last access: 2018.
- Estilow, T. W., Young, A. H., and Robinson, D. A.: A long-term Northern Hemisphere snow cover extent data record for climate studies and monitoring, *Earth Syst. Sci. Data*, 7, 137–142, doi:10.5194/essd-7-137-2015, 2015.
- Feng, X., Vonk, J. E., van Dongen, B. E., Gustafsson, Ö., Semiletov, I. P., Dudarev, O. V., Wang, Z., Montluçon, D. B., Wacker, L., and Eglinton, T. I.: Differential mobilization of terrestrial carbon pools in Eurasian Arctic river basins, *Proceedings of the National Academy of Sciences of the United States of America*, 110, 14168–14173, doi:10.1073/pnas.1307031110, 2013.
- Feynman, R. P. and Leighton, R.: 'What do you care what other people think?': Further adventures of a curious character / Richard P. Feynman as told to Ralph Leighton, Penguin, London, 2007.
- Flannigan, M., Stocks, B., Turetsky, M., and Wotton, M.: Impacts of climate change on fire activity and fire management in the circumboreal forest, *Global change biology*, 15, 549–560, doi:10.1111/j.1365-2486.2008.01660.x, 2009.

- Fox, J. and Weisberg, S.: *An R Companion to Applied Regression*, Second, Sage, Thousand Oaks CA, 2011.
- Freymond, C. V., Kündig, N., Stark, C., Peterse, F., Buggle, B., Lupker, M., Plötze, M., Blattmann, T. M., Filip, F., Giosan, L., and Eglinton, T. I.: Evolution of biomolecular loadings along a major river system, *Geochimica et Cosmochimica Acta*, 223, 389–404, doi:10.1016/j.gca.2017.12.010, 2018.
- Fry, B.: *Stable isotope ecology*, Springer, New York, N.Y., London, 2006.
- Gaillardet, J., Viers, J., and Dupré, B.: Trace Elements in River Waters, in: *Treatise on Geochemistry*, Elsevier, 195–235, 2014.
- Galy, V., France-Lanord, C., Beyssac, O., Faure, P., Kudrass, H., and Palhol, F.: Efficient organic carbon burial in the Bengal fan sustained by the Himalayan erosional system, *Nature*, 450, 407–410, doi:10.1038/nature06273, 2007.
- Galy, V., Peucker-Ehrenbrink, B., and Eglinton, T.: Global carbon export from the terrestrial biosphere controlled by erosion, *Nature*, 521, 204–207, doi:10.1038/nature14400, 2015.
- Gareis, J. A. L. and Lesack, L. F. W.: Fluxes of particulates and nutrients during hydrologically defined seasonal periods in an ice-affected great Arctic river, the Mackenzie, *Water Resour. Res.*, 53, 6109–6132, doi:10.1002/2017WR020623, 2017.
- Gilvear, D. (Ed.): *River systems: Research and management for the 21st century*, John Wiley & Sons, Hoboken NJ, pages cm, 2016.
- Glaser, B., Haumaier, L., Guggenberger, G., and Zech, W.: Black carbon in soils: The use of benzenecarboxylic acids as specific markers, *Organic Geochemistry*, 29, 811–819, doi:10.1016/S0146-6380(98)00194-6, 1998.
- Global Carbon Project: *Global Carbon Atlas*: <http://www.globalcarbonatlas.org/en/CO2-emissions>, last access: 28 April 2019.
- Grabowski, R. C., Droppo, I. G., and Wharton, G.: Erodibility of cohesive sediment: The importance of sediment properties, *Earth-Science Reviews*, 105, 101–120, doi:10.1016/j.earscirev.2011.01.008, 2011.
- Grabowski, R. C., Wharton, G., Davies, G. R., and Droppo, I. G.: Spatial and temporal variations in the erosion threshold of fine riverbed sediments, *J Soils Sediments*, 12, 1174–1188, doi:10.1007/s11368-012-0534-9, 2012.
- Griffiths, P. R. and Haseth, J. A. de: *Fourier Transform Infrared Spectrometry*, John Wiley & Sons, Inc, Hoboken, NJ, USA, 2007.
- Grotzinger, J. P. and Jordan, T. H.: *Understanding Earth*, 6th ed., W.H. Freeman, New York, 1 v. (various pagings), 2010.
- Guo, L., Ping, C.-L., and Macdonald, R. W.: Mobilization pathways of organic carbon from permafrost to arctic rivers in a changing climate, *Geophys. Res. Lett.*, 34, n/a-n/a, doi:10.1029/2007GL030689, 2007.

- Guo, Y., Yang, S., Su, N., Li, C., Yin, P., and Wang, Z.: Revisiting the effects of hydrodynamic sorting and sedimentary recycling on chemical weathering indices, *Geochimica et Cosmochimica Acta*, 227, 48–63, doi:10.1016/j.gca.2018.02.015, 2018.
- Hammes, K. and Abiven, S.: Identification of Black Carbon in the Earth System, in: *Fire phenomena and the Earth system: An interdisciplinary guide to fire science*, Belcher, C. M. (Ed.), Wiley-Blackwell, Chichester West Sussex UK, Hoboken NJ, 2013.
- Hammes, K., Schmidt, M. W. I., Smernik, R. J., Currie, L. A., Ball, W. P., Nguyen, T. H., Louchouart, P., Houel, S., Gustafsson, Ö., Elmquist, M., Cornelissen, G., Skjemstad, J. O., Masiello, C. A., Song, J., Peng, P. a., Mitra, S., Dunn, J. C., Hatcher, P. G., Hockaday, W. C., Smith, D. M., Hartkopf-Fröder, C., Böhmer, A., Luer, B., Huebert, B. J., Amelung, W., Brodowski, S., Huang, L., Zhang, W., Gschwend, P. M., Flores-Cervantes, D. X., Largeau, C., Rouzaud, J.-N., Rumpel, C., Guggenberger, G., Kaiser, K., Rodionov, A., Gonzalez-Vila, F. J., Gonzalez-Perez, J. A., La Rosa, J. M. de, Manning, D. A. C., López-Capél, E., and Ding, L.: Comparison of quantification methods to measure fire-derived (black/elemental) carbon in soils and sediments using reference materials from soil, water, sediment and the atmosphere, *Global Biogeochem. Cycles*, 21, n/a-n/a, doi:10.1029/2006GB002914, 2007.
- Hammes, K., Smernik, R. J., Skjemstad, J. O., Herzog, A., Vogt, U. F., and Schmidt, M. W. I.: Synthesis and characterisation of laboratory-charred grass straw (*Oryza sativa*) and chestnut wood (*Castanea sativa*) as reference materials for black carbon quantification, *Organic Geochemistry*, 37, 1629–1633, doi:10.1016/j.orggeochem.2006.07.003, 2006.
- Heininger, P. and Cullmann, J.: *Sediment matters*, Springer, Cham, 2015.
- Hilton, R. G., Galy, A., Hovius, N., Horng, M.-J., and Chen, H.: The isotopic composition of particulate organic carbon in mountain rivers of Taiwan, *Geochimica et Cosmochimica Acta*, 74, 3164–3181, doi:10.1016/j.gca.2010.03.004, 2010.
- Hilton, R. G., Galy, V., Gaillardet, J., Dellinger, M., Bryant, C., O'Regan, M., Gröcke, D. R., Coxall, H., Bouchez, J., and Calmels, D.: Erosion of organic carbon in the Arctic as a geological carbon dioxide sink, *Nature*, 524, 84–87, doi:10.1038/nature14653, 2015.
- Holmes, R. M., McClelland, J. W., Peterson, B. J., Tank, S. E., Bulygina, E., Eglinton, T. I., Gordeev, V. V., Gurtovaya, T. Y., Raymond, P. A., Repeta, D. J., Staples, R., Striegl, R. G., Zhulidov, A. V., and Zimov, S. A.: Seasonal and Annual Fluxes of Nutrients and Organic Matter from Large Rivers to the Arctic Ocean and Surrounding Seas, *Estuaries and Coasts*, 35, 369–382, doi:10.1007/s12237-011-9386-6, 2012.
- Honjo, S., Krishfield, R. A., Eglinton, T. I., Manganini, S. J., Kemp, J. N., Doherty, K., Hwang, J., McKee, T. K., and Takizawa, T.: Biological pump processes in the cryopelagic and hemipelagic Arctic Ocean: Canada Basin and Chukchi Rise, *Progress in Oceanography*, 85, 137–170, doi:10.1016/j.pocean.2010.02.009, 2010.

- Hugelius, G., Strauss, J., Zubrzycki, S., Harden, J. W., Schuur, E. A. G., Ping, C.-L., Schirmer, L., Grosse, G., Michaelson, G. J., Koven, C. D., O'Donnell, J. A., Elberling, B., Mishra, U., Camill, P., Yu, Z., Palmtag, J., and Kuhry, P.: Estimated stocks of circumpolar permafrost carbon with quantified uncertainty ranges and identified data gaps, *Biogeosciences*, 11, 6573–6593, doi:10.5194/bg-11-6573-2014, 2014.
- IPCC: Climate Change 2013: The Physical Science Basis.: Contribution of Working Group I to the Fifth Assessment Report of the Intergovernmental Panel on Climate Change, Cambridge University Press, Cambridge, United Kingdom and New York, NY, USA, 1535 pp., 2013.
- Jenkins, R.: X-Ray Fluorescence Spectrometry, 2. ed., Chemical Analysis, Wiley, New York, 230 pp., 2012.
- Koiter, A. J., Owens, P. N., Petticrew, E. L., and Lobb, D. A.: The behavioural characteristics of sediment properties and their implications for sediment fingerprinting as an approach for identifying sediment sources in river basins, *Earth-Science Reviews*, 125, 24–42, doi:10.1016/j.earscirev.2013.05.009, 2013.
- Kuhnle, R. A.: 9.9 Suspended Load, in: *Treatise on Geomorphology*, Elsevier, 124–136, 2013.
- Lalande, C., Forest, A., Barber, D. G., Gratton, Y., and Fortier, L.: Variability in the annual cycle of vertical particulate organic carbon export on Arctic shelves: Contrasting the Laptev Sea, Northern Baffin Bay and the Beaufort Sea, *Continental Shelf Research*, 29, 2157–2165, doi:10.1016/j.csr.2009.08.009, 2009.
- Lange, M. F. de, Vlugt, T. J.H., Gascon, J., and Kapteijn, F.: Adsorptive characterization of porous solids: Error analysis guides the way, *Microporous and Mesoporous Materials*, 200, 199–215, doi:10.1016/j.micromeso.2014.08.048, 2014.
- Laudon, H., Berggren, M., Ågren, A., Buffam, I., Bishop, K., Grabs, T., Jansson, M., and Köhler, S.: Patterns and Dynamics of Dissolved Organic Carbon (DOC) in Boreal Streams: The Role of Processes, Connectivity, and Scaling, *Ecosystems*, 14, 880–893, doi:10.1007/s10021-011-9452-8, 2011.
- Laxon, S. W., Giles, K. A., Ridout, A. L., Wingham, D. J., Willatt, R., Cullen, R., Kwok, R., Schweiger, A., Zhang, J., Haas, C., Hendricks, S., Krishfield, R., Kurtz, N., Farrell, S., and Davidson, M.: CryoSat-2 estimates of Arctic sea ice thickness and volume, *Geophys. Res. Lett.*, 40, 732–737, doi:10.1002/grl.50193, 2013.
- Le Fouest, V., Babin, M., and Tremblay, J.-É.: The fate of riverine nutrients on Arctic shelves, *Biogeosciences*, 10, 3661–3677, doi:10.5194/bg-10-3661-2013, 2013.
- Lecce, S. A. and Pavlowsky, R. T.: Spatial and temporal variations in the grain-size characteristics of historical flood plain deposits, Blue River, Wisconsin, USA, *Geomorphology*, 61, 361–371, doi:10.1016/j.geomorph.2004.01.008, 2004.

- LibreTexts: Infrared Spectroscopy Absorption Table: https://chem.libretexts.org/Ancillary_Materials/Reference/Reference_Tables/Spectroscopic_Parameters/Infrared_Spectroscopy_Absorption_Table, last access: 28 April 2019.
- Mann, P. J., Eglinton, T. I., McIntyre, C. P., Zimov, N., Davydova, A., Vonk, J. E., Holmes, R. M., and Spencer, R. G. M.: Utilization of ancient permafrost carbon in headwaters of Arctic fluvial networks, *Nature communications*, 6, 7856, doi:10.1038/ncomms8856, 2015.
- Martin, A. C., Jeffers, E. S., Petrokofsky, G., Myers-Smith, I., and Macias-Fauria, M.: Shrub growth and expansion in the Arctic tundra: An assessment of controlling factors using an evidence-based approach, *Environ. Res. Lett.*, 12, 85007, doi:10.1088/1748-9326/aa7989, 2017.
- Mayer, L. M.: Relationships between mineral surfaces and organic carbon concentrations in soils and sediments, *Chemical Geology*, 114, 347–363, doi:10.1016/0009-2541(94)90063-9, 1994.
- McClelland, J. W., Holmes, R. M., Peterson, B. J., Raymond, P. A., Striegl, R. G., Zhulidov, A. V., Zimov, S. A., Zimov, N., Tank, S. E., Spencer, R. G. M., Staples, R., Gurtovaya, T. Y., and Griffin, C. G.: Particulate organic carbon and nitrogen export from major Arctic rivers, *Global Biogeochem. Cycles*, 30, 629–643, doi:10.1002/2015GB005351, 2016.
- McGuire, A. D., Chapin, F. S., Walsh, J. E., and Wirth, C.: Integrated Regional Changes in Arctic Climate Feedbacks: Implications for the Global Climate System, *Annu. Rev. Environ. Resour.*, 31, 61–91, doi:10.1146/annurev.energy.31.020105.100253, 2006.
- McKelvy, M. L.: Infrared Spectroscopy: Introduction, in: *Encyclopedia of analytical chemistry: Applications, theory and instrumentation*, Meyers, R. A. (Ed.), Wiley, Chichester, 2000.
- Mevik, B.-H. and Wehrens, R.: The pls Package: Principal Component and PartialLeast Squares Regression in R, *Journal of Statistical Software*, 18, 2007.
- Mevik, B.-H. and Wehrens, R.: Introduction to the pls Package, University Center for Information Technology, University of Oslo, Norway; Wageningen University & Research, Netherlands, 24 pp., 2018a.
- Mevik, B.-H. and Wehrens, R.: Introduction to the pls Package: Vignette, 2018b.
- Milliman, J. D. and Farnsworth, K. L.: *River Discharge to the Coastal Ocean*, Cambridge University Press, Cambridge, 2011.
- MilliporeSigma: Milli-Q: Integral Water Purification System for Ultrapure Water: http://www.emdmillipore.com/US/en/product/Milli-Q-Integral-Water-Purification-System-for-Ultrapure-Water,MM_NF-C72876?bd=1, last access: 28 April 2019.
- Mook, W. G.: *Environmental Isotopes in the Hydrological Cycle: Principles and Applications*, Volume 2; Atmospheric Water, International Atomic Energy Agency, Internet, 73 pp., 2001.

- Natural Resources Canada: Orthoimages of Canada 1999-2003: <https://open.canada.ca/data/en/dataset/560351c7-061f-442f-9539-e38bb453ccbf>, last access: 28 April 2019.
- NIST: Certificate of Analysis: Standard Reference Material 1941b, Organics in Marine Sediment, Internet, 2015.
- NWT Centre for Geomatics: GNWT Simplified Basemap: https://www.apps.geomatics.gov.nt.ca/arcgis/rest/services/GNWT_Basemaps/GNWT_Simplified_Basemap/MapServer/info/iteminfo, last access: 28 April 2019.
- Osborne, E., Richter-Menge, J., and Jeffries, M. (Eds.): Arctic Report Card 2018, National Oceanic and Atmospheric Administration, 114 pp., 2018.
- Overeem, I. and Syvitski, J. P. M.: Shifting discharge peaks in arctic rivers, 1977–2007, *Geografiska Annaler: Series A, Physical Geography*, 92, 285–296, doi:10.1111/j.1468-0459.2010.00395.x, 2016.
- Owens, P. N.: Sediment behaviour, functions and management in river basins, in: *Sediment Management at the River Basin Scale, Sustainable Management of Sediment Resources*, Elsevier, 1–29, 2008.
- Parsons, A. J., Cooper, J., and Wainwright, J.: What is suspended sediment?, *Earth Surf. Process. Landforms*, 40, 1417–1420, doi:10.1002/esp.3730, 2015.
- Parsons, A. J., Cooper, J., Wainwright, J., and Sekiguchi, T.: Virtual velocity of sand transport in water, *Earth Surf. Process. Landforms*, 43, 755–761, doi:10.1002/esp.4262, 2018.
- PICARRO: Picarro G2131-i Datasheet 171227: https://www.picarro.com/support/library/documents/g2131_i_analyzer_datasheet_data_sheet, last access: 28 April 2019.
- PICARRO: Cavity Ring-Down Spectroscopy: <https://www.picarro.com/company/technology/crds>, last access: 28 April 2019.
- Power, M. J.: A 21 000-Year History of Fire, in: *Fire phenomena and the Earth system: An interdisciplinary guide to fire science*, Belcher, C. M. (Ed.), Wiley-Blackwell, Chichester West Sussex UK, Hoboken NJ, 2013.
- Preston, C. M. and Schmidt, M. W. I.: Black (pyrogenic) carbon: A synthesis of current knowledge and uncertainties with special consideration of boreal regions, *Biogeosciences*, 3, 397–420, doi:10.5194/bg-3-397-2006, 2006.
- QGIS Development Team: QGIS Geographic Information System: Open Source Geospatial Foundation Project: <https://qgis.org/en/site/>, last access: 28 April 2019.
- Quantachrome Instruments: FloVac® Degasser: Gas Sorption Sample Preparation: http://quantachrome.com/gassorption/flovac_degasser.html, last access: 28 April 2019.
- Quantachrome Instruments: NOVA SURFACE AREA AND PORE SIZE BY GAS SORPTION: http://www.quantachrome.com/gassorption/nova_series.html, last access: 28 April 2019.

- Randerson, J. T., Chen, Y., van der Werf, G. R., Rogers, B. M., and Morton, D. C.: Global burned area and biomass burning emissions from small fires, *J. Geophys. Res.*, 117, n/a-n/a, doi:10.1029/2012JG002128, 2012.
- Raymond, P. A., McClelland, J. W., Holmes, R. M., Zhulidov, A. V., Mull, K., Peterson, B. J., Striegl, R. G., Aiken, G. R., and Gurtovaya, T. Y.: Flux and age of dissolved organic carbon exported to the Arctic Ocean: A carbon isotopic study of the five largest arctic rivers, *Global Biogeochem. Cycles*, 21, n/a-n/a, doi:10.1029/2007GB002934, 2007.
- Regnier, P., Friedlingstein, P., Ciais, P., Mackenzie, F. T., Gruber, N., Janssens, I. A., Laruelle, G. G., Lauerwald, R., Luysaert, S., Andersson, A. J., Arndt, S., Arnosti, C., Borges, A. V., Dale, A. W., Gallego-Sala, A., Godd eris, Y., Goossens, N., Hartmann, J., Heinze, C., Ilyina, T., Joos, F., LaRowe, D. E., Leifeld, J., Meysman, F. J. R., Munhoven, G., Raymond, P. A., Spahni, R., Suntharalingam, P., and Thullner, M.: Anthropogenic perturbation of the carbon fluxes from land to ocean, *Nature Geosci*, 6, 597–607, doi:10.1038/NGEO1830, 2013.
- Reichle, L. M., Epstein, H. E., Bhatt, U. S., Raynolds, M. K., and Walker, D. A.: Spatial Heterogeneity of the Temporal Dynamics of Arctic Tundra Vegetation, *Geophys. Res. Lett.*, 45, 9206–9215, doi:10.1029/2018GL078820, 2018.
- Reisser, M., Purves, R. S., Schmidt, M. W. I., and Abiven, S.: Pyrogenic Carbon in Soils: A Literature-Based Inventory and a Global Estimation of Its Content in Soil Organic Carbon and Stocks, *Front. Earth Sci.*, 4, 1856, doi:10.3389/feart.2016.00080, 2016.
- Retsch: Mixer Mill MM 400: <https://www.retsch.com/products/milling/ball-mills/mixer-mill-mm-400/function-features/>, last access: 28 April 2019.
- Retsch: Vibratory Sieve Shaker AS 200 basic: <https://www.retsch.com/products/sieving/sieve-shakers/as-200-basic/function-features/>, last access: 28 April 2019.
- Retsch: Woven Wire Mesh Sieves: <https://www.retsch.com/products/sieving/test-sieves/mesh-sieves-200-203-mm/function-features/>, last access: 28 April 2019.
- Sant n, C., Doerr, S. H., Preston, C. M., and Gonz lez-Rodr guez, G.: Pyrogenic organic matter production from wildfires: A missing sink in the global carbon cycle, *Global change biology*, 21, 1621–1633, doi:10.1111/gcb.12800, 2015.
- S ntis Analytical AG: S ntis Analytical AG: <https://www.saentis-analytical.com/>, last access: 28 April 2019.
- Schmidt, M. W. I., Skjemstad, J. O., Gehrt, E., and Kogel-Knabner, I.: Charred organic carbon in German chernozemic soils, *Eur J Soil Science*, 50, 351–365, doi:10.1046/j.1365-2389.1999.00236.x, 1999.
- Schneider, M. P.W., Hilf, M., Vogt, U. F., and Schmidt, M. W.I.: The benzene polycarboxylic acid (BPCA) pattern of wood pyrolyzed between 200 C and 1000 C, *Organic Geochemistry*, 41, 1082–1088, doi:10.1016/j.orggeochem.2010.07.001, 2010.

- Schramel, P., Wolf, A., Seif, R., and Klose, B.-J.: Eine neue Apparatur zur Druckveraschung von biologischem Material, *Z. Anal. Chem.*, 302, 62–64, doi:10.1007/BF00469765, 1980.
- Schwab, M. S.: Coupled Organic and Inorganic Tracers of Particle Flux Processes in the North American Arctic Ocean, Master Thesis, Department of Earth Sciences, ETH Zürich, Zurich, 91 pp., 2016.
- Scott, A. C., Bowman, D. M. J. S., Bond, W. J., Pyne, S. J., and Alexander, M. E.: Fire on earth: An introduction / Andrew C. Scott, David M.J.S. Bowman, William J. Bond, Stephen J. Pyne, Martin E. Alexander, John Wiley & Sons, Chichester, West Sussex, 2014.
- Sigma-Aldrich: IR Spectrum Table by Frequency Range: <https://www.sigmaaldrich.com/technical-documents/articles/biology/ir-spectrum-table.html>, last access: 28 April 2019.
- Sly, P. G. and Hart, B. T.: Sediment/Water Interactions, Springer Netherlands, Dordrecht, 1989.
- Smith, S. L., Romanovsky, V. E., Lewkowicz, A. G., Burn, C. R., Allard, M., Clow, G. D., Yoshikawa, K., and Throop, J.: Thermal state of permafrost in North America: A contribution to the international polar year, *Permafrost Periglac. Process.*, 21, 117–135, doi:10.1002/ppp.690, 2010.
- Spencer, R. G. M., Mann, P. J., Dittmar, T., Eglinton, T. I., McIntyre, C., Holmes, R. M., Zimov, N., and Stubbins, A.: Detecting the signature of permafrost thaw in Arctic rivers, *Geophys. Res. Lett.*, 42, 2830–2835, doi:10.1002/2015GL063498, 2015.
- Stein, R. and Macdonald, R. W. (Eds.): The Organic Carbon Cycle in the Arctic Ocean, Springer Berlin, Berlin, XIX, 363 S. in 1 Teil, 2013.
- Stocks, B. J., Mason, J. A., Todd, J. B., Bosch, E. M., Wotton, B. M., Amiro, B. D., Flannigan, M. D., Hirsch, K. G., Logan, K. A., Martell, D. L., and Skinner, W. R.: Large forest fires in Canada, 1959–1997, *J. Geophys. Res.*, 108, 512, doi:10.1029/2001JD000484, 2003.
- Stuart, B. H.: Infrared Spectroscopy: Fundamentals and Applications, John Wiley & Sons, Ltd, Chichester, UK, 2004.
- Supelco: Bulletin 910: Guide to Solid Phase Extraction: <https://www.sigmaaldrich.com/Graphics/Supelco/objects/4600/4538.pdf>, last access: 28 April 2019.
- Tarnocai, C., Canadell, J. G., Schuur, E. A. G., Kuhry, P., Mazhitova, G., and Zimov, S.: Soil organic carbon pools in the northern circumpolar permafrost region, *Global Biogeochem. Cycles*, 23, n/a-n/a, doi:10.1029/2008GB003327, 2009.
- Team, R.: RStudio: Integrated Development Environment for R, Boston, MA: <http://www.rstudio.com/>, 2016.
- Team, R. C.: R: A Language and Environment for Statistical Computing, Vienna, Austria: <https://www.R-project.org/>, 2017.

- Turnewitsch, R., Springer, B. M., Kiriakoulakis, K., Vilas, J. C., Arístegui, J., Wolff, G., Peine, F., Werk, S., Graf, G., and Waniek, J. J.: Determination of particulate organic carbon (POC) in seawater: The relative methodological importance of artificial gains and losses in two glass-fiber-filter-based techniques, *Marine Chemistry*, 105, 208–228, doi:10.1016/j.marchem.2007.01.017, 2007.
- van Erp, T. S. and Martens, J. A.: A standardization for BET fitting of adsorption isotherms, *Microporous and Mesoporous Materials*, 145, 188–193, doi:10.1016/j.micromeso.2011.05.022, 2011.
- Venables, W. N. and Ripley, B. D.: *Modern Applied Statistics with S*, Fourth, Springer, New York, 2002.
- Viers, J., Dupré, B., and Gaillardet, J.: Chemical composition of suspended sediments in World Rivers: New insights from a new database, *The Science of the total environment*, 407, 853–868, doi:10.1016/j.scitotenv.2008.09.053, 2009.
- Vogel, H., Rosén, P., Wagner, B., Melles, M., and Persson, P.: Fourier transform infrared spectroscopy, a new cost-effective tool for quantitative analysis of biogeochemical properties in long sediment records, *J Paleolimnol*, 40, 689–702, doi:10.1007/s10933-008-9193-7, 2008.
- Vonk, J. E., Giosan, L., Blusztajn, J., Montlucon, D., Graf Pannatier, E., McIntyre, C., Wacker, L., Macdonald, R. W., Yunker, M. B., and Eglinton, T. I.: Spatial variations in geochemical characteristics of the modern Mackenzie Delta sedimentary system, *Geochimica et Cosmochimica Acta*, 171, 100–120, doi:10.1016/j.gca.2015.08.005, 2015a.
- Vonk, J. E., Tank, S. E., Bowden, W. B., Laurion, I., Vincent, W. F., Alekseychik, P., Amyot, M., Billet, M. F., Canário, J., Cory, R. M., Deshpande, B. N., Helbig, M., Jammet, M., Karlsson, J., Larouche, J., MacMillan, G., Rautio, M., Walter Anthony, K. M., and Wickland, K. P.: Reviews and syntheses: Effects of permafrost thaw on Arctic aquatic ecosystems, *Biogeosciences*, 12, 7129–7167, doi:10.5194/bg-12-7129-2015, 2015b.
- Walling, D. E., Owens, P. N., and Leeks, G.J.L.: The characteristics of overbank deposits associated with a major flood event in the catchment of the River Ouse, Yorkshire, UK, *CATENA*, 31, 53–75, doi:10.1016/S0341-8162(97)00034-9, 1997.
- Walling, D. E., Owens, P. N., Waterfall, B. D., Leeks, G. J.L., and Wass, P. D.: The particle size characteristics of fluvial suspended sediment in the Humber and Tweed catchments, UK, *Science of The Total Environment*, 251-252, 205–222, doi:10.1016/S0048-9697(00)00384-3, 2000.
- Ward, N. D., Bianchi, T. S., Medeiros, P. M., Seidel, M., Richey, J. E., Keil, R. G., and Sawakuchi, H. O.: Where Carbon Goes When Water Flows: Carbon Cycling across the Aquatic Continuum, *Front. Mar. Sci.*, 4, GB4007, doi:10.3389/fmars.2017.00007, 2017.

- Wiedemeier, D. B., Hilf, M. D., Smittenberg, R. H., Haberle, S. G., and Schmidt, M. W. I.: Improved assessment of pyrogenic carbon quantity and quality in environmental samples by high-performance liquid chromatography, *Journal of chromatography. A*, 1304, 246–250, doi:10.1016/j.chroma.2013.06.012, 2013.
- Wiedemeier, D. B., Lang, S. Q., Gierga, M., Abiven, S., Bernasconi, S. M., Früh-Green, G. L., Hajdas, I., Hanke, U. M., Hilf, M. D., McIntyre, C. P., Scheider, M. P. W., Smittenberg, R. H., Wacker, L., Wiesenberg, G. L. B., and Schmidt, M. W. I.: Characterization, Quantification and Compound-specific Isotopic Analysis of Pyrogenic Carbon Using Benzene Polycarboxylic Acids (BPCA), *Journal of visualized experiments JoVE*, doi:10.3791/53922, 2016.
- Williams, N. D., Walling, D. E., and Leeks, G. J. L.: An analysis of the factors contributing to the settling potential of fine fluvial sediment, *Hydrol. Process.*, 22, 4153–4162, doi:10.1002/hyp.7015, 2008.
- Woodward, J. C. and Walling, D. E.: Composite suspended sediment particles in river systems: Their incidence, dynamics and physical characteristics, *Hydrol. Process.*, 21, 3601–3614, doi:10.1002/hyp.6586, 2007.
- Yamada, M., Fujino, S., Goff, J., and Chagué-Goff, C.: Large-scale erosion and overbank deposition caused by the July 2013 flood of the Abu River, Yamaguchi City, Japan, *Island Arc*, 25, 386–399, doi:10.1111/iar.12162, 2016.
- Zimmerman, A. R. and Mitra, S.: Trial by Fire: On the Terminology and Methods Used in Pyrogenic Organic Carbon Research, *Front. Earth Sci.*, 5, 354, doi:10.3389/feart.2017.00095, 2017.
- Ziolkowski, L. A., Chamberlin, A. R., Greaves, J., and Druffel, E.R.M.: Quantification of black carbon in marine systems using the benzene polycarboxylic acid method: A mechanistic and yield study, *Limnol. Oceanogr. Methods*, 9, 140, doi:10.4319/lom.2011.9.140, 2011.

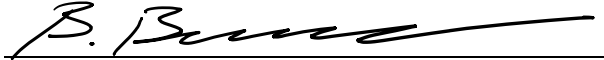
Declaration of Originality

Personal declaration: I hereby declare that the submitted thesis is the result of my own, independent work. All external sources are explicitly acknowledged in the thesis.

Place, Date

Windisch, April 28, 2019

Signature



Bastian S. Buman

Supplements

S-1. Methods

Sieving and Drying

About 200 g of sample were wet sieved into the different size fractions. In a first round, sieves of sizes 250 μm , 150 μm and 63 μm were used. The sample was sieved using Milli-Q ultra-pure water (MilliporeSigma, 2018), Retsch analysis sieves (Retsch, 2018c) and a Retsch sieve shaker AS 200 basic at 2 mm/g (Retsch, 2018b). Material was collected in plastic bags and frozen overnight. The frozen samples were subsequently freeze-dried ($-80\text{ }^{\circ}\text{C}$, 100 Pa, see Christ, 2018) until all water was removed. From the size fraction $< 63\text{ }\mu\text{m}$ about 90 % was further sieved down using sieves of sizes 32 μm and 20 μm (undergoing the exact same protocol).

Area under the curve

To calculate the area under the curve for aromatics-related bands, the libraries MESS (miscellaneous useful and semi-useful functions, Venables and Ripley, 2002) and CAR (companion to applied regression, Fox and Weisberg, 2011) were used inside the R (Team, 2017) and Rstudio (Team, 2016) statistical environment. Linear interpolation was used with 50 equally spaced points over the selected interval and the integration was done using 100 subintervals.

Partial Least Squares Regression

For this the R statistical software (Team, 2017) and the integrated development environment Rstudio (Team, 2016) with the pls package (Mevik and Wehrens, 2007; Mevik and Wehrens, 2018b) was used.

As in total only 18 samples had both OC and IR measured by primary means, the whole 18 samples were used for the training of the PLSR, thereby omitting a split of the samples with known composition into a training set (2/3) and a test set (1/3), to avoid poor PLSR quality (i.e. optimize learning). However, since a Leave-One-Out cross-validation procedure was selected, the model performance can still be evaluated.

S-2. Treatise of XRF Reproducibility and Error

XRF yields a final overview of the total element concentration as a sum of all the measurement elements, which should theoretically amount to near 100 % as otherwise something might not have been properly measured, this is a device internal processing that is not accessible for evaluation. For the present samples these summed-up concentration values ranged from around 60 % to around 100 %. Due to this, affected samples with very low total concentrations were measured again, to find out if these low values were reproducible. The selected samples are given in Table S-1 with the results for selected elements as well as the summed-up concentration values and the reference material series (soil standard).

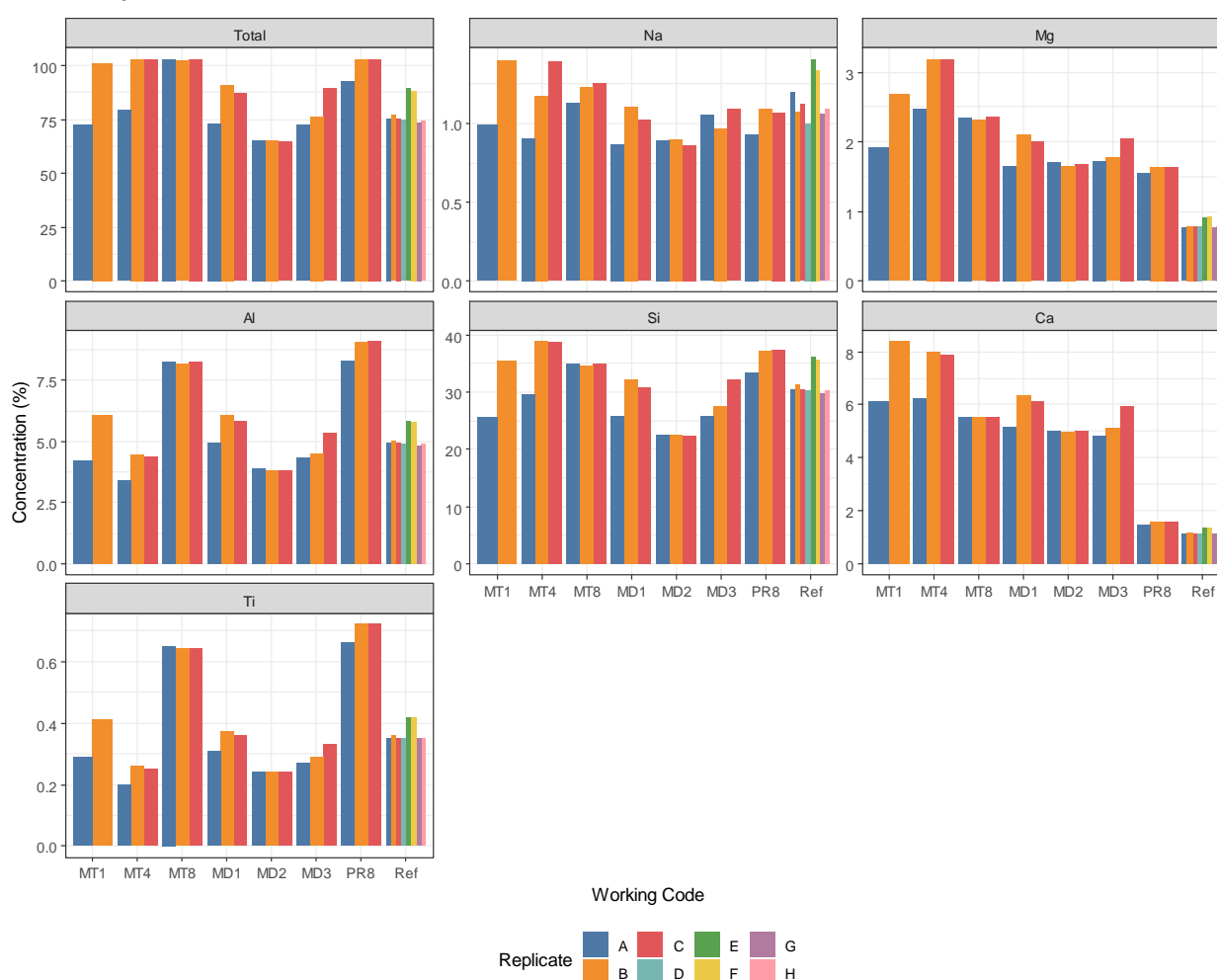


Figure S-1 Overview of the selected samples (MT1, MT4, MT8, MD1, MD2, MD3, PR8) and elements (Na, Mg, Al, Si, Ca, Ti), as well as the total concentration and the reference series (Ref), see Table S-1. Concentration has variable scales in this figure! Samples are indicated using their working code, where MT refers to Tsiigehtchic / Mackenzie, AR to Tsiigehtchic / Arctic Red, PR to Fort McPherson / Peel and MD to Inuvik / Mackenzie, the number refers to the particle size, with 1 being associated with bulk and 8 with <math>< 20 \mu\text{m}</math> (more details in Table 3-1).

The total amount (panel 1) shows strong changes between replicates, interestingly, sample MT8, which was chosen as a control (having around 100 % total concentration in

the very first measurement run,) shows little changes between runs, indicating good measurement reproducibility. The reference soil material however shows quite some changes between replicates. Also, very interesting is sample MD2 which consistently shows low total concentrations at around 65 %. When looking at the element concentrations, clear differences between replicates are visible, for sodium changes of up to 0.75 % can be found (MT1), magnesium measurements differed up to about 0.7 % (for MT1 and MT4 relative increase of > 25 %). The other elements also show clear and strong differences, especially silicon, with an increase from about 25 % to 35 % for MT1 and from about 28 % to 39 % for MT4.

Furthermore, a pattern can be found when looking at the reference material. A clear change in total concentration (panel 1, replicates E and F)) is accompanied by clear changes in the elemental concentrations (panels 2 – 7). This pattern is also well visible for the samples and their replicates. This means that accompanied to a change in total concentration, the relative share of a sample changes (which is somewhat logical). This highlights that the total concentration amount in some cases can give an indication of the measurement quality, but this is not necessarily always true, as shows sample MD2, which ranks amongst the lowest total concentration values, but shows very good reproducibility.

Between the runs the samples were not modified in any way, except that care was taken to get a smooth surface on the sample cup membrane. In consequence this means that XRF on powdered samples may exhibit drastic changes between runs and multiple runs are advisable to check consistency and derive relative measurement errors (which in this case are orders of magnitude larger than the devices internally reported measurement error, in the order of fractions of a percent). Furthermore, sample preparation seems also very important, as homogeneity is a key factor since otherwise the X-Rays and thus the resulting fluorescence signal can be very different between runs (especially when the sample cup was removed and later placed differently in subsequent runs).

Table S-1 Overview of the XRF elemental composition for selected samples and selected elements as well as the total summed up concentration (device internal processing). Samples are indicated using their working code, where MT refers to Tsiigehtchic / Mackenzie, AR to Tsiigehtchic / Arctic Red, PR to Fort McPherson / Peel and MD to Inuvik / Mackenzie, the number refers to the particle size, with 1 being associated with bulk and 8 with < 20 μm (more details in Table 3-1).

Sample	Replicate	Na	Mg	Al	Si	Ca	Ti	Total
MT1	A	0.99	1.91	4.22	25.56	6.11	0.29	72.53
	B	1.40	2.68	6.09	35.52	8.38	0.41	101.24
MT4	A	0.91	2.47	3.42	29.53	6.23	0.20	78.99
	B	1.18	3.19	4.44	38.81	7.98	0.26	103.00
	C	1.39	3.19	4.42	38.78	7.89	0.25	103.00
MT8	A	1.13	2.35	8.29	34.89	5.53	0.65	102.98
	B	1.23	2.32	8.17	34.58	5.51	0.64	102.18
	C	1.25	2.36	8.25	34.86	5.50	0.64	102.89
MD1	A	0.87	1.65	4.96	25.82	5.17	0.31	73.25
	B	1.11	2.11	6.11	32.06	6.33	0.37	90.80
	C	1.02	2.00	5.83	30.87	6.13	0.36	87.27
MD2	A	0.89	1.70	3.88	22.67	5.01	0.24	65.46
	B	0.90	1.65	3.80	22.57	4.99	0.24	65.00
	C	0.86	1.67	3.81	22.48	5.00	0.24	64.82
MD3	A	1.05	1.73	4.34	25.85	4.85	0.27	72.57
	B	0.97	1.77	4.52	27.40	5.11	0.29	76.45
	C	1.09	2.06	5.33	32.12	5.93	0.33	89.43
PR8	A	0.93	1.55	8.31	33.33	1.44	0.66	92.81
	B	1.09	1.64	9.04	37.17	1.59	0.72	102.74
	C	1.07	1.63	9.09	37.31	1.58	0.72	103.00
Ref	A	1.2	0.77	4.95	30.43	1.12	0.35	75.03
	B	1.08	0.79	5.06	31.31	1.16	0.36	77.08
	C	1.12	0.79	4.94	30.53	1.13	0.35	75.25
	D	1	0.79	4.9	30.23	1.13	0.35	74.49
	E	1.41	0.91	5.85	36.06	1.35	0.42	89.06
	F	1.34	0.93	5.81	35.82	1.34	0.42	88.43
	G	1.06	0.77	4.87	29.74	1.11	0.35	73.47
	H	1.09	0.78	4.92	30.12	1.12	0.35	74.34

S-3. BPCA Statistics

Descriptive statistics for the distribution of BPCAs in the different rivers.

Table S-2 Descriptive statistics of the BPCA distribution across measurement sites. MT = Mackenzie at Tsiigehtchic, AR = Arctic Red (at Tsiigehtchic), PR = Peel River, MD = Mackenzie Delta (at Inuvik). For each of the four BPCAs a test of normal distribution was conducted by using the Shapiro method, subsequently a Levene test was used to test for equal variances and finally either a Kruskal-Wallis (K-W.) or an analysis of variance (ANOVA; AOV) was conducted to see if measurement sites have significantly different BC quality. A Dunn post-hoc test, using the Bonferroni method, was used to find the different groups. Correlation coefficient was calculated using $r = \left| \frac{z}{\sqrt{n}} \right|$, effect size is based on Cohen (1992).

BPCA	Shapiro	Levene	Grouping	Post-Hoc	Grouping				Effect Size (Cohen, 1992)
					MT	AR	PR	MD	
B3	sig.	sig *	K.-W. **	Du. - Bo. *	a	b	b	b	r = 1.18, large
B4	n.s.	sig ***	K.-W. *	Du. - Bo. **	a	b	ab	ab	r = 1.15, large
B5	sig	sig **	K.-W. **	Du. - Bo. **	a	b	ab	ab	r = 1.24, large
B6	n.s.	n.s.	AOV. n.s.	—	a	a	a	a	—

S-4. Mid-infrared spectrometry

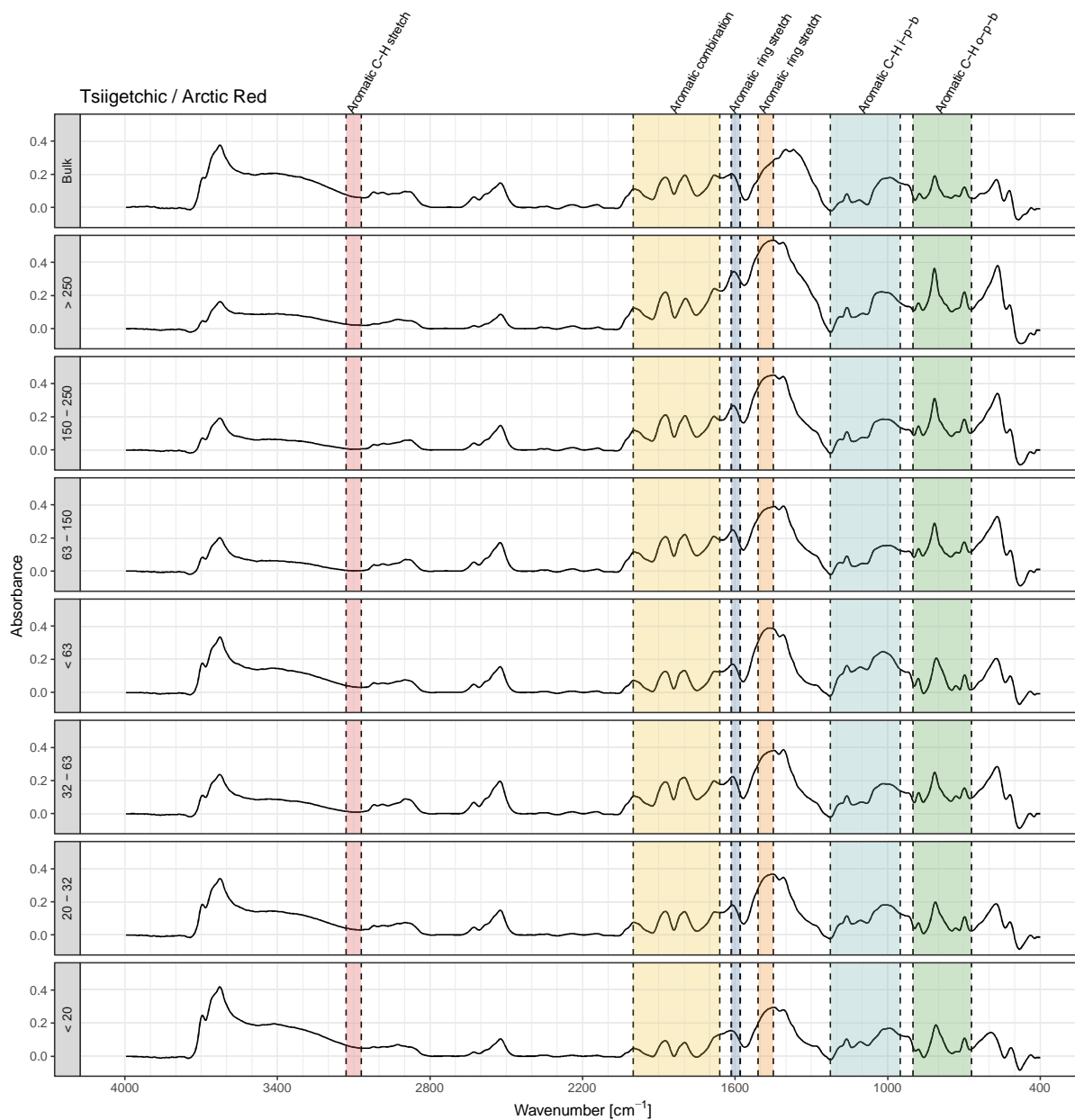


Figure S-2 Mid-infrared spectral data from diffuse reflectance spectrometry for the site Tsiigetichic / Arctic Red. Dashed lines indicate absorption bands of compounds related to aromatic structures. Aromatic C-H i-p-b refers to aromatic C-H in-plane bending. Aromatic C-H o-p-b denotes aromatic C-H out-of-plane bending. For more details about the bands and the spectra refer to the text and Table 3-3. Absorbance is a unitless ratio defined as $A = -\log\left(\frac{I}{I_0}\right)$, where I is the measured light intensity and I_0 is the initial intensity.

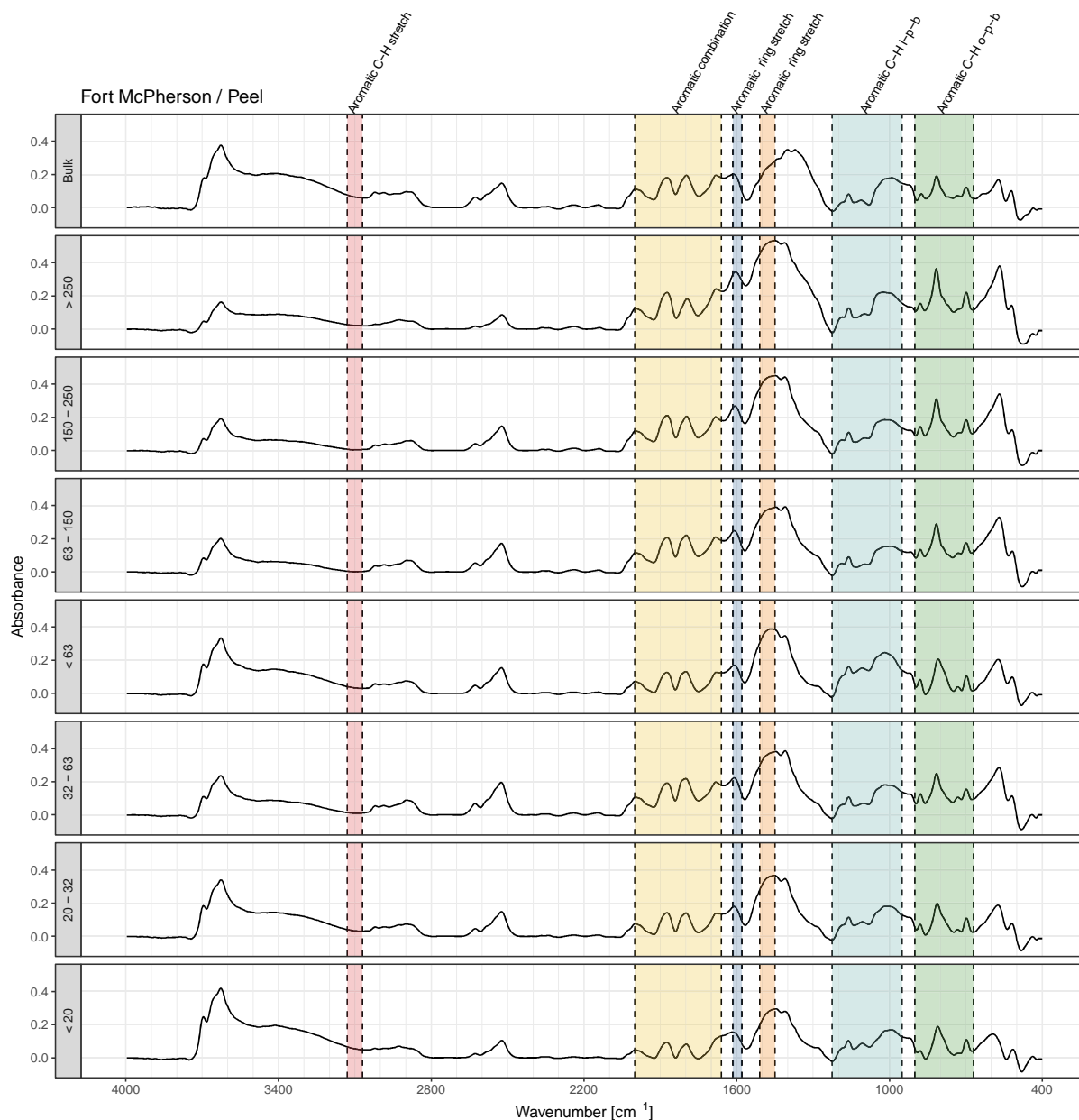


Figure S-3 Mid-infrared spectral data from diffuse reflectance spectrometry for the site Fort McPherson / Peel. Dashed lines indicate absorption bands of compounds related to aromatic structures. Aromatic C-H i-p-b refers to aromatic C-H in-plane bending. Aromatic C-H o-p-b denotes aromatic C-H out-of-plane bending. For more details about the bands and the spectra refer to the text and Table 3-3. Absorbance is a unitless ratio defined as $A = -\log\left(\frac{I}{I_0}\right)$, where I is the measured light intensity and I_0 is the initial intensity.

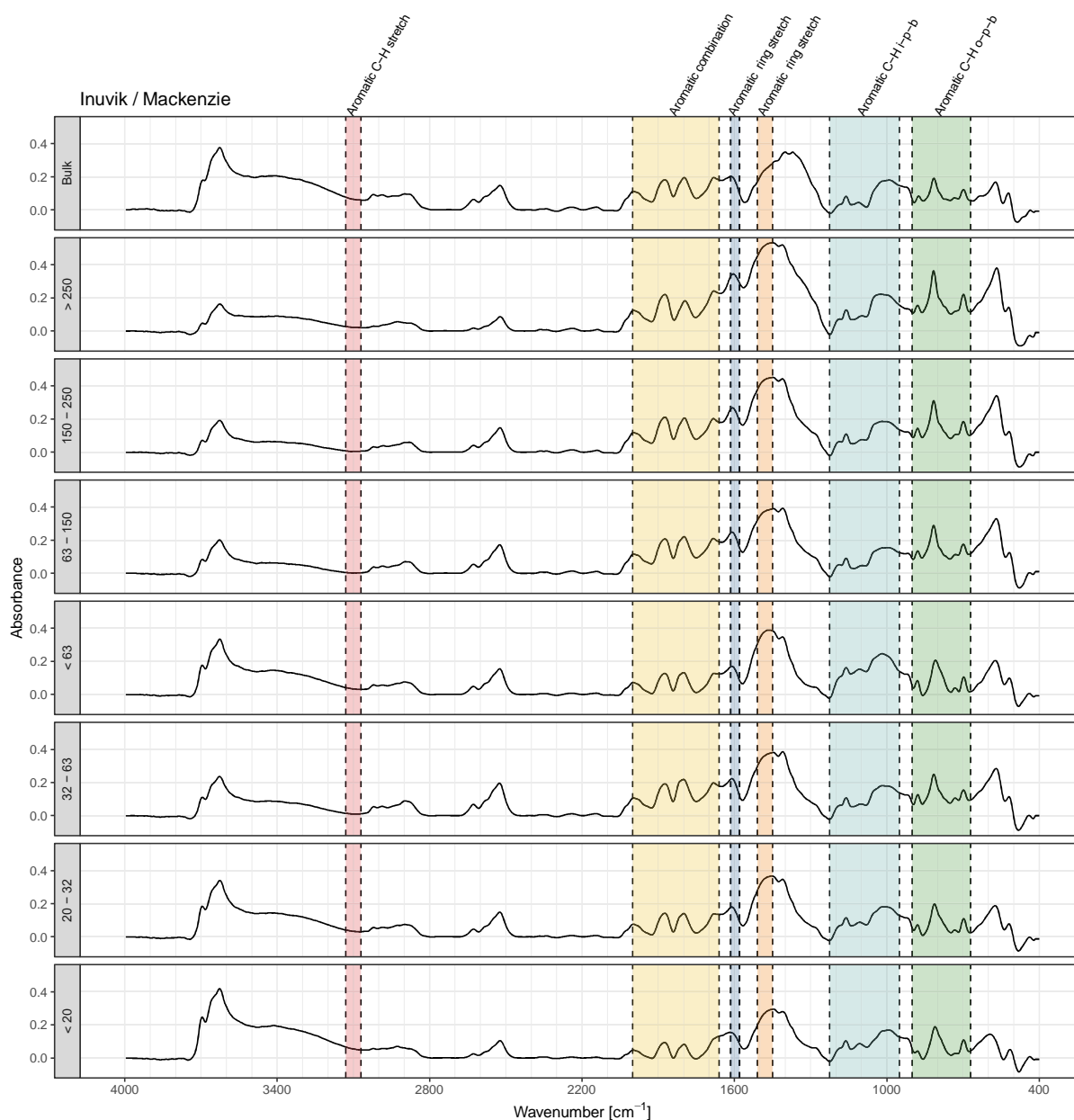


Figure S-4 Mid-infrared spectral data from diffuse reflectance spectrometry for the site Inuvik / Mackenzie. Dashed lines indicate absorption bands of compounds related to aromatic structures. Aromatic C-H i-p-b refers to aromatic C-H in-plane bending. Aromatic C-H o-p-b denotes aromatic C-H out-of-plane bending. For more details about the bands and the spectra refer to the text and Table 3-3. Absorbance is a unitless ratio defined as $A = -\log\left(\frac{I}{I_0}\right)$, where I is the measured light intensity and I_0 is the initial intensity.

Table S-3 Descriptive statistics for the relationship between aromatic C-H stretch AUC and BPCA [g/kg sample]. No autocorrelation according to D-W statistics, residuals normally distributed and homoscedastic.

Coefficients:	Estimate	Std. Error	t value	Pr(> t)
Intercept	0.35	0.085	4.18	0.000232 ***
AUC-A3	0.20	0.026	7.70	1.37e-08 ***
Multiple R-squared: 0.66				
F-statistic: 59.3 on 1 and 30 DF p-value: 1.369e-08				

S-5. Estimating the Organic Carbon Content

To get an estimate of the amount of C_{org} in samples that had no primary method yield this information, a partial least squares regression (PLSR) was conducted. First off, the number of components or latent variables (see Mevik and Wehrens, 2018a) to be used in the regression was set to six, because this amount minimizes the residual mean square error of prediction (RMSEP, see Figure S-5). RMSEP compares the predicted values with the measured values and should be as low as possible. In this case the minimum, found for 6 components is about 0.44, which is rather high, but since the sample amount is rather low, nothing can be changed to further decrease RMSEP. In their example, based on 50 samples and a higher scan resolution, Mevik and Wehrens (2018a) achieve an RMSEP of 0.297 with only two components. However, their samples being of type gasoline, are rather simple mixtures, showing only a couple of peaks.

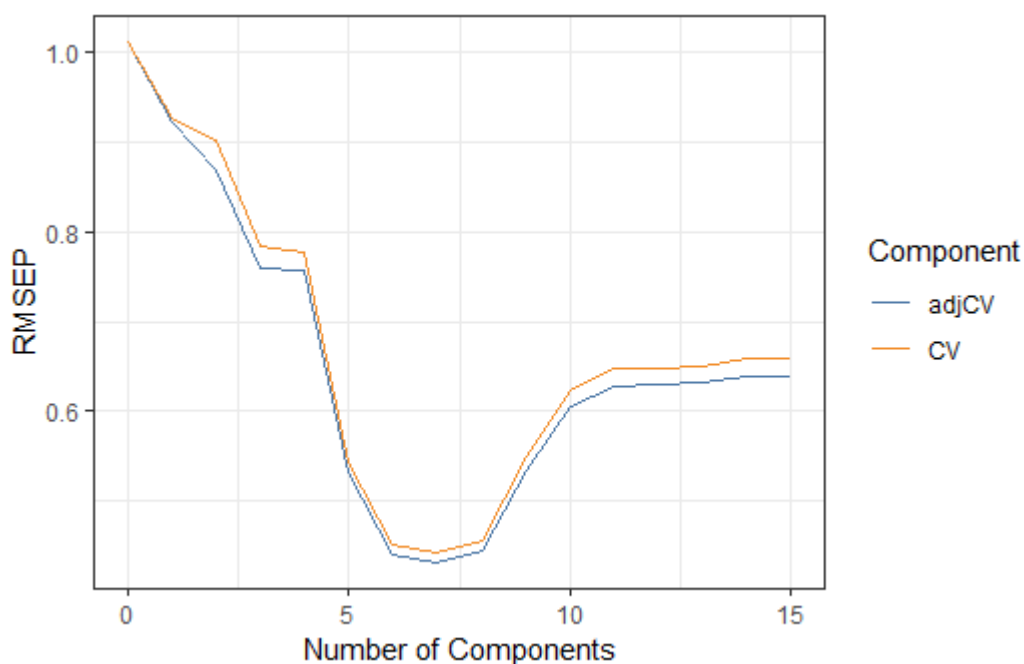


Figure S-5 Number of components vs. residual mean squared error of prediction (RMSEP) for the prediction of organic carbon by PLSR on DR-spectrometry data.

The relationship between different components can be analyzed by comparing the different combinations in a scatterplot matrix or a score plot (see Figure S-6). The percentage behind the name of the component gives the amount of variance explained. No special patterns, grouping or outliers can be found here.

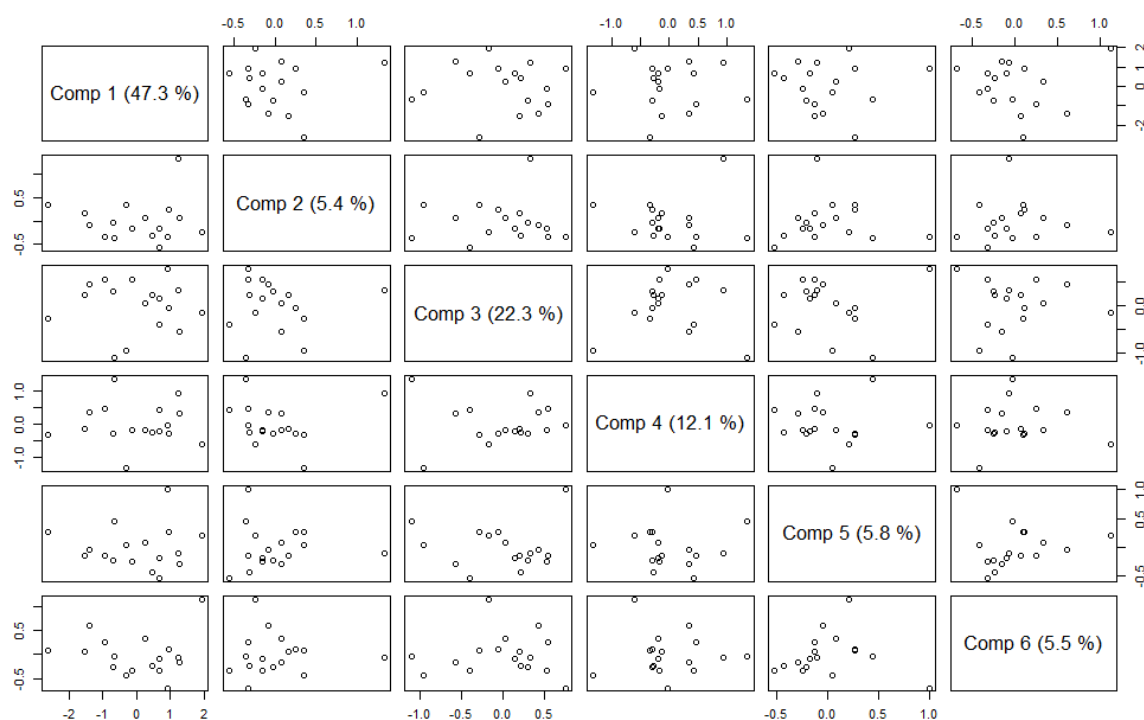


Figure S-6 Scatterplot matrix of the combinations of the 6 components, percentages in braces indicate the amount of variance explained by the component.

When comparing measured values in relation to the predicted values, the points closely follow the 1:1 line, with only one major outlier in the top right corner, otherwise no curvature or clustering is clearly visible (Figure S-7).

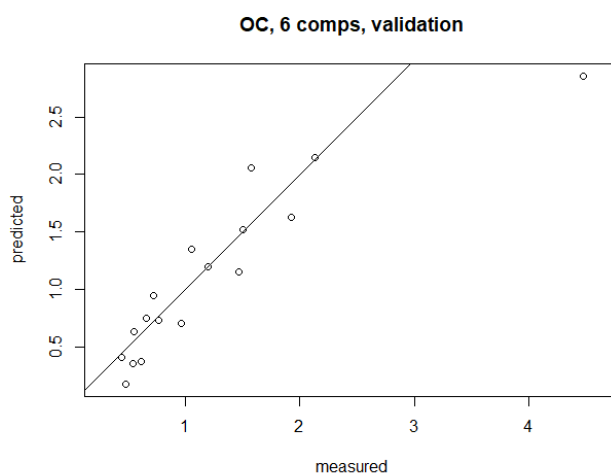


Figure S-7 Measured vs. predicted values, the line indicates a 1:1 relationship.

The loadings can finally be investigated individually over the whole spectrum by a spectral loadings plot (Figure S-8). Interestingly the alcohol peak and the CO₂ peak seem to have some biased influence on the prediction (having both negative and positive values

at the same position). The region from 400 cm^{-1} to $2'200\text{ cm}^{-1}$ looks chaotic, with no clear bands or peaks. Ideally the components would not differ as strongly as presented here, they would tend to highlight the same indicative or important bands and regions in the spectrum. Thus, as a final note, it should be stated that the analysis and regression conducted here presents only a very rough estimate of organic carbon, this is clear from the amount of components required (6), from the rather high RMSEP (0.44) as well as from the loadings plot (Figure S-8). Nonetheless it allowed to continue with the BC analysis, that would otherwise have been hindered by missing C_{org} data.



Figure S-8 Components and their loading values.



*What will become of you and me;
Besides the photo and the memory?
This is the school in which we learn,
That time is the fire in which we burn.
What is the self amid this blaze?
What am I now, that I was then,
Which I shall suffer and act again.
The children shouting are bright as they run,
Ravished entirely in their passing play!
This is the school in which they learn,
That time is the fire in which they burn.*

— *Adaptation from Delmore Schwartz's "Calmly We Walk through This April's Day".*